

Characterisation of the neuronal microcircuitry and adenosine modulation of layer 6 neurons in rat medial prefrontal cortex

Inaugural dissertation

for the attainment of the title of doctor
in the Faculty of Mathematics and Natural Sciences
at the Heinrich Heine University Düsseldorf

presented by

Chao Ding

from Wuwei, Anhui, China

Jülich, August 2018

from the INM2, Institute of Neuroscience and Medicine
at the Forschungszentrum Jülich

Published by permission of the
Faculty of Mathematics and Natural Sciences at
Heinrich Heine University Düsseldorf

Supervisor: Prof. Dr. Andreas Bauer (Department of Neurology Heinrich Heine
University; Institute of Neuroscience and Medicine, Forschungszentrum Jülich)
Co-supervisor: Prof. Dr. Christoph Fahlke (Institute of Complex Systems,
Forschungszentrum Jülich)

Date of the oral examination: 30/10/2018

To my family

Table of Contents

1. Introduction	1
1.1 The mammalian neocortex	1
1.2 The role of prefrontal cortex	2
1.3 Neuronal classification and microcircuit in neocortex	5
1.4 Adenosine and adenosine receptors	9
1.5 Aim of this study	13
2. Materials and Methods	15
2.1 Slice Preparation	15
2.2 Solution	15
2.3 Identification of cortical layers and neurons in mPFC	16
2.4 Patch clamp technique	17
2.4.1 Single cell recordings	17
2.4.2 Pair recordings	18
2.5 Drug Application	20
2.6 Analysis of electrophysiological data	20
2.6.1 Passive membrane properties of single neuron	20
2.6.2 Active properties of single neuron	21
2.6.3 Miniature spontaneous synaptic activity	22
2.6.4 Properties of synaptic physiology in paired recordings	23
2.7 Morphological reconstructions and analysis	25
2.7.1 Histological procedures	25
2.7.2 Morphological 3D reconstructions	25
2.7.3 Axonal density map	26
2.8 Cluster analysis	26
2.9 Statistical analysis	27
3. Results	28
3.1 Neuronal classification in L6 of mPFC	28
3.1.1 Morphological classification of excitatory neurons	28
<i>Comparison of electrophysiological properties between 2 morphological clusters</i>	33

3.1.2 Morphological and electrophysiological classification of L6 inhibitory interneurons ...	37
<i>Morphological classification</i>	38
<i>Electrophysiological classification</i>	42
<i>Correlation between morphological and electrophysiological clusters</i>	44
3.2 Monosynaptic connections in L6 of mPFC	46
3.2.1 Synaptic connectivity between L6 excitatory neurons	47
3.2.2 Synaptic connectivity between L6 excitatory and inhibitory neurons	54
<i>Excitatory connections from L6 excitatory neurons to inhibitory neurons</i>	54
<i>Inhibitory connections from L6 inhibitory neurons to excitatory neurons</i>	57
3.3 Adenosine effects on excitatory neurons and microcircuits of mPFC	60
3.3.1 Adenosine modulates single neuron activities in L5 and L6	61
<i>Effect of adenosine on the single neuron activities in L5</i>	61
<i>Adenosine effects on single neuron activity in L6</i>	66
3.3.2 Adenosine modulates excitatory synaptic transmission in L6	69
4. Discussion	76
4.1 Classification of excitatory neurons in L6 of mPFC	76
4.2 Classification of inhibitory neurons in L6 of mPFC	78
4.3 Monosynaptic connections in L6 of mPFC	79
4.4 Adenosine modulation on cortical microcircuitry of mPFC	82
Summary	86
Zusammenfassung	88
References	90
Abbreviations	102
Acknowledgement	104
Curriculum Vitae	106
Eidesstattliche Erklärung	107

1. Introduction

1.1 The mammalian neocortex

From an evolutionary point of view is the neocortex the newest part of cerebral cortex. It is involved in higher order brain functions, such as sensory perception, motor control, cognition and social activity (Baumgartner 2009; Lui et al. 2011; Lodato and Arlotta 2015). The shape, size and neuron number of different neocortical areas vary widely through different mammalian species (Herculano-Houzel 2009). In humans, the neocortex constitutes 90% of the cerebral cortex (Nieuwenhuys et al. 1998), which is considered to be a key evolutionary advance because it enabled higher cognitive function (Lui et al. 2011). Brodmann's map, which was defined by the German anatomist Korbinian Brodmann, is one of the most influential works illustrating the cytoarchitectural organisation of neurons in the human brain. In Brodmann's map, the cerebral cortex is subdivided into 52 areas (Fig. 1.1). Each area has distinct cytoarchitectural properties and correlates closely with diverse cortical functions. Therefore, abnormal functions of the neocortex are usually associated with different psychiatric illnesses (Kaufmann and Moser 2000; Luna et al. 2002; Thompson and W Toga 2003; Mueller et al. 2009; Zilles and Amunts 2010; Lewis et al. 2011).

The neocortex is a multi-layered structure that usually consists of six horizontally oriented layers from outside (pial surface) to inside (white matter, WM), segregating by morphological, physiological and genetical characteristics, such as soma density, cell type and axonal projection patterns of pyramidal cells (Brodmann and Gary 2006; Meyer et al. 2010). Exceptions exist in some cortices such as the primary motor cortex and the prefrontal cortex where layer 4 (L4) is small or missing. Layer 1 (L1) neurons are primarily inhibitory interneurons and do not project extrinsically. Pyramidal neurons (PNs) in layer 2 (L2) and layer 3 (L3) project their long-range collaterals within their home cortical area and to other cortical regions, while layer 5 and 6 are the primary output layers of the neocortex that send the projections to subcortical structures such as the thalamic nuclei, brainstem and spinal cord. L4 is regarded as the major thalamorecipient layer and distributes the incoming information to other cortical layers (Feldmeyer 2012; Narayanan et al. 2017; Rockland 2017).

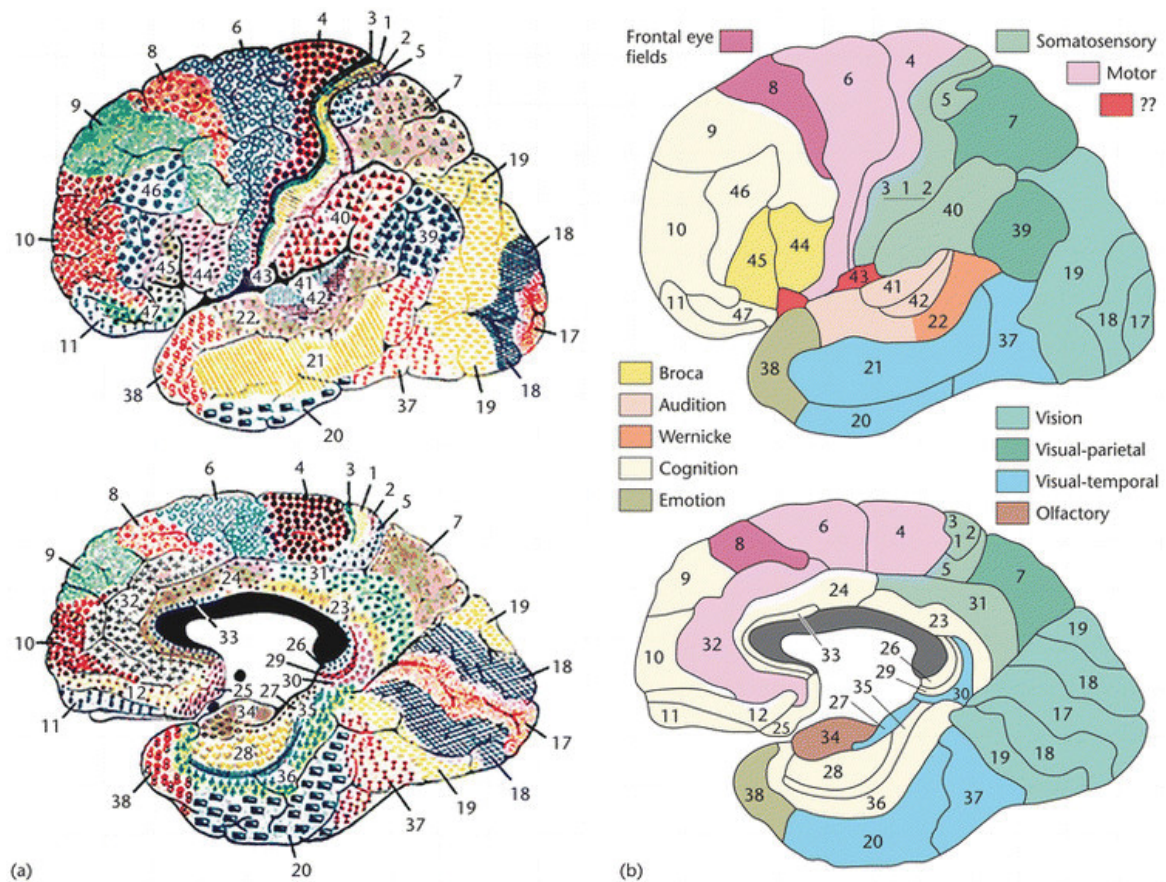


Fig. 1.1 Brodmann' maps and functions of different areas. *The human cortex was divided into 52 regions by the German anatomist Kobinian Brodmann in 1909. Different regions were considered to have distinct cytoarchitectural organisation and involved in specific function. Parts of these functions were indicated in (b). (Adapted from Thompson and W Toga 2003, the images source was from Mark Dubin, University of Colorado, Boulder)*

In addition, sensory cortices are also organised into vertically oriented columns (Mountcastle 1957). Neurons within a cortical column are activated by the same area of the associated receptive field, same modality and through similar dynamic stimulus conditions (Baumgartner 2009). To better understand the structure and function of cortical areas, it is important to investigate the connectivity characteristics between different neuronal cell types in the local microcircuits.

1.2 The role of prefrontal cortex

The areas of cerebral cortex are organised in a hierarchical fashion during development (Fuster 2001). Sensory and motor areas, which support the specific sensory and motor functions are at the bottom of this organisation. Sensory association areas, which support more integrative functions are

progressively higher-order areas. At the highest level of the neocortical hierarchy, the prefrontal cortex (PFC) integrates information from several cortical areas, including sensory and motor cortices and is considered to be responsible for cognitive processes (Damasio et al. 1985; Stuss et al. 1986; Wood and Grafman 2003; Wood et al. 2003).

The PFC is located in the anterior portion of the frontal lobe. In human brain, PFC contains areas 8-14, 24, 25, 32, 44-47 according to the Brodmann's map (Murray et al. 2017). In the development of the human brain, the PFC shows a larger increase in size compared to other brain regions and constitutes almost one-third of the neocortex (Fuster 2001). Based upon Brodmann's map, PFC is subdivided to caudal, ventrolateral, dorsolateral, medial and orbitofrontal cortex. Extensive connections between these subregions support an integrating of disparate information and distribute information from regional afferents to other parts of PFC. Thus, PFC integrates inputs and information from wide-ranging brain systems and processes these in a relatively local circuit. By working with the extrinsic inputs and outputs, PFC plays a central role in a wide variety of brain processes and complex behaviours (Miller and Cohen 2001).

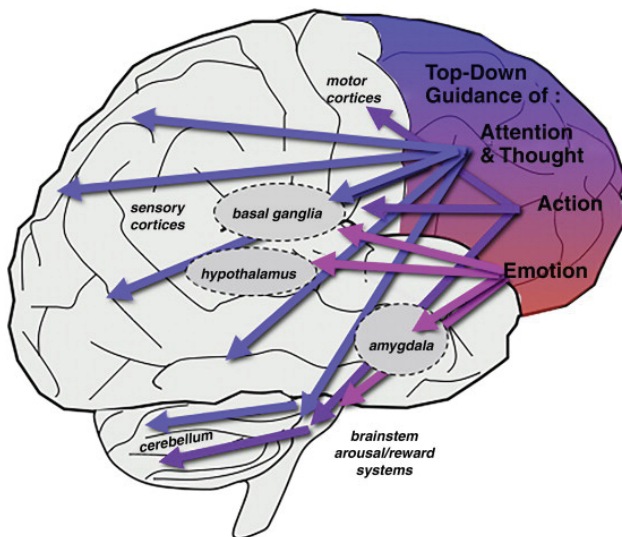


Fig. 1.2 Top-down control of behaviour, thought and emotion provided by PFC. *Subregions of PFC form intensive connections with many cortical and subcortical brain areas. Topographically speaking, the dorsal and lateral part of PFC regulate attention, thought and actions, while the more ventral and medial parts regulate emotion. (Adapted from Berridge and Arnsten 2015)*

The PFC interconnects with almost all sensory systems (Goldman-Rakic and Schwartz 1982; Petrides and Pandya 1984; Barbas and Pandya 1989; Seltzer and Pandya 1989; Pandya and Yeterian 1990; Petrides and Pandya 1999), with cortical and subcortical motor system structures (Goldman and Nauta 1976; Alexander et al. 1986; Bates and Goldman-Rakic 1993; Lu et al. 1994;

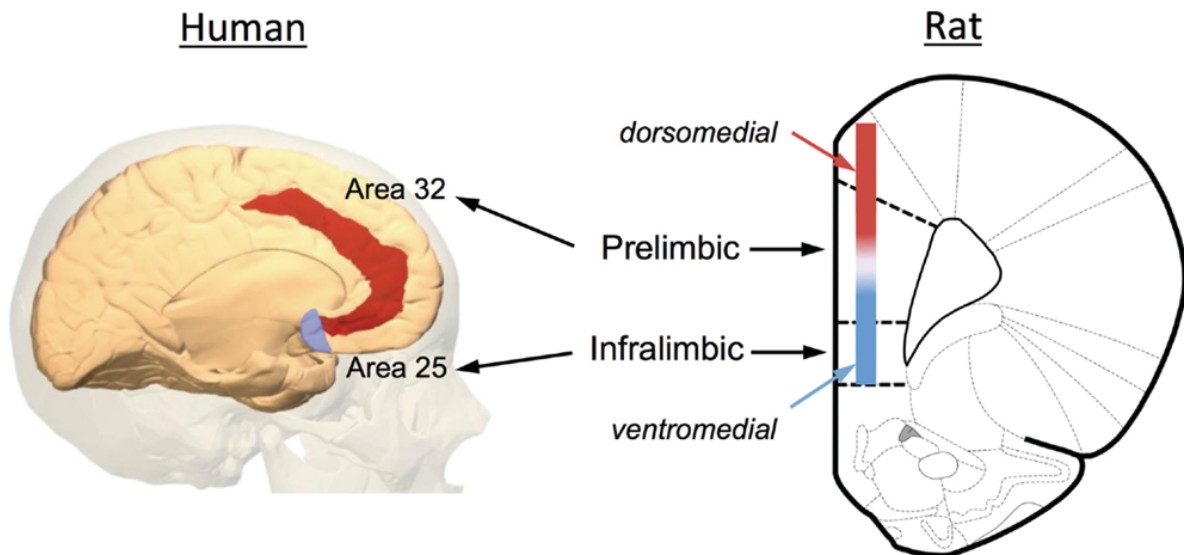


Fig. 1.3 Anatomical depiction of rat prelimbic (PrL) and infralimbic (IfL) cortex of medial PFC and their equivalent regions in human brain. *Based on the commonality of thalamic input, the rat PrL cortex is homologous to Brodmann area 32 while IfL cortex is homologous to Brodmann area 25 which belong to the medial PFC. In some circumstance, the mPFC in rat is also divided simply to a dorsomedial and a ventromedial region because of the uncertain borders between PrL and IfL cortex (Adapted from Gass and Chandler 2013).*

Schmahmann and Pandya 1997) and with limbic structures including direct and indirect connections with hippocampus, amygdala and hypothalamus (Van Hoesen et al. 1972; Porrino et al. 1981; Amaral and Price 1984; Goldman-Rakic et al. 1984; Barbas and Pandya 1989; Barbas and De Olmos 1990). PFC projects widely to most of the other neocortical areas (Pandya and Yeterian 1990) and send the feedback signals or top-down commands (Berridge and Arnsten 2015) during PFC-associated functions like memory retrieval (Tomita et al. 1999). All these characteristics of PFC show that it plays an important role in the central nervous system and that it is involved in many complex neuronal and behavioural activities including decision making (Euston et al. 2012), learning and memory (Fuster 2001; Miller and Cohen 2001), addiction (Davis et al. 2006; Gass and Chandler 2013), sleep (Muzur et al. 2002; Elmenhorst et al. 2007; Elmenhorst et al. 2009) and social activity (Wang et al. 2011; Bicks et al. 2015).

However, the structural organisation of rodent brain is different from that of human brain. The PFC of rodents is anatomically located in the anterior part of the frontal cortex and is roughly divided to anterior cingulate cortex (ACC), medial prefrontal cortex (mPFC) and orbital frontal cortex (OFC)

(Van Eden and Uylings 1985; Uylings et al. 2003; Hoover and Vertes 2007; Gass and Chandler 2013). The homologous subregions of PFC in rodents and human are difficult to define due to its massive expansion during mammalian evolution. Rodent mPFC can be further subdivided into prelimbic (PrL) cortex and infralimbic (IfL) cortex; based on similarities in the thalamic inputs, the PrL cortex is homologous to Brodmann area 32 while IfL cortex is homologous to Brodmann area 25 in the human brain (Gass and Chandler 2013). Among all the subregions of PFC, mPFC is one of the most extensively investigated area with its well studied role in error detection (Holroyd et al. 2002), executive control (Posner et al. 2007), conflict monitoring (Botvinick et al. 2004), reward-guided learning (Rushworth et al. 2011) and consolidation (Takashima et al. 2006), retrieval (Bontempi et al. 1999; Frankland et al. 2004) and extinction (Gass and Chandler 2013) of both recent and remote memory. To better understand the fundamental neuronal circuitry in mPFC and to associate the microcircuit to the complex functions, rat mPFC is one of the most popular cortical areas for both *in vivo* and *in vitro* studies.

1.3 Neuronal classification and microcircuit in neocortex

The neocortex comprises diverse types of excitatory and inhibitory neurons in different layers. These neurons differ in their electrophysiological, molecular, morphological and biochemical properties. In the neocortex, most of the excitatory neurons, also known as the principal cells that project to distant intra- and subcortical target regions are pyramidal neurons (PNs) that the soma is shaped like a pyramid and with a long, thick apical dendrite extending towards the cortical surface and several basal dendrites (Megias et al. 2001). Notably, there are inverted PNs in layer 6 (L6) with main dendrites pointing towards the WM instead of the pial surface (van Aerde and Feldmeyer 2013; Radnikow and Feldmeyer 2018). The electrophysiological characteristics including passive electrical properties, action potential (AP) firing pattern and synaptic properties differ throughout layers and brain regions. Morphologically, different excitatory neuron types can be distinguished by the shape and length of their apical dendrites (Fig. 1.4) (Radnikow and Feldmeyer 2018). The classification has also been done based on the projection pattern of their axons, such as corticocortical and corticothalamic neurons in L6 of somatosensory cortex (Zhang and Deschenes 1997; Kumar and Ohana 2008). In mPFC, PNs in layer 5 (L5) have been studied most comprehensively due to their special role as the main output layer of neocortex (Molnar and Cheung 2006). Previous studies indicated that different pyramidal cell types in this area form

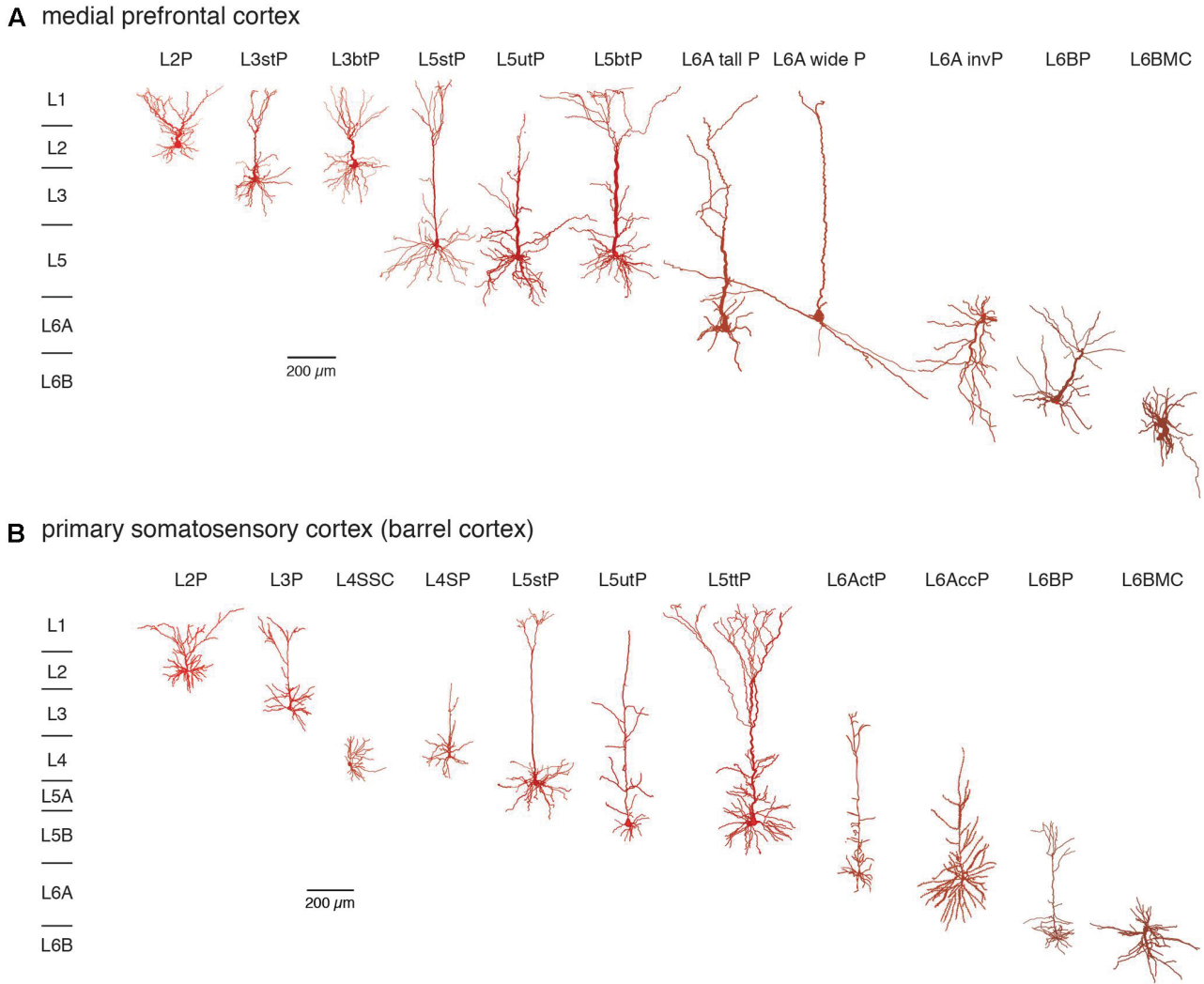


Fig. 1.4 Excitatory neuron types in layer 2-6 of the medial prefrontal (A) and primary somatosensory cortex (B). The excitatory neurons in cortical layer 2-6 of rat mPFC and S1 barrel cortex can be classified based on their dendritic pattern (from superficial to deep layer, the somatodendritic domains are shown in different shades of red, from bright red to dark red). Most neuron types are pyramidal cells with apical dendrites of different shape and length, except the spiny stellate cells in L4 and multipolar neurons in L6B (from Radnikow and Feldmeyer, 2018 with permission).

Abbreviations: L2P - L2 pyramidal cell; L3stP - L3 slender-tufted pyramidal cell, L3btP - L3 broad-tufted pyramidal cell; L3P - L3 pyramidal cell; L4SSC - L4 spiny stellate cell; L4SP - L4 star pyramidal cell; L5stP - L5 slender-tufted pyramidal cell; L5utP - L5 untufted pyramidal cell; L5btP - L5 broad-tufted pyramidal cell; L5ttP - L5 thick-tufted pyramidal cell; L6A tall P - L6A tall pyramidal cell; L6A wide P - L6A wide pyramidal cell; L6A invP - L6A inverted pyramidal cell; L6AccP - L6A corticocortical pyramidal cell; L6ActP - L6A corticothalamic pyramidal cell; L6BP - L6B pyramidal cell; L6BMC - L6B multipolar cell.

different subcortical projections, intralaminar connections and subnetworks (Otsuka and Kawaguchi 2008; Brown and Hestrin 2009; Dembrow et al. 2010). On the other hand, the morphology of

excitatory neuron in L6 shows a remarkably high degree of diversity (Marx and Feldmeyer 2013; van Aerde and Feldmeyer 2013; van Aerde et al. 2013; Radnikow and Feldmeyer 2018). However, only few studies have investigated synaptic interactions in the excitatory neuronal network in mPFC.

GABAergic inhibitory interneurons, are so named after their release of neurotransmitter *gamma*-aminobutyric acid (GABA), share only 12% of the total number of neurons in neocortex (Meyer et al. 2011) but play important roles in the development of central nervous system (Wonders and Anderson 2006) and functions of the cerebral cortex, such as balancing neuronal excitation, synchronising cortical activities and maintaining regional oscillation (McBain and Fisahn 2001; Markram et al. 2004; Klausberger and Somogyi 2008). In principle, the subtypes of GABAergic interneurons are systematically classified based upon the expression of neurochemical markers, electrophysiological properties and morphological characteristics including dendritic and axonal projection patterns (Ascoli et al. 2008; DeFelipe et al. 2013; Feldmeyer et al. 2018).

GABAergic interneurons have been characterised previously based on the specific expression of molecular markers including calcium-binding proteins, neuropeptides, enzymes, receptors, ion channels and structural proteins (Kawaguchi and Kubota 1993, 1996; Cauli et al. 1997; Monyer and Markram 2004; Ascoli et al. 2008). Nevertheless, the existence of three basically non-overlapping interneuron subpopulations has been proposed. The subpopulations show differential expression of parvalbumin (PV), somatostatin (SST) or the ionotropic serotonin receptor 3A (5HT_{3a} receptor) (Rudy et al. 2011; Tremblay et al. 2016; Feldmeyer et al. 2018).

Interneurons in the neocortex can be classified also by their electrophysiological characteristics. The time course of the action potential (AP) and the characteristics of the AP spiking behaviour including frequency, initial onset and steady-state response, decide the types of physiological properties of interneurons (Markram et al. 2004; Ascoli et al. 2008; DeFelipe et al. 2013; Feldmeyer et al. 2018). Fast-spiking (FS) neurons fire at a continuous high frequency with little to no frequency adaptation during prolonged stimulation and display a smaller AP half-width compared to non-fast spiking interneurons (Feldmeyer et al. 2018). Irregular-spiking (IS) neurons display high frequency initial burst firing followed by irregular spaced spikes during the initial onset (Cauli et al.

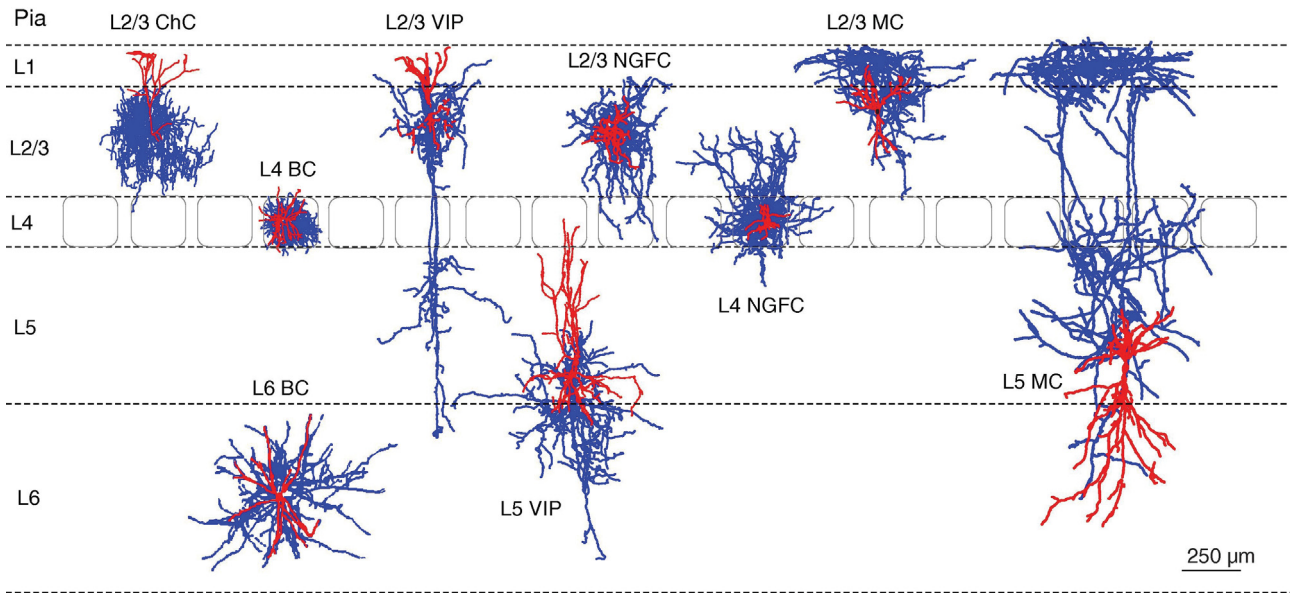


Fig. 1.5 Morphological diversity of classical interneuron types in primary somatosensory cortex. Example reconstructions of different inhibitory neuron types in different layers of rat S1 barrel cortex. Axons are labeled in blue, soma and dendrites in red. Abbreviations: ChC – Chandelier cell/axo-axonic cell, BC – Basket cell, VIP – Vasoactive intestinal polypeptide cell, NGFC – Neurogliaform cell, MC – Martinotti cell. (Adapted from Feldmeyer et al., 2018).

1997; Porter et al. 1998). The low threshold spiking (LTS) neurons show a burst of 100 Hz at a lower threshold compared with that of other interneurons (Kawaguchi and Kubota 1993, 1997). Other subtypes of interneurons show certain frequency adaptation upon strong stimulation, display a ‘stuttering’ pattern, or respond with a delay during initial onset can be easily distinguished from one to another.

GABAergic neurons show also a high heterogeneity in their morphological properties. The best-studied subgroups include basket cells, chandelier cells, Martinotti cells, neurogliaform cells and bipolar cells. They are classified based on the subcellular postsynaptic target innervation as well as dendritic and axonal projection pattern (Fig. 1.5) (Staiger et al. 2004; Ascoli et al. 2008; Helmstaedter et al. 2009; DeFelipe et al. 2013; Cauli et al. 2014; Clowry 2015; Koelbl et al. 2015; Feldmeyer et al. 2018).

Although neuronal cell types have extensively studied and classified in different neocortical areas, little is known about excitatory and inhibitory neuron types in the mPFC, especially in the deep layers. In order to arrive at a meaningful and convincing classification, it is necessary to use a

combined quantitative analysis of morphological characteristics, active and passive electrophysiological properties as well as molecular parameters.

To investigate the details of local circuit connections in neocortex, multiple recordings with different protocols were widely used (Feldmeyer et al. 1999; Feldmeyer et al. 2002; Thomson et al. 2002; Wang et al. 2006; Lefort et al. 2009; Jiang et al. 2013; Jiang et al. 2015; Koelbl et al. 2015; Lee et al. 2015; Qi et al. 2017). These studies revealed that different types of neurons form different types of connections within the same layer or between layers. Depending on the cell types and locations of the presynaptic and postsynaptic neurons, the connectivity ratio changes dramatically (Thomson et al. 2002; Lefort et al. 2009). For example, the connectivity ratio was found to be high between L4 excitatory, spiny neurons within single barrels in the barrel field of rat somatosensory cortex (Feldmeyer et al. 1999; Petersen and Sakmann 2000). The connectivity ratio is also high in L4 to L3 excitatory pairs due to the fact that axons of L4 neurons form dense projections to L3 (Valverde 1976; Parnavelas et al. 1977; Gilbert 1983; Burkhalter 1989; Feldmeyer et al. 1999; Feldmeyer et al. 2002; Lefort et al. 2009). On the other hand, the connectivity ratio is relatively low between L6 neurons (Beierlein and Connors 2002; Mercer et al. 2005; West et al. 2006; Lefort et al. 2009; Crandall et al. 2017) which might result from the high diversity of individual neurons or their low axonal density within L6. Only few studies on the synaptic connectivity in prefrontal cortex are currently available (Wang et al. 2006; Schwindel et al. 2014) and even fewer data is available for L6. Investigation of the neuronal connections and their interaction in this area is crucial for an understanding of the circuit dynamics and the complexity of mPFC-associated behaviour.

1.4 Adenosine and adenosine receptors

Adenosine is a ubiquitous nucleoside that plays important roles in many biochemical processes with different formats. As a product of the ATP metabolism, it is involved in the energy transformation. Adenosine itself also works as a key neuromodulator that regulates many physiological processes.

In the central nervous system (CNS), the main source of adenosine is from the catabolism of intracellular and extracellular ATP. As a byproduct of the cellular purine metabolism, adenosine originates from the dephosphorylation of AMP and is directly released from both neurons and glial cells (Latini and Pedata 2001). During prolonged wakefulness, hypoxia, ischemia or elevated

Introduction

Receptor	A ₁ receptors	A _{2A} receptors	A _{2B} receptors	A ₃ receptors
Adenosine affinity	~70 nM	~150 nM	~5100 nM	~6500 nM
G-Protein	G _i , G _o	G _s	G _s , G _q	G _i , G _q
Transduction mechanisms	Inhibits adenylyl cyclase Activates PLC Activates GIRKs Inhibits Ca ²⁺ channels	Activates adenylyl cyclase	Activate adenylyl cyclase Activates PLC	Inhibits adenylyl cyclase
Distribution & expression level	High expression in cortex, hippocampus, cerebellum, spinal cord, eye, adrenal gland, atria	High expression in olfactory bulb, spleen, thymus, leukocytes	High expression in Cecum, colon, bladder	High expression in testis (rat), mast cell (rat)
	Intermediate expression in other brain regions, skeletal muscles, liver, kidney, adipose tissue	Intermediate expression in heart, lung, blood vessels, peripheral nerves	Intermediate expression in lung, blood vessels, eye, mast cells	Intermediate expression in cerebellum, hippocampus
	Low expression in lungs, pancreas	Low expression in other brain regions	Low expression in adipose tissue, adrenal gland, brain, kidney	Low expression in thyroid, most of brain, adrenal gland, spleen, liver, kidney, heart

Table 1.1 Characters and distribution of adenosine receptors.

GIRKs, G-protein-dependent inwardly rectifying K⁺ channels; PLC, phospholipase C

Adapted from Dunwiddie and Masino 2001, Sachdeva and Gupta 2013

metabolic demand, a high intracellular adenosine concentration will result in a net efflux via nucleoside transporters and leads to an increase in the extracellular adenosine concentration (Dunwiddie and Masino 2001). During these processes, the adenosine concentrations can rise from nanomolar to micromolar levels indicating the crucial role of adenosine in both physiological and pathological CNS function (van Calker and Biber 2005; Fredholm 2007).

There are four known subtypes of adenosine receptors, the A₁, A_{2A}, A_{2B} and A₃ adenosine receptors (A₁AR, A_{2A}AR, A_{2B}AR, A₃AR). All adenosine receptor types are G-protein-coupled receptors with seven transmembrane domains, but display distinct tissue distribution, pharmacological characteristics and down-stream cellular signal transduction mechanisms (Dunwiddie and Masino 2001; Jacobson and Gao 2006). Among the four types of adenosine receptors, the A₁AR shows the highest adenosine affinity and is the most abundant receptor in the brain. It is densely expressed in the CNS including neocortex, hippocampus, cerebellum and spinal cord (Dunwiddie and Masino 2001; Bauer et al. 2003; Bauer et al. 2005; Meyer et al. 2006; Sachdeva and Gupta 2013). A₁AR is

also found in the eye, heart, adrenal gland, adipose tissue and inflammatory cells (Olah and Stiles 1995; Townsend-Nicholson et al. 1995; Poulsen and Quinn 1998; Sachdeva and Gupta 2013). It couples to G_i proteins which inhibit adenylyl cyclase (AC) activity leading to the decrease of cAMP level and increased activity of phospholipase C (PLC) that hydrolyses phosphatidylinositol 4,5-bisphosphate (PIP_2) to triphosphoinositol (IP_3) and diacylglycerol (DAG) (Gerwins and Fredholm 1992; Rogel et al. 2005; Tawfik et al. 2005). These second messenger molecules then activate the signalling cascade and make a long-term effect to cell growth, differentiation, survival and death (Jacobson and Gao 2006). Adenosine acting via A_1AR , also depresses the release of excitatory neurotransmitters by reducing presynaptic calcium influx (Wu and Saggau 1994; Arrigoni et al. 2001) and inhibits the intrinsic excitability of glutamatergic neurons by increasing postsynaptic inwardly rectifying potassium conductance (Rainnie et al. 1994; Luscher et al. 1997). Taking the wide distribution and high adenosine affinity of A_1AR s into account, adenosine is generally treated as an inhibitory neuromodulator that suppresses the neuronal activity in the CNS.

In contrast to A_1AR , stimulation of the $A_{2A}AR$ results in an increasing of AC activity through activation of the G_s proteins and in turn leads to an elevation of intracellular cAMP level (Jacobson and Gao 2006). $A_{2A}AR$ s are found only in a few brain regions at high expression levels including primarily the striatum, the olfactory tubercle and the nucleus accumbens; it is expressed only at very low levels elsewhere in the CNS (Fredholm et al. 2003; Boison et al. 2012; Sachdeva and Gupta 2013). $A_{2B}AR$ s are widely expressed all over the brain but have a very low adenosine affinity. Because of this, it is relatively difficult to associate $A_{2B}AR$ to a certain adenosine effect neither in cellular level nor at the behavioural level (Feoktistov and Biaggioni 1997).

A_3AR s are similar to $A_{2B}AR$ s with respect to receptor distribution and adenosine affinity, but are coupled to G_i proteins as A_1AR . Reports concerning the characterisation of A_3AR s are rare; it has been suggested that it may modulate the activity of other adenosine receptors such as A_1AR s (Dunwiddie et al. 1997; Macek et al. 1998).

The role of adenosine in sleep homeostasis has been widely documented. It has been shown that adenosine can promote and maintain sleep (Porkka-Heiskanen et al. 1997; Strecker et al. 2000; Basheer et al. 2004). Adenosine receptor antagonists such as caffeine can promote wakefulness and

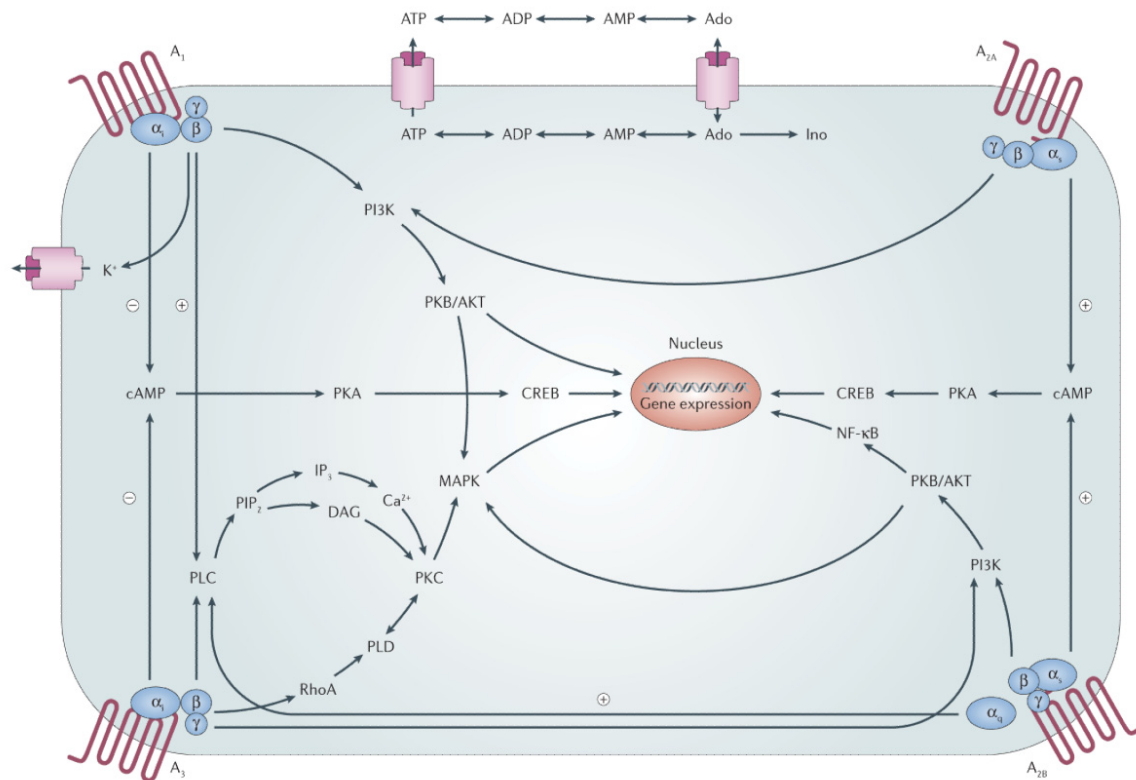


Fig. 1.6 Adenosine receptor signalling pathways. Activation of A_1 and A_3 adenosine receptors inhibits adenylyl cyclase activity via G_i proteins while activation of A_{2A} and A_{2B} adenosine receptors facilitated adenylyl cyclase activity through G_s proteins. These processes affect the intracellular cAMP level, and together with other secondary messenger molecules, influence long-term cellular activities by activate or deactivate different kinds of protein kinase. CREB, cAMP response element binding protein; DAG, diacylglycerol; IP₃, inositol 1,4,5- trisphosphate; PI3K, phosphatidylinositol 3-kinase; PIP₂, phosphatidylinositol-4,5- bisphosphate; PK, protein kinase; PLD, phospholipase D; NF- κ B, nuclear factor- κ B. (Adapted from Jacobson and Gao 2006)

influence normal sleep. A_1 AR and A_{2A} AR have been demonstrated to be responsible for these processes. Furthermore, agonists of the A_1 AR have been shown to induce sleep (Portas et al. 1997), whereas its antagonist reduce sleep demand (Lin et al. 1997). In the radioligand imaging studies higher A_1 AR binding was found after sleep deprivation throughout the entire brain (Basheer et al. 2007; Elmenhorst et al. 2007). Adenosine exerts a negative control on the cholinergic system, which is known as an arousal centre in the brain. High local energy consumption will result in an increase of extracellular adenosine. Via a combinatorial regulation of A_1 AR and A_{2A} AR, this increased adenosine level can reduce cholinergic release and facilitate the transition from wake to sleep (Rainnie et al. 1994; Portas et al. 1997; Van Dort et al. 2009). This results from the fact that adenosine modulates excitatory glutamatergic neurotransmission and plays a role in the interaction

between energy metabolism and neuronal excitability. The activation of glutamatergic NMDA receptors may cause the release of adenosine, the concentration of which is sufficiently high to induce an inhibition of glutamate release at the presynaptic axon terminals (Manzoni et al. 1994; Brambilla et al. 2005). This is in line with the finding that A₁ARs are richly expressed at synaptic sites instead of dendrites and cell bodies (Rebola et al. 2003). Via A₁AR-mediated reduction of the open probability of presynaptic Ca²⁺ channels, adenosine-induced suppression of presynaptic release therefore causes an overall shift to lower excitability in cortical microcircuits (Prince and Stevens 1992; Scanziani et al. 1992; Arrigoni et al. 2001; Qi et al. 2017; Radnikow and Feldmeyer 2018).

1.5 Aim of this study

The heterogeneity of pyramidal cells and interneurons in sensory and motor areas of the neocortex is well characterised in different cortical areas and layers (Yang et al. 1996; Markram et al. 2004; Ascoli et al. 2008; Helmstaedter et al. 2009; Rudy et al. 2011; DeFelipe et al. 2013; Marx and Feldmeyer 2013; van Aerde and Feldmeyer 2013; Tremblay et al. 2016; Emmenegger et al. 2018; Feldmeyer et al. 2018). However, the structural and functional properties of neurons in L6 of mPFC are less well known. One aim of this study is to quantitatively classify excitatory and inhibitory neurons based on their electrophysiological, morphological and molecular properties. This will help to better understand the functional roles of different neuronal types in the L6 microcircuitry and eventually provide an insight into the complex mPFC-associated functions.

To date only few reports about the excitatory and inhibitory synaptic connections in mPFC are available. It was the aim of this work to investigate the anatomical and functional characteristics of intralaminar excitatory and inhibitory connections in L6 of rat mPFC. With the quantitative classification of excitatory and inhibitory neurons, we wished to determine the types of connections based on the pre- and postsynaptic neuronal types, thereby providing a basic understanding of the local connectivity.

On the other hand, although the effects of adenosine on cortical neurons and networks through different brain regions have been well studied, especially in recent years (Lopes et al. 1999; Arrigoni et al. 2006; van Aerde et al. 2013; Yang et al. 2013; Bannon et al. 2014; Zhang et al. 2015;

Introduction

Qi et al. 2017), the impact of adenosine on the microcircuitry of L6 in mPFC has so far not been investigated. Here, we used pharmacological procedures including adenosine, agonist and antagonist of adenosine receptors to explore the adenosinergic modulation on single neuronal activity and moreover, on different types of L6 synaptic connections.

2. Materials and Methods

2.1 Slice Preparation

Coronal sections were prepared from Wistar rats (Charles River, either sex) aged 17-42 postnatal days (P17-P42) in accordance with the guidelines of the Federation of European Laboratory Animal Science Association and the German Animal Welfare Act. The rats were anaesthetised with isoflurane, decapitated and the brains were quickly transferred to ice-cold extracellular solution containing 4 mM $MgCl_2$ and 1mM $CaCl_2$ to reduce synaptic activity and bubbled with 95% O_2 and 5% CO_2 . Brains were cut with blade at the position shown in Fig. 2.1 and glued with the frontal part (the cut surface) on the cooled metal stage of a vibration microtome (MICROM HM 650V, Walldorf, Germany). The tissue was fully immersed in the ice-cold extracellular solution, depending on the size of the brain, 4-5 coronal slices with a thickness of 350 μ m were cut and then incubated in the same solution at room temperature to recover for at least 1 hour (21-24 °C).

2.2 Solution

Slices were transferred to the recording chamber of the patch clamp set-up; they were continuously perfused (~5 ml/min) with artificial cerebrospinal fluid (ACSF) containing (in mM): 125 NaCl, 2.5 KCl, 25 glucose, 2 $CaCl_2$, 1 $MgCl_2$, 1.25 NaH_2PO_4 and 25 $NaHCO_3$, bubbled with 95% O_2 and 5%

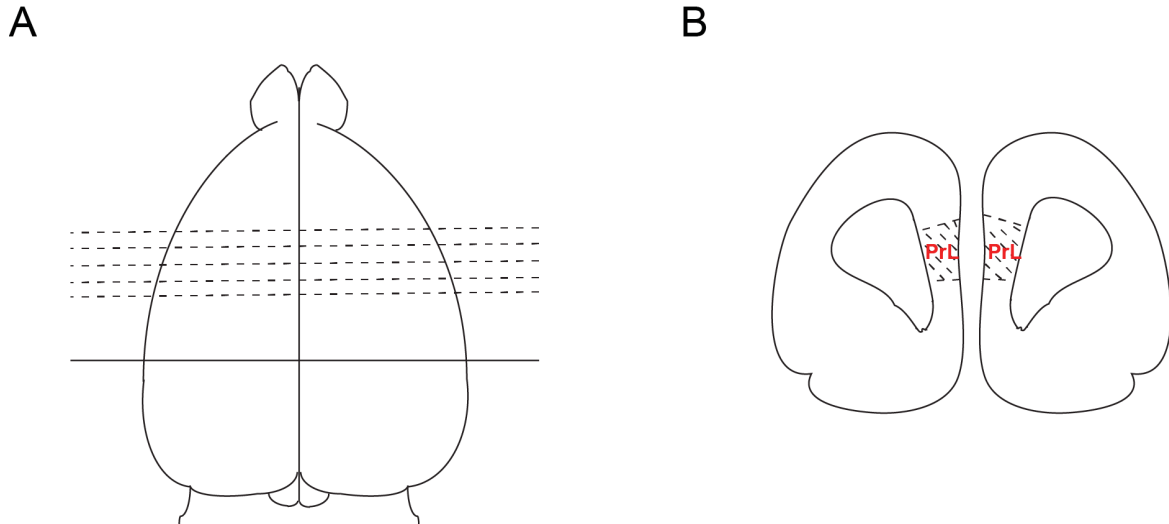


Fig. 2.1 Coronal slice preparations of rat prelimbic mPFC. (A) Dorsal view of rat brain, the whole brain was cut into two parts and glued on the metal stage at the position of solid line. Dash lines indicate the serial sections at a thickness of 350 μ m. (B) Rostral view of the coronal slices; the prelimbic mPFC lies in the area marked by dashed lines. Both the right and left hemisphere were used in the experiments.

CO₂, with a heater to keep the temperature between 30.5-31.5 °C. The intracellular solution, with which the recording pipette was filled, contained (in mM): 135 K-Gluconate, 4 KCl, 10 HEPES, 10 Phosphocreatine, 4 Mg-ATP and 0.3 GTP (PH 7.4, ~300mOsm). Biocytin (4.5-5 mg/ml, Sigma, Munich, Germany) was added to the intracellular solution to stain neurons during the electrophysiological recording. For searching pipettes used for paired recordings, a different solution was used containing 105 Na-gluconate, 30 NaCl, 10 HEPES, 10 Phosphocreatine, 4 Mg-ATP and 0.3 GTP.

2.3 Identification of cortical layers and neurons in mPFC

Slices were placed in the recording chamber under an upright microscope (fitted with 4×/ 0.13 numerical aperture (NA) and 40×, water immersion/ 0.80 NA objective, Olympus, Tokyo, Japan) with the pial surface pointing forward. The layer borders were visualised under bright-field illumination at low magnification. Because of the high density of neuron somata, L2 is easily

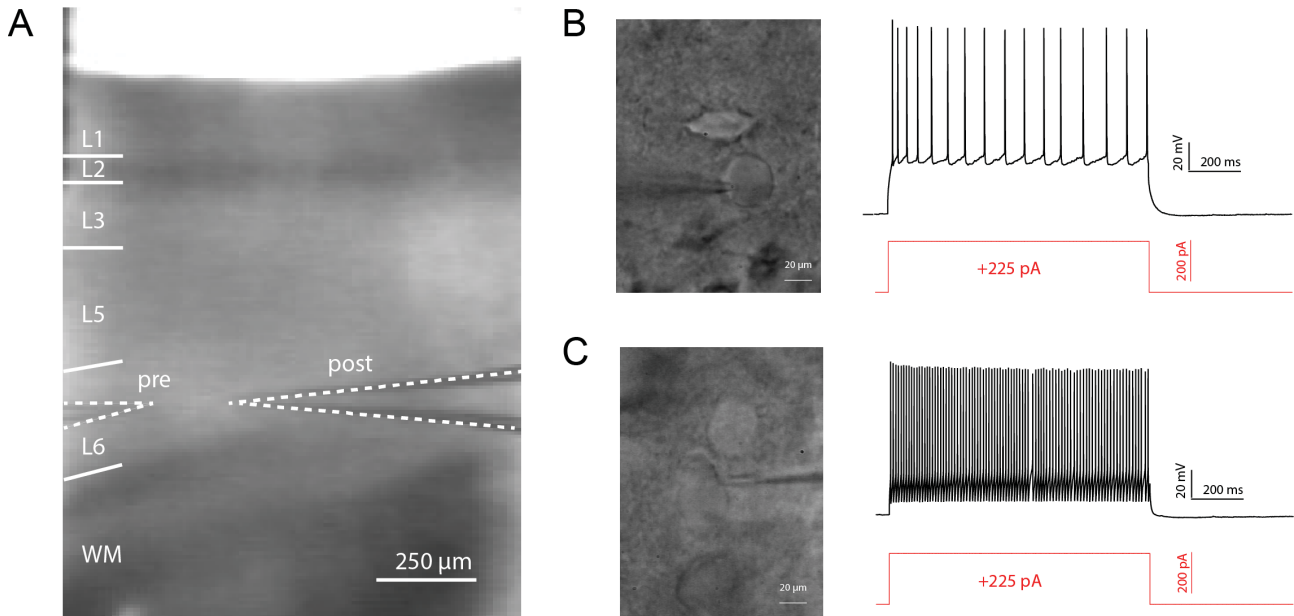


Fig. 2.2 Identification of cortical layers and neurons in mPFC. (A) Identification of cortical layers in mPFC during paired recording. Approximately, L1, L2 and L3 comprise one third of the prelimbic cortex, L5 and L6 equally separate the rest. The pipettes for patching Presynaptic and postsynaptic neuron were marked in dash line. (B) High magnification image of the presynaptic excitatory neuron (left) and its firing pattern with relatively low frequency (right). (C) High magnification image of the postsynaptic inhibitory neuron (left) and the firing pattern with high frequency (right).

identified as a dark thin band between L1 and L3. L3 has about the same width as L1 and they situated directly beneath and above L2 respectively. In the mPFC of rodents, there is no L4 so that L3 borders directly on L5. L5 is clearly discriminated from L3 and L6 by the large soma size of excitatory neurons with their thick, long apical dendrites under high magnification (40× objective). The total distance from pia to WM is about 1100-1400 μm depending on the age of the animal and the numbers of slice in preparation as the areas of mPFC increased from the first slice and normally show biggest proportion at the 4th or 5th slice. L1-3 share one third of the prelimbic cortex whereas L5 and L6 equally separate the rest (Fig. 2.2). In this study, all the neurons of L5 were recorded between 600-850 μm from pia and all the neurons of L6 were acquired at the range between 850-1200 μm from pia.

Excitatory neurons and interneurons were differentiated by their appearance under high magnification and their AP firing pattern. A post hoc identification was based on 3D reconstructions of their axonal and dendritic arbours. The thick apical dendrites of excitatory neurons were clearly visible before patching; these neurons showed a regular firing pattern with no or only little adaptation whereas interneurons display a high frequency firing pattern and lacked apical dendrites (Fig. 2.2). Fast spiking (FS) interneurons exhibit a higher firing frequency, a shorter action potential (AP) half-width, a larger after-hyperpolarisation potential (AHP) amplitude and rheobase current when compared with non-fast spiking (non-FS) interneurons.

2.4 Patch clamp technique

2.4.1 Single cell recordings

Whole-cell patch-clamp recordings from single excitatory neurons in layers 5 and L6 of the mPFC were made using patch pipettes of 4-8 M Ω resistance pulled from thick borosilicate glass capillaries (outer diameter, 2.0 mm; inner diameter, 1.0 mm). Recording pipettes were filled with intracellular solution and biocytin (4.5-5 mg/ml) to label the patched neurons. We used infrared differential interference contrast (IR-DIC) video microscopy to visualise individual neurons in mPFC. Voltage and current signals were recorded using a HEKA EPC10 amplifier (Lambrecht, Germany). Stimulation protocols were programmed with the “Patch Master” software (HEKA, Lambrecht, Germany). An Ag/AgCl bath electrode was used as reference electrode. All components of the set-up were grounded in order to reduce interference and electrical noise. High precision

micromanipulators (SM-5, Luigs & Neumann, Ratingen, Germany) were used to move the pipette in three dimensions with micrometer-speed to the neuron under investigation.

To prevent a blockage of the pipette tip during the movement through the slice, a weak positive pressure was applied to the pipette to blow away the tissue in the path to the neurons. The pipette was moved gently to the neuronal cell body and a dimple was visible on the soma membrane due to this positive pressure. Releasing the positive pressure and applying suction resulted in the formation of a tight seal – a so called ‘gigaseal’ - between the recording pipette and the soma membrane. Resistance values of 1 G Ω or more were obtained and guaranteed a good signal-to-noise ratio. Additional suction broke the soma membrane attached to the pipette and formed a direct channel between the neuronal cytoplasm and the patch pipette.

The resting membrane potential (V_m) was measured directly after forming the whole-cell configuration. The series resistance (R_s) was compensated by 80%. If the series resistance was >50 M Ω at the beginning of or changed by more than 25% during an experiment, the recordings were excluded from the analysis. Current steps of 1 s duration were applied in current clamp mode, starting at -100 pA with 10 pA step size or at -20 pA in the beginning with 25 pA step size to elicit action potentials. The first super-threshold AP was identified by the 10 pA step size protocol, which ensures that the initiated AP is close to the native threshold. Single AP characteristics were analysed later (see next section) using this first super-threshold AP to avoid the short-term changes caused by sustained stimulation. The 25 pA step size protocol was used to analyse the active properties of action potential trains (see next section) by using the first train with a minimum 10 spikes. Continuous recordings of membrane potential change were made in current clamp mode without current injection. Miniature spontaneous activity was recorded in voltage clamp mode at a holding potential of -70 mV; tetrodotoxin (TTX, 0.5 μ M) and gabazine (10 μ M) were applied to prevent the generation of APs in the recorded neurons and to block GABA-mediated inhibitory postsynaptic currents (IPSCs). All experiments were performed at 31 ± 0.5 °C to maintain adequate levels of oxygenation.

2.4.2 Pair recordings

To obtain synaptically coupled neurons, two different methods were used. Direct dual patch clamp recording, or random double patch clamp recording, was normally performed when the connectivity ratio between two synaptically coupled neurons was high. After successfully establishing the whole-cell configuration in a potential postsynaptic neuron, another, putative presynaptic neuron was patched to check whether they are synaptically coupled.

If the connectivity ratio between two neurons was low, random dual patch clamp recording become ineffective. A modified paired-recordings technique with searching procedure (Qi et al. 2015; Feldmeyer and Radnikow 2016) was used to find the presynaptic neuron of a synaptically coupled neuron pair in L6 of mPFC. A searching pipette of 8-11 M Ω , filling with an internal solution in which Na⁺ replaced K⁺ in order to prevent a depolarisation of searched neurons was used. These relatively high resistance pipettes with a high Na⁺-internal solution ensure that the searched neurons remains healthy by preventing accidental break-through into the neuron and AP firing of neurons.

A postsynaptic neuron was patched first in whole-cell current-clamp mode. Subsequently, surrounding neurons were tested for synaptic connection using the searching pipette. After a 'loose' cell- attached patch with a seal resistance of 30-300 M Ω was established, large current pulses (0.2-2 nA) were applied to elicit an action potential in the potential presynaptic cell, which can be seen as a small spikelet on the voltage response. If the two neurons were synaptically coupled the postsynaptic neuron would respond with an excitatory postsynaptic potential (EPSP) or an inhibitory postsynaptic potential (IPSP) to the stimulation of the potential presynaptic neuron. Searching pipettes could be used more than 20 times for further cell-attached recordings until a connection was found or the tip of pipette was contaminated (and thus failed to form the seal with a resistance >30 M Ω in searching mode). Once a response was found in postsynaptic neuron, the searching pipette was slowly removed and replaced by a patch pipette with biocytin-containing, regular internal solution. The presynaptic neuron was then recorded in whole-cell mode. APs were elicited in the presynaptic neurons using short (5 ms) depolarising current and postsynaptic EPSPs or IPSPs were recorded in current clamp mode. The postsynaptic neurons were held at resting membrane potential during recordings of EPSPs. As the reversal potential of IPSPs was calculated to be -85 mV (Koelbl et al. 2015) in this study when considering the internal and external solution, the postsynaptic neurons were held at -55 mV during recordings of IPSPs by injecting a constant

positive current to increase the driving force of Cl^- thereby facilitating the detection of inhibitory connections.

2.5 Drug Application

All drugs used in this study were from Sigma-Aldrich (Steinheim, Germany) or Tocris (Bristol, UK). Adenosine (30 μM and 100 μM in single recording mode, 10 μM and 30 μM in paired recording mode, prepared in the perfusion solution), N^6 -cyclopentyladenosine (CPA, 1 μM , an agonist of adenosine A_1 receptor), 8-cyclopentyl-1,3-dimethylxanthine (CPT, 1 μM , an antagonist of adenosine A_1 receptor), CGS21680 (30 nM, an agonist of adenosine A_{2a} receptor), TTX (0.5 μM , a sodium channel blocker) and gabazine (10 μM , an antagonist of GABA_A receptor) were bath applied. In the miniature spontaneous activity experiments, a perfusion solution with TTX and gabazine was used as a control for all experimental phases. 30-50 sweeps were obtained as a baseline followed by a 'drug phase' consisting of another 30-50 sweeps; a 'wash out phase' or 'antagonist' phase with 30-60 sweeps was recorded after the 'drug phase'. Six concentrations (1, 3, 10, 30, 100, 300 μM) of adenosine were applied sequentially to the same neuron to acquire a dose-response curve of adenosine. Higher concentrations were only used after complete wash-out of the previous concentrations.

2.6 Analysis of electrophysiological data

2.6.1 Passive membrane properties of single neuron

After establishing the whole-cell configuration, V_m and R_s were measured immediately. Neurons were selected for analysis when V_m was between -55 to -75 mV and R_s less than 50 $\text{M}\Omega$ at the beginning of recording and did not change by more than 25% during the experiment to ensure a high quality of the recording. The input resistance (R_{in}) of the membrane was measured as the slope of the linearly fitting I-V-curves with the current injection between -50 to 50 pA (0 pA was excluded). The time constant (τ , Tau) was calculated as the mean value of individuals obtained by fitting the I-V-curves with an exponential function at the same range of current injection. At hyperpolarising voltage steps, a voltage sag was observed due to the activation of a hyperpolarisation-activated, cyclic-nucleotide gated (HCN) channel. It was measured as the difference between the most hyperpolarised voltage and the steady voltage deflection, divided by the steady voltage deflection.

The continuous membrane potential was recorded in current clamp mode without current injection, at least 30 sweeps for each group were collected. For comparison the ‘control phase’ and the ‘drug phase’, two windows of membrane potential were chosen before and after the drug effect and the difference was calculated as the drug-induced voltage deflection (Fig. 2.4 A).

2.6.2 Active properties of single neuron

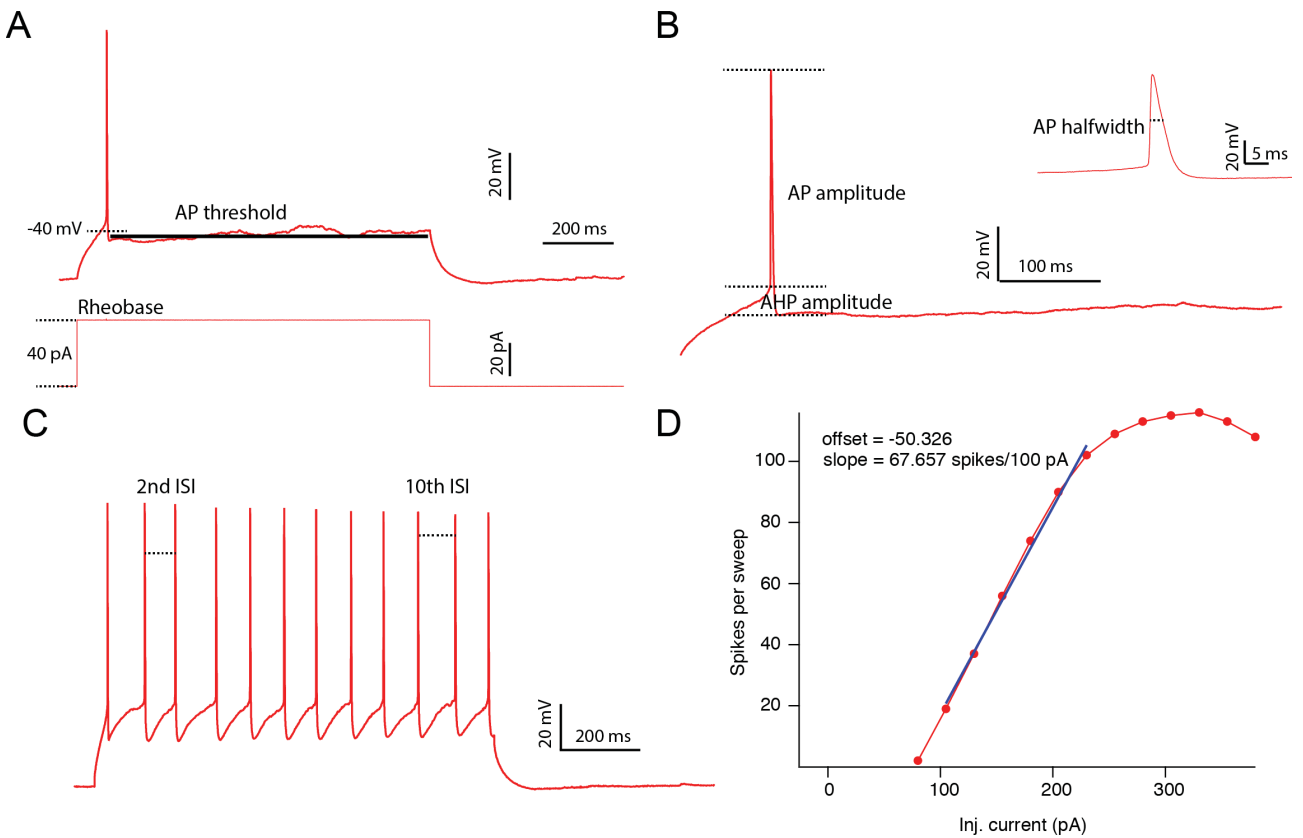


Fig. 2.3 Analysis of active properties of single neuron. (A) The AP threshold and rheobase were measured as the minimum voltage and current that observed at the first-elicited AP. (B) AP amplitude was the difference between the AP peak voltage and the threshold. AHP amplitude was determined as the difference between threshold and the minimum voltage during hyperpolarisation. AP half-width was calculated as the AP width (time) at half-maximal amplitude. (C) The inter-spike-interval (ISI) was calculated as the average time between two individual spikes during the first train with a minimum of 10 spikes, the adaptation ratio was measured as the ratio of the tenth ISI and the second ISI. (D) The average firing frequency per 100 pA was acquired as the slope of linearly fitting curve by plotting number of spikes against injected current.

The active properties of a neuron (i.e. its excitability) were determined by the characteristics of action potentials (AP), which were evoked by inception of current pulse of variable amplitude (see 2.4.1). The AP threshold, AP time, AP amplitude, AP half-width and after-hyperpolarisation (AHP) amplitude were measured at the first elicited AP with the smaller increase in step size of 10pA to avoid the influence from sustained stimulation and make it close to the native threshold. Rheobase current (pA) was determined as the minimal current that elicited an AP. AP threshold (mV) and AP time (ms) were measured as the minimum voltage and time respectively, which were required for the initiation of first spike. AP amplitude (mV) was the difference between the AP peak voltage and the threshold. AP half-width (ms) was calculated as the AP width at half-maximal amplitude (time between rising phase and decaying phase) and the AHP amplitude (mV) was determined as the difference between threshold and the minimum voltage during hyperpolarisation (Fig. 2.3). AP firing properties were characterised using a larger current step size of 25 pA. The average firing frequency per 100 pA was determined as the slope of a linear fit, which shows the spikes per sweep response to the injected current. The maximum firing frequency was measured from the sweep of APs that has a maximal firing frequency and constant AP amplitudes. The inter-spike-interval (ISI) was calculated as the average time between two individual spikes during the first train with a minimum of 10 spikes. In some of the firing patterns, the second spike comes immediately after the first spike and shows a ‘burst firing’ which make the first and second ISIs much smaller than others, thus the adaptation ratio was measured as the ratio of the ninth ISI and the third ISI (ninth ISI/ third ISI) (Fig. 2.3).

2.6.3 Miniature spontaneous synaptic activity

Miniature spontaneous EPSCs were recorded in voltage clamp by holding the voltage to -70 mV in the condition with TTX and gabazine. Data were analysed using SpAcAn (Spontaneous Activity Analysis, designed by Guillaume Dugué and Charly Rousseau) analysis software programmed in Igor Pro. Stable recordings of 90 seconds for each group (control, drug or wash-out) were used for analysis, and a defined threshold for the mEPSC amplitude was set to detect the potential events. All the events detected by the software were inspected visually and verified; only events with typical mEPSC shape were selected as the real events. The mEPSC frequency was calculated as total number of synaptic events per second. The inter-event interval (IEI) was obtained by the time difference between two consecutive event foot time (EFT), which describes the time of the peak of

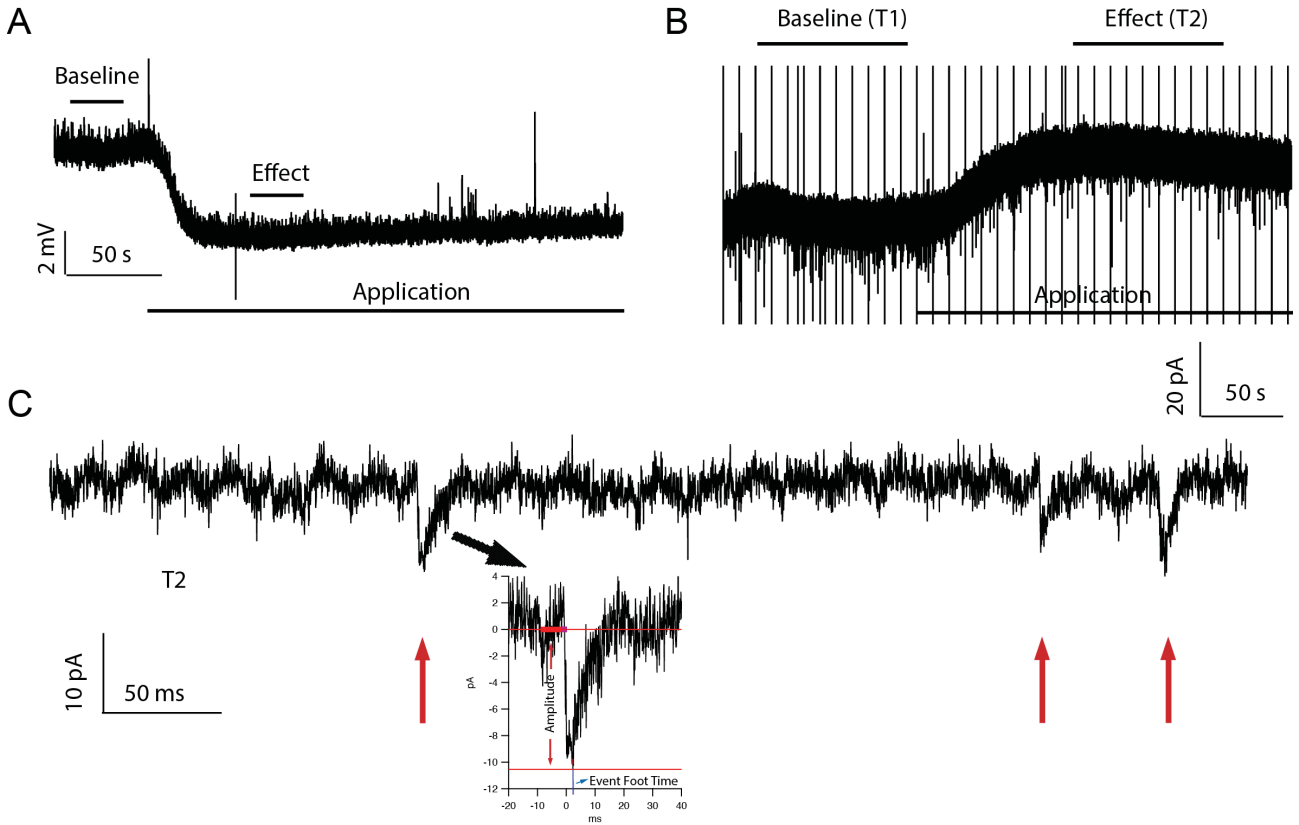


Fig. 2.4 Analysis of spontaneous membrane potential change and synaptic activity. (A) Full sweeps of continuous recordings in current clamp mode, membrane potential change was calculated as the difference of the mean potential of two selected windows before and during drug application (baseline and effect). (B) Full sweeps of continuous recordings in voltage clamp mode (holding potential of -70mV), 90 seconds for two time window (T1 and T2) before and during drug application were chosen for detecting of mEPSC. (C) 0.5 second of T2 window in (B). Automatically detected events will be confirmed again and only the events with correct shape were selected as the real events (red arrow). High resolution image of first mEPSC indicated the value of amplitude and the event foot time.

mEPSC. The average amplitude for one neuron was calculated as the mean value of all events (Fig. 2.4).

2.6.4 Properties of synaptic physiology in paired recordings

Following previous studies (Feldmeyer et al. 1999), the synaptic properties of excitatory and inhibitory connections were analysed using custom-written algorithms (Igor Pro, WaveMetrics, Lake Oswego, OR). After excluding sweeps with high spontaneous activity, all sweeps were aligned to the peak of the AP and then the EPSPs were averaged (Feldmeyer et al. 1999). The PSP amplitude was calculated as the difference between the mean baseline amplitude and the maximum

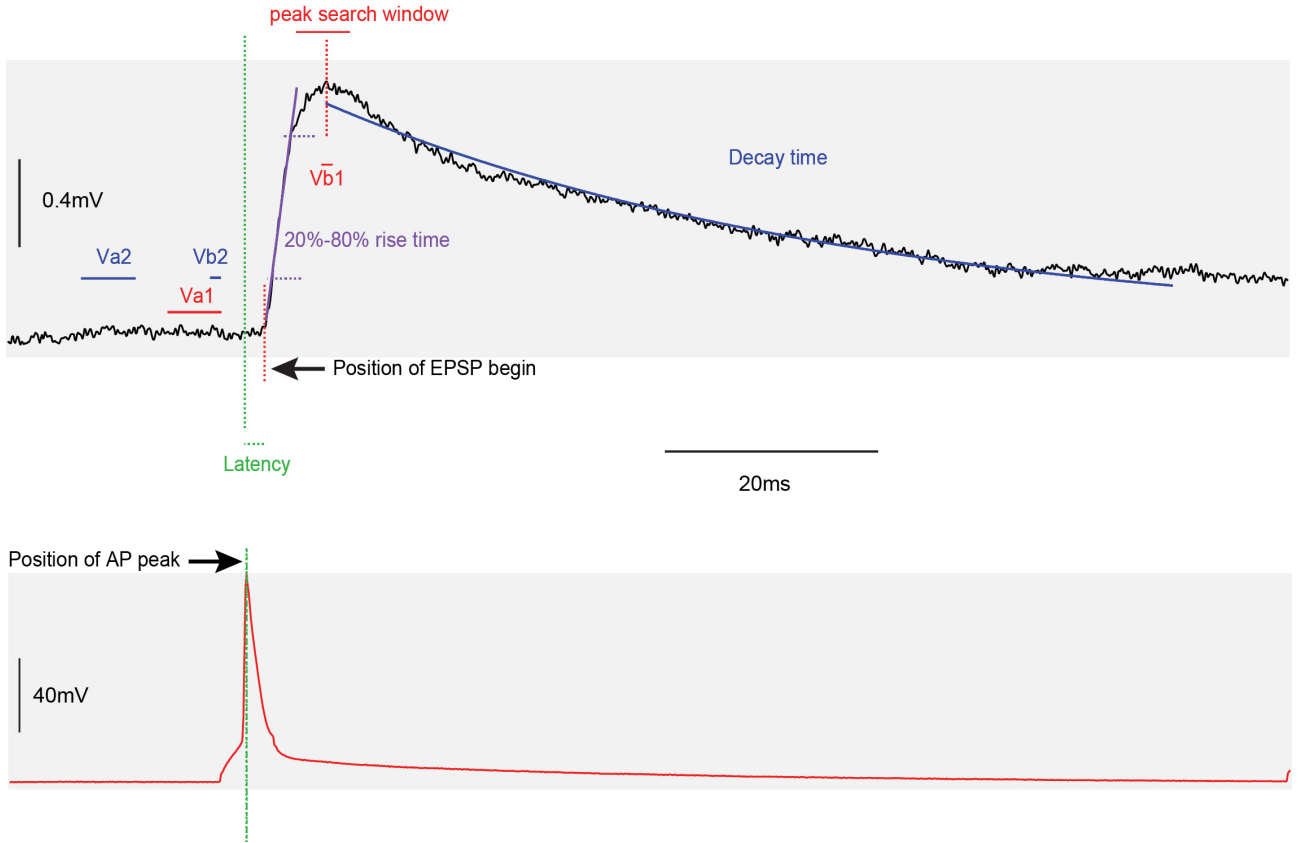


Fig. 2.5 Analysis of synaptic properties. A single sweep of the first PSP from a paired post neuron was shown in top, the presynaptic action potential was shown in bottom. The AP-EPSP latency was calculated as the time difference between the position of presynaptic AP peak (green dash line) and the position of the postsynaptic PSP initiation. The EPSP amplitude was calculated as the difference between mean baseline amplitude ($Va1$) and maximum voltage of the postsynaptic EPSP ($Vb1$). The baseline noise was measured as the voltage difference between $Va2$ and $Vb2$. Rise time was evaluated as the time from 20% to 80% of the peak EPSP amplitude (marked in purple). Decay time was obtained from a single exponential fit to the decay phase of the EPSP (shown in blue).

voltage of the postsynaptic PSP. The mean baseline amplitude was determined with a baseline region of 5 ms just preceding the PSP. A ‘peak search window’ of 5 ms was selected to determine the maximum amplitude and averaged over 1 ms. The baseline noise was evaluated with the similar manner as PSP amplitude, where a second baseline amplitude and a second maximum voltage were measured before the PSP initiation. Decay time constants were obtained from single exponential fits to the decay phase of individual and averaged response. The rise time was calculated as the average time between 20% to 80% of the peak amplitude from linear fit. The latency of PSP was defined as the time interval between the peak of presynaptic AP and the onset of the PSP (Fig. 2.4). The paired pulse ratio (PPR) was calculated as the ratio of the second PSP amplitude divided by the first PSP

amplitude elicited by a train of two-three APs at a stimulation frequency of 10 Hz. The coefficient variation (CV) was determined as the standard deviation divided by the mean of PSP amplitude. An individual response amplitude, which was smaller than 1.5x the standard deviation of the baseline noise, was defined as a failure. The failure rate was calculated as the numbers of failures divided by the number of the recorded sweeps.

2.7 Morphological reconstructions and analysis

2.7.1 Histological procedures

After recordings, slices containing biocytin-filled neurons were immediately fixed in 4% paraformaldehyde (PFA) in 100 mM phosphate buffer (PB, pH 7.4) at 4 °C for at least 24 hours. To quench any endogenous peroxidase activity, the slices were incubated in 2 ml H₂O₂ for 20 min after fixation. After rinsing the slices several times in 100 mM PB solution, they were then incubated in 1% avidin-biotinylated horseradish peroxidase (Vector ABC staining kit, Vector Lab. Inc.) containing 0.1% Triton X-100 at room temperature for 1 hour. To visualise the axonal and dendritic branches of biocytin-filled neurons 3,3-diaminobenzidine (Sigma-Aldrich, USA) was added as a chromogen. This resulted in the formation of a black-brown precipitate in the cells. Slices were then slowly dehydrated using ethanol and xylene after several times of rinsing with 100 mM PB and finally mounted on gelatinised slides and embedded using Eukitt medium (Otto Kindler GmbH) (Marx et al. 2012).

2.7.2 Morphological 3D reconstructions

Biocytin-labelled excitatory and inhibitory neurons in L5 and L6 of mPFC were morphological reconstructed using Neurolucida software (MicroBrightField, USA) and Olympus BX61 microscopy at 1000 X magnification (100x objective and 10x eyepiece). Slices were considered for reconstruction only when the neuron was clearly labelled and background staining was low. Layer borders, WM and pial surface were marked; the final 3D reconstruction were then rotated so that the pial surface is aligned at the horizontal plane. Tissue shrinkage was corrected in all spatial dimensions (factor 1.1 in the x and y axes, factor 2.1 in the z axes) (Marx et al. 2012) and the morphological properties were analysed using Neuroexplorer software (MicroBrightField, Colchester, USA).

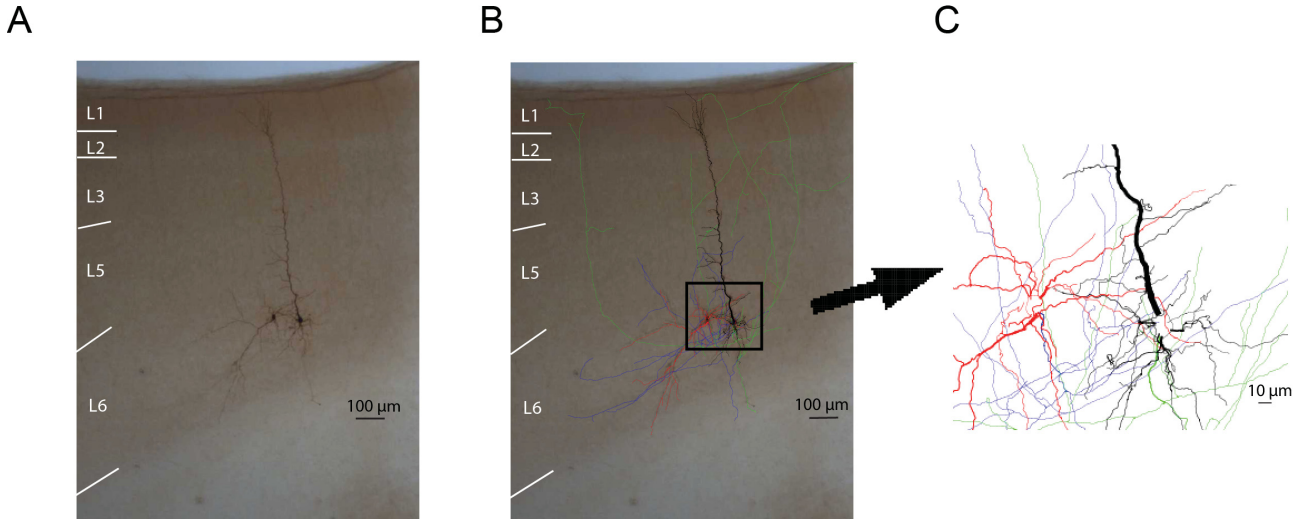


Fig. 2.6 Reconstruction of an excitatory-excitatory pair in L6 of prefrontal cortex. (A) Photomicrograph of a biocytin-labelled pair between an ‘inverted’ pyramidal neuron and a ‘slender tufted’ upright pyramidal cell. (B) Reconstruction of this pair, the presynaptic soma & dendrites and axons were shown in red and blue respectively, the postsynaptic soma & dendrites and axons were shown in black and green respectively. (C) Enlarged portion of the reconstruction shown in the boxed area in (B), the thickness of the structures was marked during reconstruction.

2.7.3 Axonal density map

3D maps of axonal density were made using computerised 3D reconstructions. The soma centre of each neuron in a single cluster was aligned and given the coordinates of X, Y, Z = (0, 0, 0). By using the segment point analysis in the Neurolucida Explorer, The relative coordinate of the beginning and endpoint of each segment in the axonal trace were acquired. The 3D density map for a cluster was constructed for each reconstructed neurons in this cluster and then averaged in Matlab using custom-written software (courtesy of Dr. G. Qi and Dr. H. Wang). The averaged density maps were smoothed using the 3D smoothing function in Matlab with a Gaussian kernel (s.d = 50 μm) and isosurfaces were calculated at the 80 percentile.

2.8 Cluster analysis

Morphological and electrophysiological parameters were normalised. The normalised dataset having mean 0 and standard deviation 1 retained the parameters of the original dataset. Principal component analysis (PCA) was used to analyse the interrelation between variables and to eliminate correlated variables. This approach avoided double weighing of parameters and hence a

misinterpretation of cluster analysis (CA). PCA creates linear combinations of the original variables and generates new axes, which are known as principal components (PCs). The variances explained by each PC are represented as eigenvalues and all components that with a eigenvalue less than one are excluded by using Kaiser's rule. Unsupervised CA was then performed using Euclidean distances and Ward's method to calculate the linkage distance and to combine clusters in each stage (Ward 1963). The final number of clusters was determined using Thorndike procedure, where the linkage step with the maximal linkage distance was taken for cutoff.

2.9 Statistical analysis

All data are represented as mean \pm standard deviation. Paired Student's t-test or Wilcoxon signed-rank test ($n < 10$) was used for statistical comparisons between two groups. Tukey's test was used when the sample size is different between two groups. Correlation analysis was performed by calculating Pearson correlation coefficients.

3. Results

3.1 Neuronal classification in L6 of mPFC

Previous studies in other neocortical areas revealed a large degree of morphological diversity of both excitatory and inhibitory neuron in L6 (Zhang and Deschenes 1997; Thomson 2010; Marx et al. 2012; Pichon et al. 2012; Arzt et al. 2017; Cotel et al. 2017). However, so far only few studies are available on L6 of prefrontal cortex (Yang et al. 1996; van Aerde and Feldmeyer 2013). A systematic and objective classification of excitatory and inhibitory neurons in L6 of prefrontal cortex therefore become significantly important.

Whole-cell patch clamp recordings with simultaneous biocytin fillings were made from neurons in L6 of rat mPFC. After histochemical processing, slices with high background staining or neurons with incomplete filling were not reconstructed. After morphological reconstructions, neurons were carefully inspected for the presence of dendritic (excitatory neurons) or axonal (inhibitory neurons) truncations. For excitatory neurons that with truncations at the main branch of the dendrites were excluded from the final analysis. And inhibitory neurons that exhibited more than 15% truncations of the terminal axonal branches or less than 40% of the average axonal length were not taken into the final analysis. These criterion result in 79 excitatory neurons and 38 inhibitory neurons with high quality 3D reconstructions.

3.1.1 Morphological classification of excitatory neurons

In a coronal slice, L6 excitatory neurons of mPFC normally show a high ratio of axonal truncation due to their wide range projections. The apical dendritic pattern of these neurons showed a high degree of heterogeneity which is likely to have implications for their local synaptic connectivity. Therefore, the classification of excitatory neurons was based mainly on their apical dendritic properties with reference to cortical layers and relation with basal dendrites.

Eight morphological parameters including the principal dendritic length in L1, L2, L3, L5, L6 and the WM, the length of longest basal dendrite and the ratio between the longest basal dendrite and principal dendrite were measured for the cluster analysis (CA). Bipolar neurons have two major dendrites that predominantly longer and thicker than the other dendrites and they point towards pia surface and WM respectively. In our study, the thickest dendrite was selected as the principal

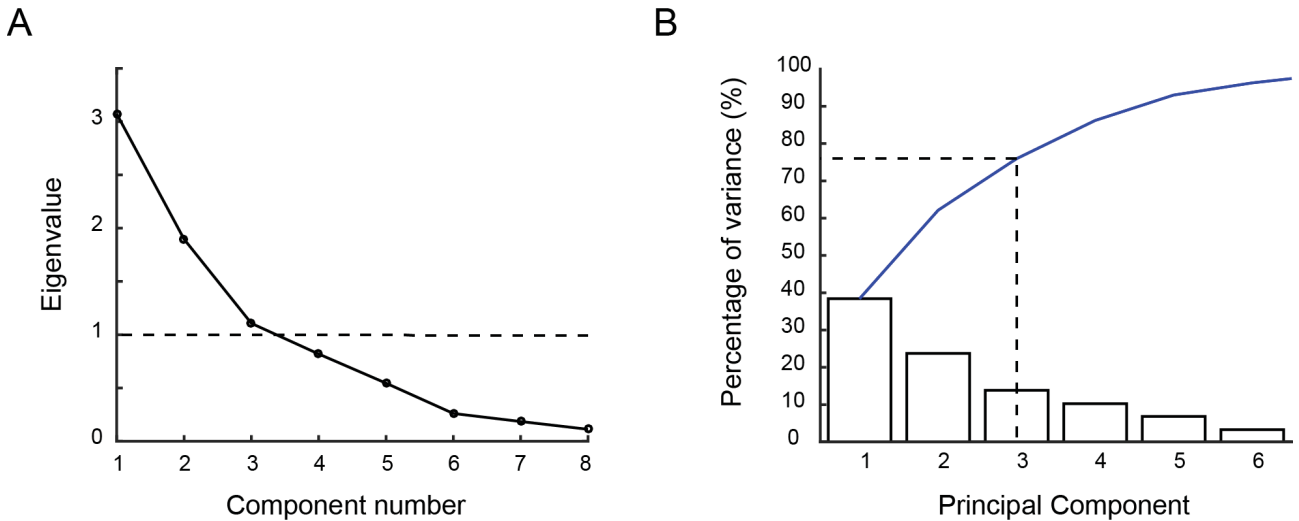


Fig. 3.1.1 Morphological analysis of L6 excitatory neurons using principal component analysis. (A) The first three principal components with eigenvalues greater than one were retained for cluster analysis. (B) The Pareto plot shows the individual (bars) and cumulative (blue curve) variance explained by the PCA components. The first three PCs explain around 76% of the total variance.

dendrite where the second thick dendrite was selected as the longest basal dendrite. The dendrites of multipolar neurons have the similarities in length and thickness. For the sake of analysis, the dendrite projecting to the pia surface was selected as the ‘principal dendrite’.

Principal Component Analysis (PCA) was used to analyse the interdependence between variables to avoid double weighting of the correlated variables in the cluster analysis (CA). The first three principal components (PCs) with eigenvalues larger than one were retained for CA; they explained around 76% of the total variance (Fig. 3.1.1). CA based on morphological parameters grouped 79 L6 excitatory neurons in 2 main clusters: 48 ‘upright’ neurons (61%) with principal dendrites projecting to the pia that spanned superficial layers and terminated in L5 to L1; 31 inverted/horizontally oriented neurons (39%), which had a prominent main dendrite pointing towards the WM or oriented sideways. The two main clusters can be further classified into six sub-clusters (cluster 1) and two sub-clusters (cluster 2) (Fig. 3.1.2 A). The optimal number of clusters was decided using the Thorndike method, where the cut-off point show the largest linkage distance (Fig. 3.1.2 B).

Cluster 1: Upright neurons with a principal dendrite projecting to the pia

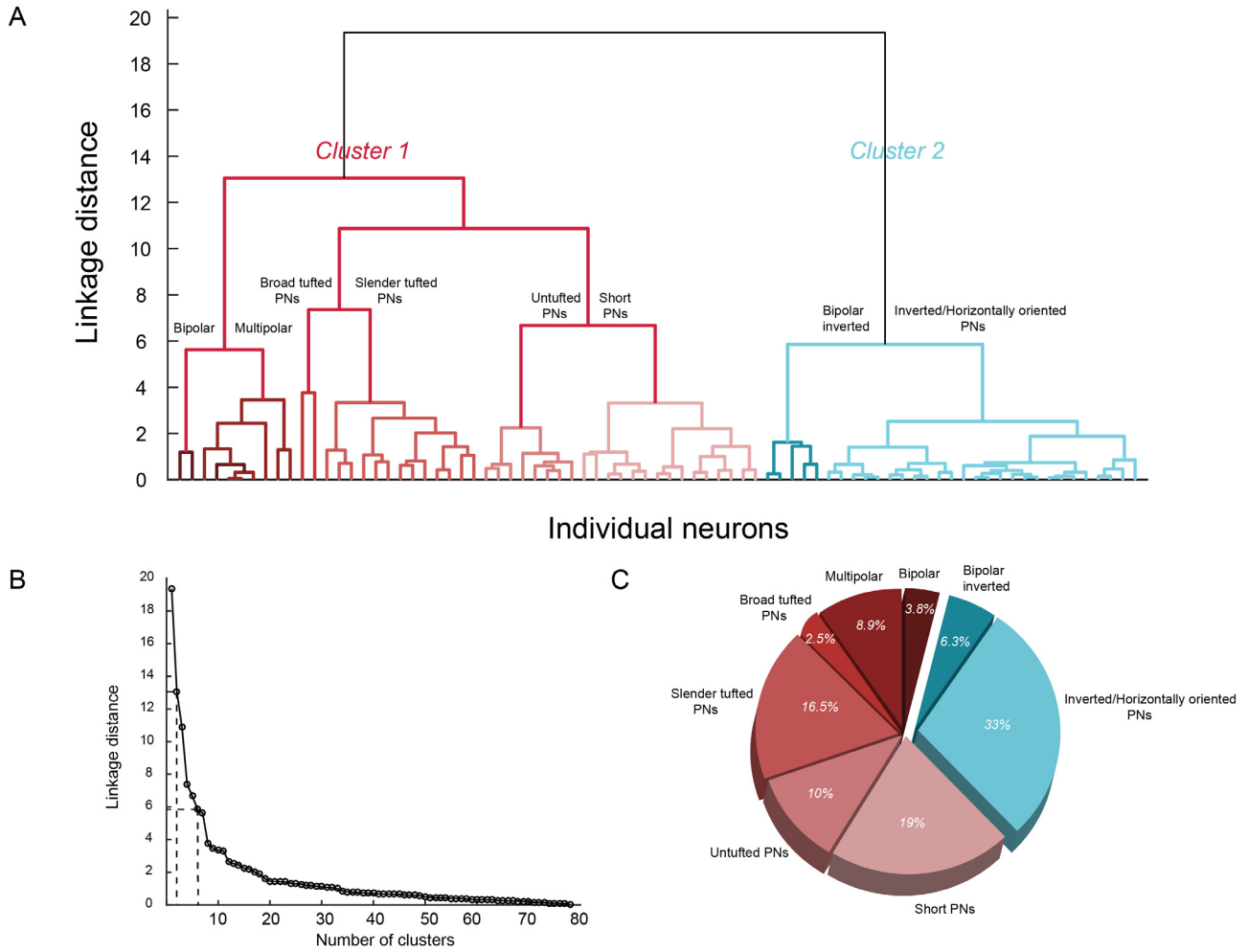


Fig. 3.1.2 Morphological analysis of L6 excitatory neurons using cluster analysis. (A) Dendrogram from cluster analysis of morphological parameters reveals 2 main clusters and 8 distinct sub-clusters ($n=79$). The X-axis shows individual neurons, and the Y-axis corresponds to the linkage distance measured by Euclidean distance. Cluster 1 and cluster 2 are shown in gradient of red and blue. (B) The cut-off for significant clusters was determined using the Thorndike method. Two dashed line indicate the cut-off position of 2 main clusters and 8 sub-clusters. (C) The percentage of each subcluster is shown in the pie chart, sub-clusters are marked by the same colour as shown in (A).

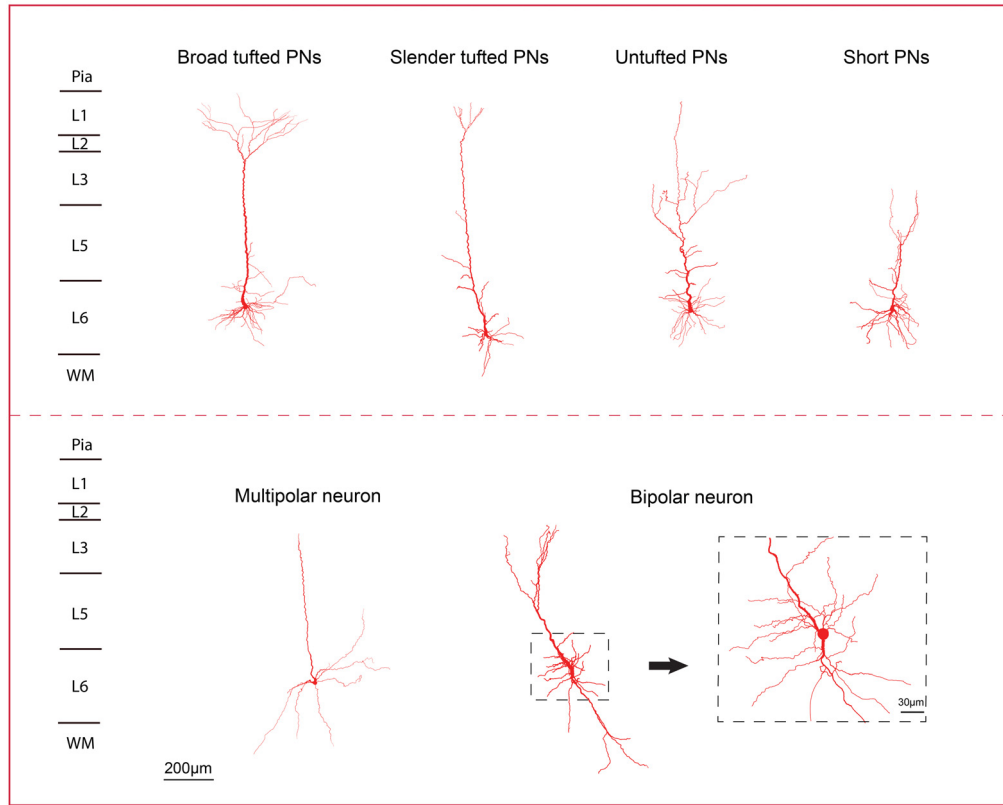
In the 48 upright neurons, there were 2 broad tufted PNs, 13 slender tufted PNs, 8 untufted PNs, 15 short PNs, 3 bipolar neurons and 7 multipolar neurons.

Broad tufted PNs, slender tufted PNs, untufted PNs and short PNs were named basing on their apical dendritic distribution in different cortical layers. Broad and slender tufted PNs had a tall apical dendrite that terminated close the pial surface and neurons in only these 2 sub-clusters have a

Results

A

Cluster 1



B

Cluster 2

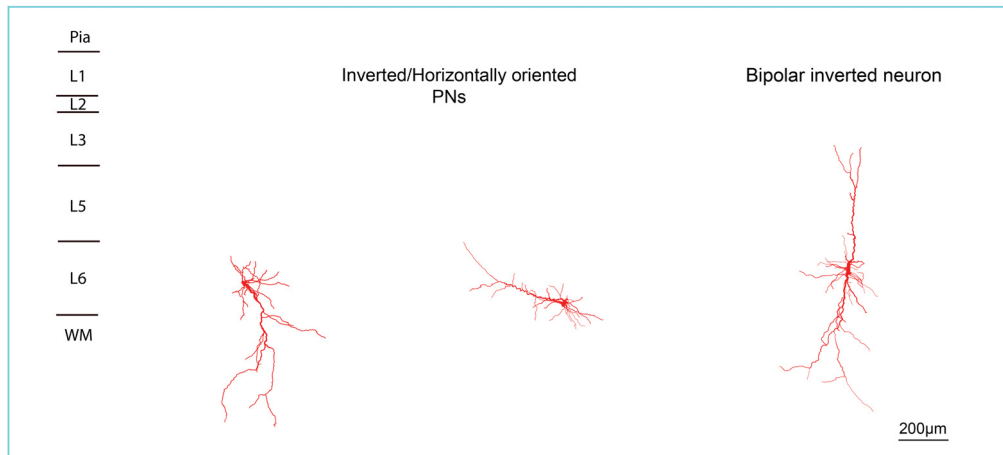


Fig. 3.1.3 Morphological examples of 8 sub-clusters under 2 main clusters in L6. Morphological reconstruction of L6 excitatory neurons are classified into 2 main clusters and 8 sub-clusters basing on the distribution of principal dendrite in different layers and the properties of the longest basal dendrite. (A) 6 sub-clusters were found in cluster 1, which called ‘upright excitatory neurons’. The principal dendrites in these neurons point toward the pia surface. Enlarged portion of the bipolar neuron indicates the differences between 2 ‘major dendrites’. (B) 2 sub-cluster were found in cluster 2, which called ‘inverted excitatory neurons’. The principal dendrites are pointing toward the WM (inverted neurons,) or horizontally (oriented neurons).

Results

substantial fraction of their dendrite in L1. The tips of apical dendrites were widely tufted in the broad tufted PNs and were sparsely tufted in the slender tufted PNs. To be more specific, the apical dendrites of broad tufted PNs distributed $60.1\pm20.9\%$ in L1, $5.4\pm5.0\%$ in L2, $3.8\pm2.1\%$ in L3, $11.7\pm8.1\%$ in L5, $26.0\pm24.4\%$ in L6 and $0.5\pm0.8\%$ in WM; while the apical dendrites of slender tufted PNs distributed $28.1\pm12.5\%$ in L1, $5.9\pm3.3\%$ in L2, $10.1\pm4.5\%$ in L3, $26.2\pm7.8\%$ in L5, $29.5\pm11.0\%$ in L6 and $0.1\pm0.3\%$ in WM (Fig. 3.1.3, Fig. 3.1.4).

Seven out of 8 untufted PNs had apical dendrites terminating in L1 but only small fraction of the total apical dendritic length resided in that layer. In one of these PNs the apical dendrite terminated already in L2. Apical dendrites of the PNs in this sub-cluster frequently form apical oblique dendrites in L3 and L5. These apical oblique dendrites comprised more than 70% of the total length ($23.7\pm8.0\%$ in L3, $47.1\pm9.9\%$ in L5) (Fig. 3.1.3, Fig. 3.1.4).

Apical dendrites of short PNs terminated in L5 or L6 and most of the dendritic branches were restricted in L5 ($49.9\pm14.8\%$) and L6 ($41.0\pm16.8\%$). There were also a fraction of apical dendrites in L3 ($8.1\pm6.9\%$) (Fig. 3.1.3, Fig. 3.1.4).

Apart from pyramidal cells, there were also normal bipolar neurons and multipolar L6 neurons in cluster 1. In a normal bipolar neuron, the principal dendrite terminated in L3 and there was a long secondary dendrite, which was similar in the total length and number of branches compared to the principal dendrite. In multipolar neurons, the difference on the thickness of ‘principal dendrite’ and basal dendrites was small and the number of dendritic branches was low. The dendritic length of the principal dendrites in multipolar neurons varied widely, while most of them were ending in L1-L3 (Fig. 3.1.3). In these two sub-clusters neurons the longest basal dendrite and the principal dendrite were almost similar in length as the ration of the longest basal dendrite/principal dendrites shows (0.85 ± 0.11 in bipolar neurons and 0.97 ± 0.36 in multipolar neurons; s. Table 3.3.1). This was in marked contrast to neuronal cell types of all other subclusters.

Cluster 2: Inverted/Horizontally oriented neurons

Of the 31 inverted/horizontally oriented neurons, there were 26 inverted/horizontally oriented PNs and 5 bipolar inverted neurons. In the sub-cluster of inverted/horizontally oriented PNs, most

Results

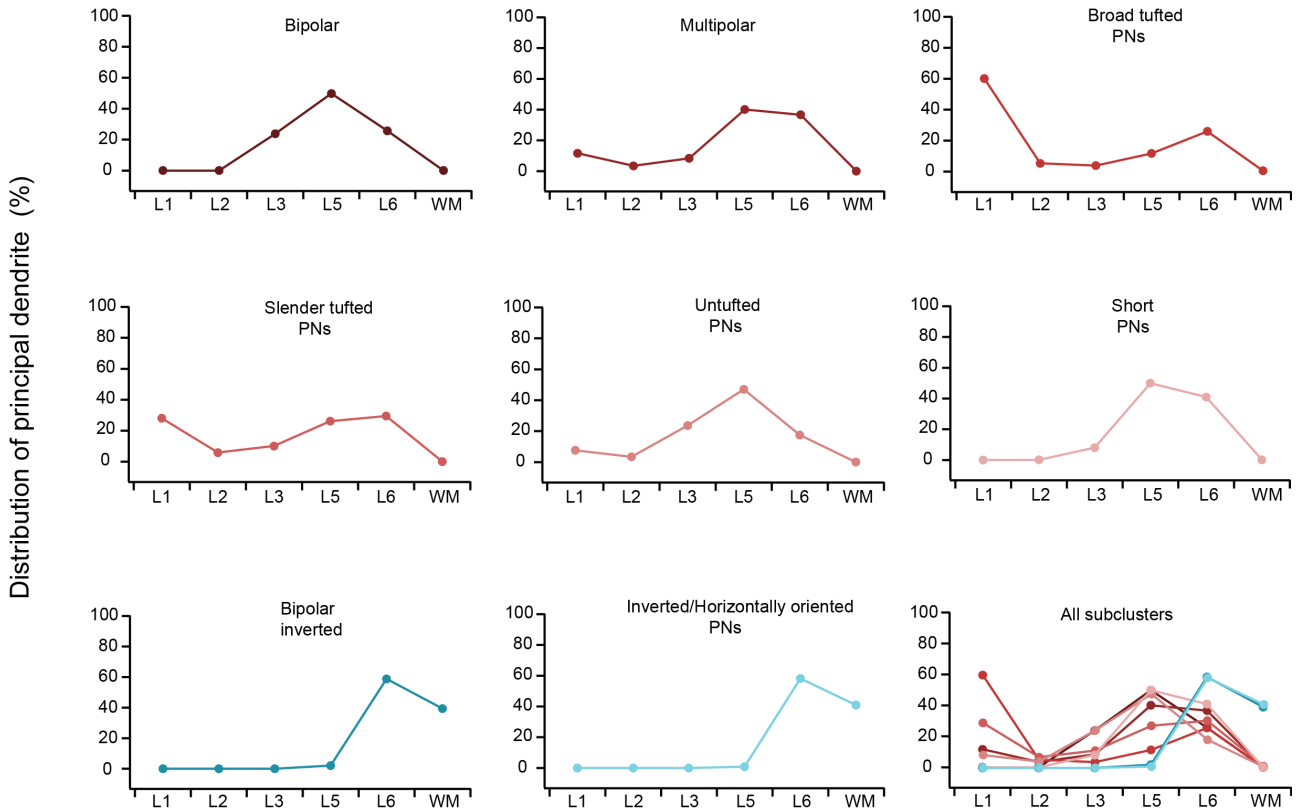


Fig. 3.1.4 Different sub-clusters of L6 excitatory neurons display distinct distribution of principal dendrite in different layers and WM. The percentage of the apical dendrite that is located in L1, L2, L3, L5, L6 and the WM is indicated by dots. All the dots are represented the average values of all neurons in the corresponding sub-clusters. Different sub-clusters are shown with the same colour code as in Fig. 3.1.2.

neurons were inverted PNs and almost all the apical dendrites of PNs in this sub-cluster were restricted in L6 ($58.2 \pm 18.6\%$) and WM ($40.8 \pm 19.1\%$). Only one horizontally oriented PN was found in this study and its principal dendrite was located predominantly in L6 (82.3%) due to that the main branch of the apical dendrite was extend parallel to the cortical layer border (Fig. 3.1.3, Fig. 3.1.4).

Unlike the bipolar neurons in cluster 1, the inverted bipolar neurons were diverse with respect to their secondary dendrites. Some neurons had secondary dendrites that bifurcated in a manner similar to that of the apical dendrite, pointing towards the pial surface or oriented sideways. While some neurons had long secondary dendrites with only few branches. (Table 3.3.1).

Comparison of electrophysiological properties between 2 morphological clusters

Results

Parameters	Cluster 1						Cluster 2	
	Bipolar (n=3)	Multipolar (n=7)	Broad tufted PNs (n=2)	Slender tufted PNs (n=13)	Untufted PNs (n=8)	Short PNs (n=15)	Bipolar inverted (n=5)	Inverted/ horizontally oriented PNs (n=26)
Length of principal dendrite in L1 (μm)	-	212 \pm 368	4180 \pm 557	1048 \pm 559	285 \pm 137	-	-	-
Length of principal dendrite in L2 (μm)	0.1 \pm 0.17	64 \pm 105	352 \pm 278	212 \pm 120	131 \pm 32	1 \pm 5	-	-
Length of principal dendrite in L3 (μm)	812 \pm 750	160 \pm 140	261 \pm 90	369 \pm 170	942 \pm 402	232 \pm 224	-	-
Length of principal dendrite in L5 (μm)	1394 \pm 572	577 \pm 362	782 \pm 403	951 \pm 305	1798 \pm 307	1213 \pm 506	66 \pm 138	27 \pm 47
Length of principal dendrite in L6 (μm)	603 \pm 337	494 \pm 362	2074 \pm 2178	1101 \pm 473	732 \pm 421	926 \pm 343	2137 \pm 1153	2100 \pm 773
Length of principal dendrite in WM (μm)	-	-	45 \pm 63	3 \pm 11	-	2 \pm 9	1290 \pm 725	1513 \pm 854
Length of longest basal dendrite (μm)	2455 \pm 1196	1266 \pm 406	841 \pm 44	603 \pm 235	608 \pm 210	656 \pm 232	1556 \pm 498	509 \pm 163
Length of longest basal dendrite / Length of principal dendrite	0.85 \pm 0.11	0.97 \pm 0.36	0.12 \pm 0.02	0.17 \pm 0.09	0.16 \pm 0.07	0.3 \pm 0.12	0.46 \pm 0.11	0.14 \pm 0.05

Table 3.1.1 Statistical analysis of the morphological parameters that were used in the cluster analysis. All data are represented as mean \pm standard deviation. The parameters that characterise the individual subclusters are marked in bold.

To find out whether these two morphological clusters had different electrophysiological properties, passive membrane properties, single AP properties and firing properties of the neurons that included in the morphological CA were analysed. Neurons with a resting membrane potential less negative than -55 mV or a series resistance larger than 40 M Ω were excluded from the final data set. Therefore, electrophysiological parameters of 20 upright neurons and 11 inverted neurons were collected for statistical comparison (Table 3.1.2).

Upright excitatory neurons and inverted excitatory neurons show significant differences in their passive properties, single AP properties and firing properties. Inverted excitatory neurons had a more depolarised resting membrane potential (-60.55 \pm 4.03 vs. -66.8 \pm 5.18 mV, $P < 0.01$) and AP

Results

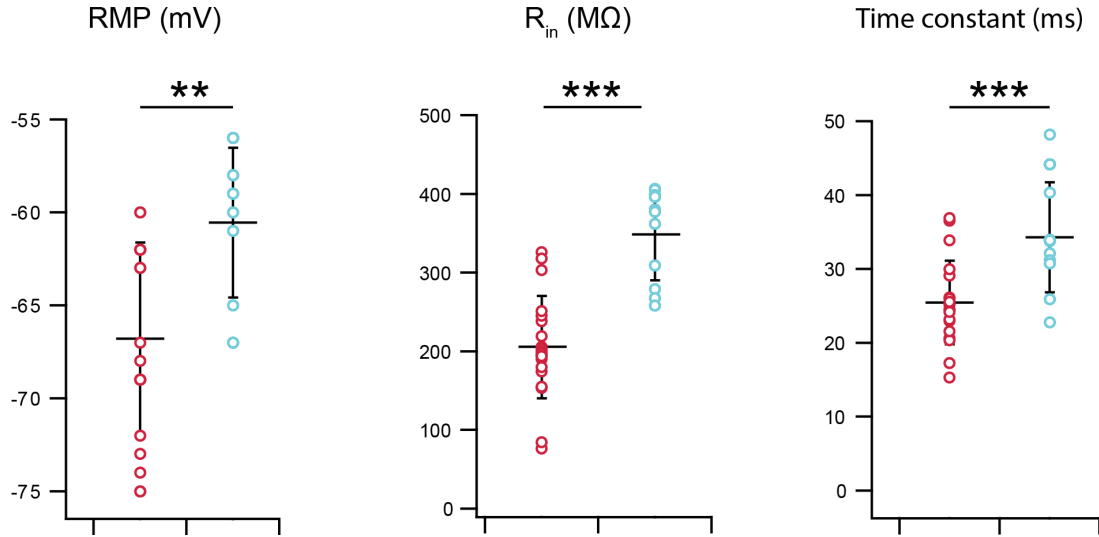


Fig. 3.1.5 Comparison of passive membrane properties between two clusters basing on the morphology. ‘Upright’ excitatory neurons (red, $n=20$) show differences in resting membrane potential (RMP), input resistance (R_{in}) and time constant compared to ‘inverted’ excitatory neurons (cyan, $n=11$). ** $P < 0.01$, *** $P < 0.001$.

threshold (-29.46 ± 3.16 vs. -33.21 ± 4.54 mV, $P < 0.05$) when compared to upright excitatory neurons (Fig. 3.1.5, Fig. 3.1.6).

Although the input resistance (R_{in}) of neurons in both clusters was relatively higher than that of neurons in other layers (van Aerde and Feldmeyer 2013), it was exceptionally high in inverted excitatory neurons, for which R_{in} was almost twice as high as for upright excitatory neurons, (396.08 ± 95.97 vs. 235.93 ± 77.26 M Ω , $P < 0.001$). This resulted in a slower membrane time constant (34.27 ± 7.46 vs. 25.35 ± 5.66 ms, $P < 0.001$). In addition, the AP half-width was much longer in inverted excitatory neurons than in upright excitatory neurons (1.34 ± 0.16 vs. 1.06 ± 0.14 ms, $P < 0.001$) (Fig. 3.1.5, Fig. 3.1.6).

The two L6 neuron clusters differed substantially in their excitability. Upright neurons were less excitable as a rheobase value of 112.5 ± 39.32 pA indicates. By comparison, in inverted neurons APs could be elicited by injecting 49.09 ± 13 pA, which was more than twofold lower than that for upright neurons ($P < 0.001$) (Fig. 3.1.6).

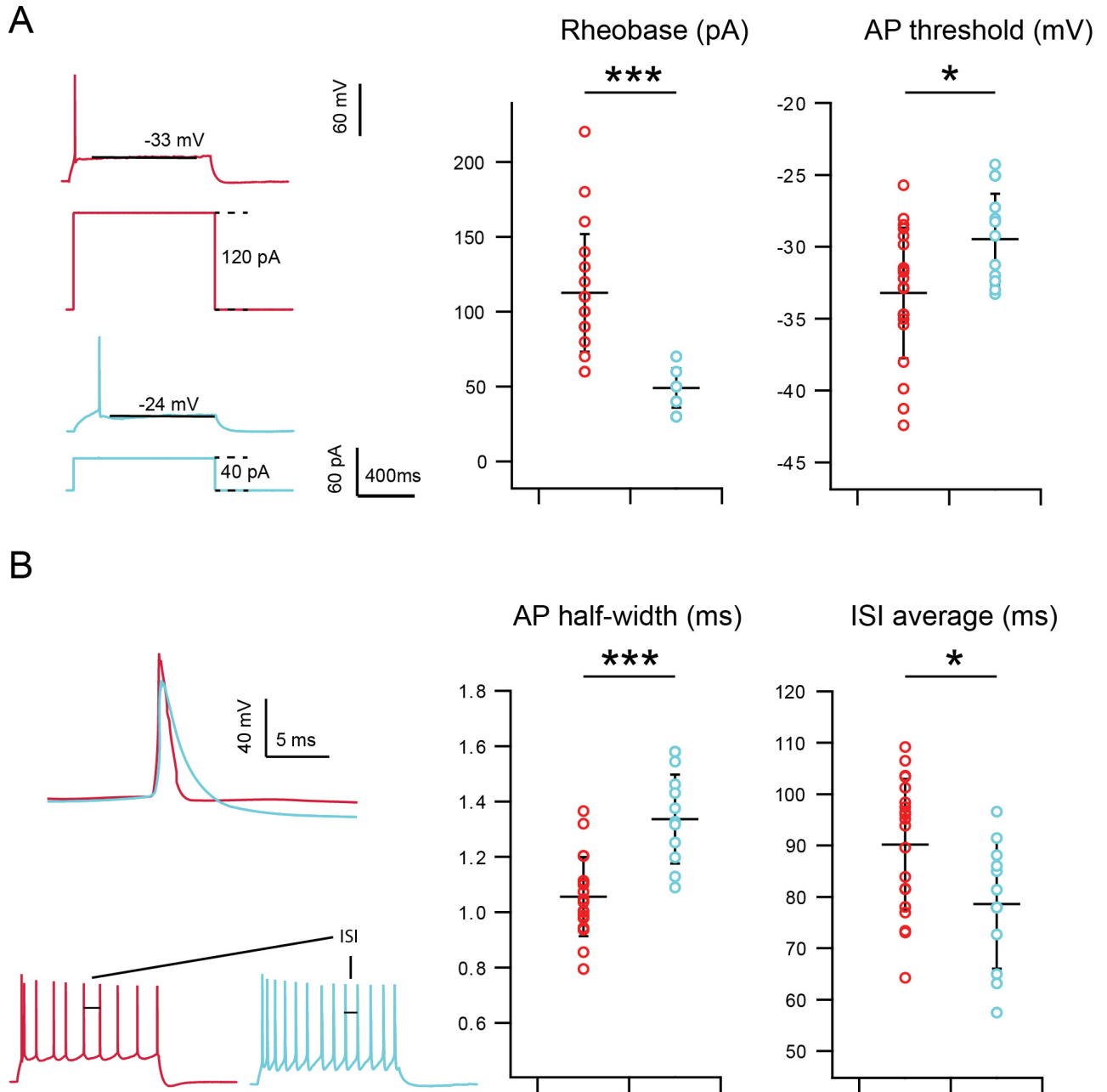


Fig. 3.1.6 Comparison of single AP and firing properties between two clusters basing on the morphology. (A) ‘Upright’ excitatory neurons show differences in Rheobase and AP threshold with ‘inverted’ excitatory neurons. Examples are shown in the left. (B) ‘Upright’ excitatory neurons show differences in AP half-width and average inter-spike interval (ISI) with ‘inverted’ excitatory neurons. Examples are shown in the left. ‘Upright’ excitatory neurons ($n=20$) and ‘inverted’ excitatory neurons ($n=11$) are displayed in red and cyan respectively. * $P < 0.05$, *** $P < 0.001$.

Most excitatory neurons in L6 of mPFC showed a regular firing pattern and some of these regular spiking neurons displayed a very short first inter-spike interval (ISI). As this will also affect the

Results

Parameters	Cluster 1 (n=20)	Cluster 2 (n=11)	P
Membrane potential (mV)	-66.8 ± 5.18	-60.55 ± 4.03	< 0.01**
Input resistance (MΩ)	235.93 ± 77.26	396.08 ± 95.97	< 0.001***
Time constant (ms)	25.45 ± 5.66	34.27 ± 7.46	< 0.001***
Voltage sag (%)	11.33 ± 8.49 (n=17)	8.56 ± 3	0.32
Rheobase (pA)	112.5 ± 39.32	49.09 ± 13	< 0.001***
AP threshold (mV)	-33.21 ± 4.54	-29.46 ± 3.16	< 0.05*
AP amplitude (mV)	88.78 ± 8.23	83.79 ± 5.95	0.09
AP half-width (ms)	1.06 ± 0.14	1.34 ± 0.16	< 0.001***
ISI average (ms)	90.19 ± 12.78	78.63 ± 12.6	< 0.05*
Adaptation ratio (ISI-3/ISI-9)	0.86 ± 0.22	1 ± 0.3	0.17
Firing frequency (Hz/100 pA)	15.86 ± 6.83	20.11 ± 3.85	0.07

Table 3.1.2 Statistical analysis of the electrophysiological parameters of L6 excitatory neurons under two morphological clusters. All data are represented as mean ± standard deviation. Tukey test was performed for the significant difference between two clusters. Significant p-values are marked in bold. * $P < 0.05$, ** $P < 0.01$, *** $P < 0.001$.

second ISI, the adaptation ratios were measured by ISI-3/ISI9 for all excitatory neurons. There was no major difference in the firing pattern of both upright and inverted excitatory neurons, although the inverted neurons showed a significantly smaller mean ISI value (78.63 ± 12.6 vs. 90.19 ± 12.78 ms, $P < 0.05$) (Fig. 3.1.6).

3.1.2 Morphological and electrophysiological classification of L6 inhibitory interneurons

The experiments in this part were performed together with Dr. Shalini Emmenegger and Kim Schaffrath; they contributed 23 interneurons in the morphological classification (total number is 38) and 3 interneurons in the electrophysiological classification (total number is 18).

The axonal projections of inhibitory neurons are normally dense and local resulting in a relatively intact axonal pattern compared to excitatory neurons. The axonal geometry is a very important morphological parameter for defining the innervation domain and hence allowing predictions about

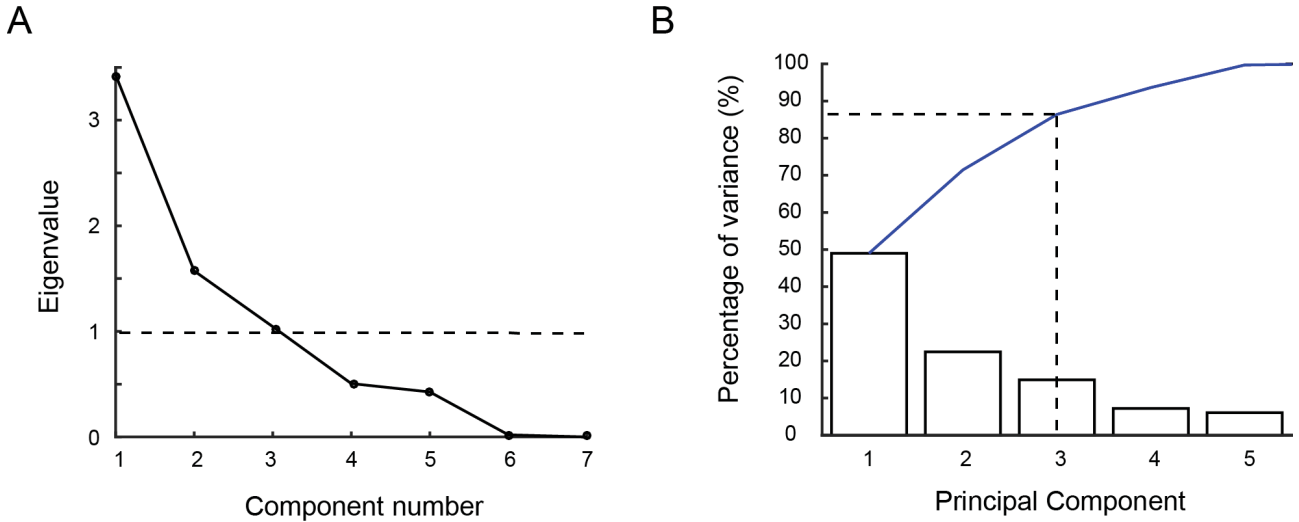


Fig. 3.1.7 Morphological analysis of L6 inhibitory neurons using principal component analysis. (A) The first three principal components with eigenvalues larger than one were used for cluster analysis. (B) The Pareto plot shows the individual (bars) and cumulative (blue curve) variance explained by the PCA components. The first three PCs explain more than 86% of the total variance.

the potential synaptic connectivity. In this study, the quantitative classification of inhibitory neurons was therefore performed based on the axonal innervation domains in different cortical layers.

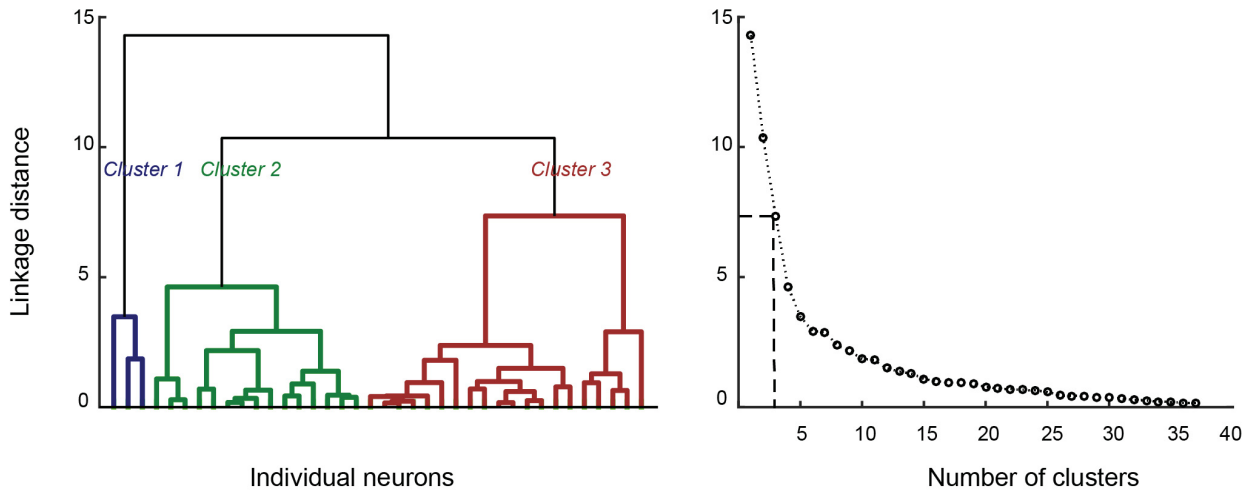
Morphological classification

Neurons that exhibited more than 15% truncations of the terminal axonal branches or less than 40% of the average axonal length were excluded from the final analysis. The average axonal length is around 19000 μm , so the reconstructions with axonal length less than 7600 μm were excluded. Based on both criteria, 38 reconstructions were included in the morphological analysis.

Parameters used for CA were the distributions of axonal length in cortical layer 1 to 6, the WM, and the axon orientation. The orientation of an axon was calculated using polar plots, from which the ratio between horizontal and vertical axonal lengths were calculated. Values larger than 1 signify a horizontal orientation, and smaller than 1 indicate a vertical orientation.

PCA was used and the first three PCs with eigenvalues greater than one were retained for CA; these accounted for ~86% of the total variance (Fig. 3.1.7). CA based on morphological parameters of the 38 L6 inhibitory neurons used here identified three clusters. The three clusters were distinct in their

A



B

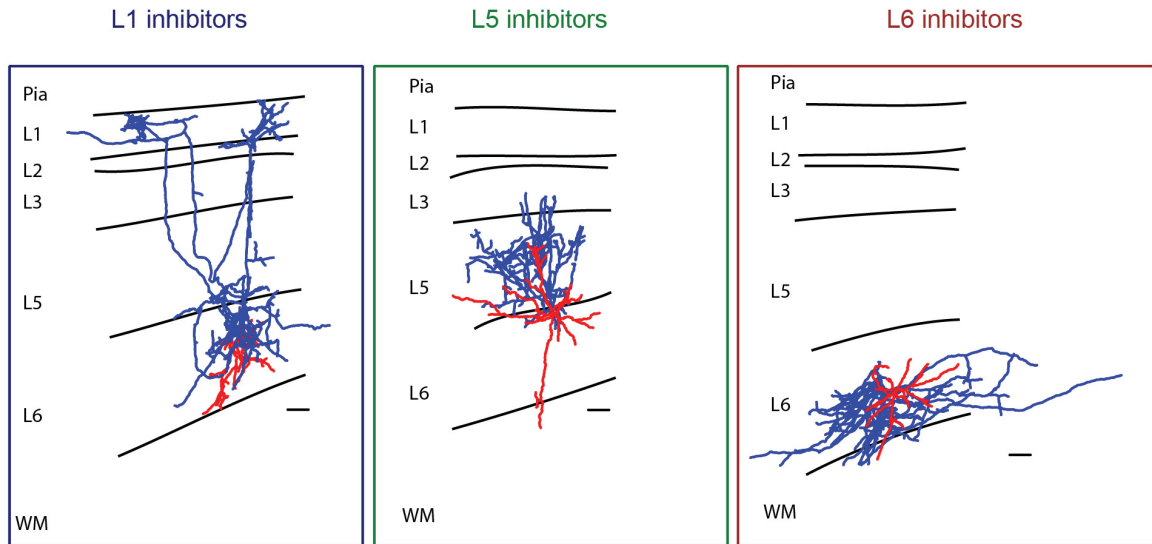


Fig. 3.1.8 Morphological analysis of L6 inhibitory neurons using cluster analysis. (A) Dendrogram from cluster analysis of morphological parameters reveals three clusters of L6 interneurons ($n=38$). The Y-axis corresponds to the linkage distance measured by Euclidean distance, and the X-axis shows individual neurons in the left and number of clusters in the right. the Cluster 1, cluster 2 and cluster 3 are shown in blue, green and red respectively. Dashed line indicates the cut-off position of three significant clusters, which was determined by using the Thorndike procedure. (B) Example reconstructions of three neurons in the three clusters, dendrites are shown in red and axons are coloured in blue. Scale bar is $100\ \mu\text{m}$.

axonal projections patterns. Cluster 1 neurons had axons that projected to L1 and were named ‘L1 inhibitors’, cluster 2 neurons had a high axonal density in L5 so they were named as ‘L5 inhibitors’,

Results

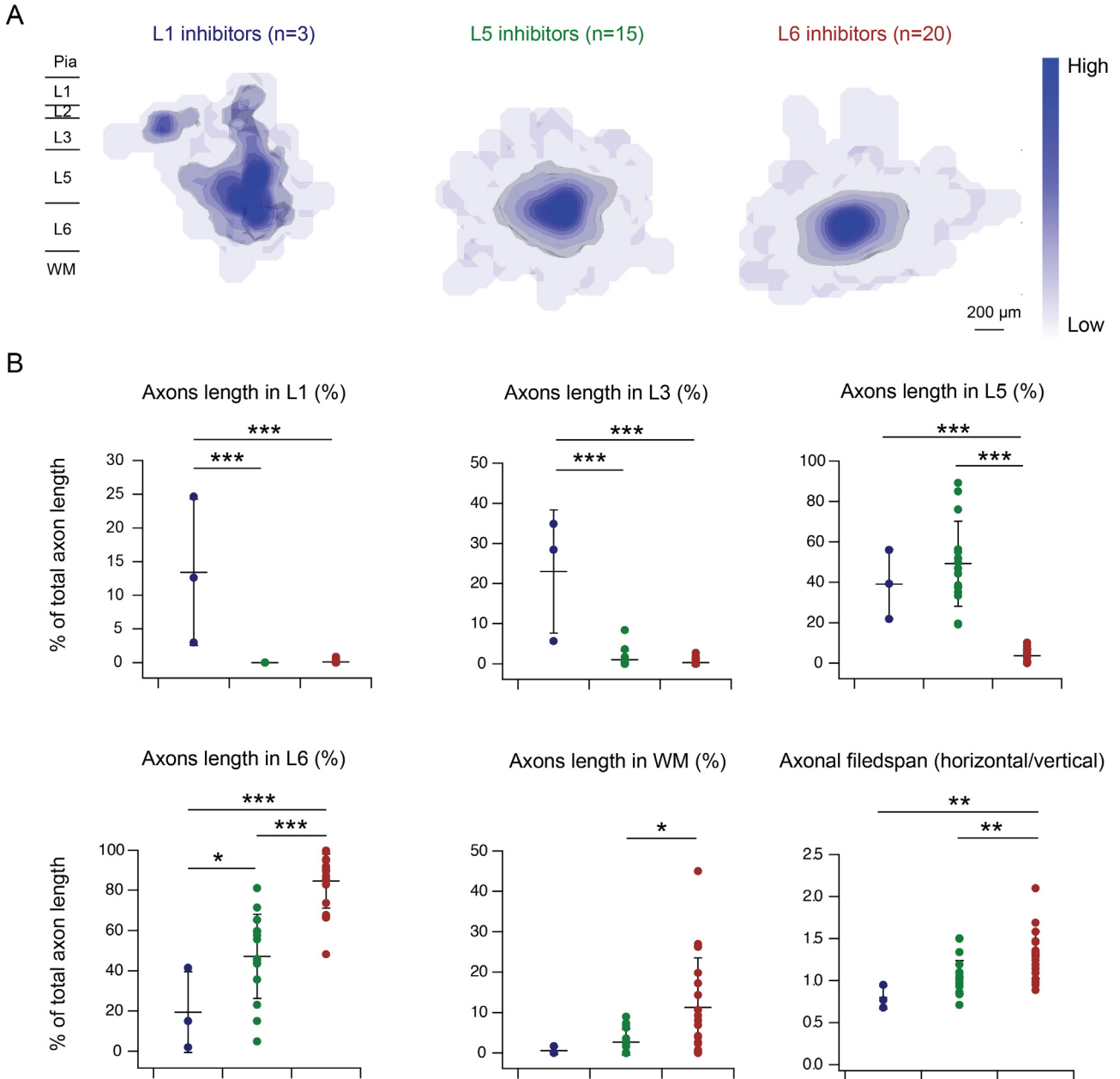


Fig. 3.1.9 Axonal properties of L6 inhibitory neurons under three morphological clusters. (A) The average axonal (blue) density maps of 3 morphological clusters. Grey isosurfaces show 80 percentile of the 3D axonal density. (B) Statistical analysis of the axonal properties of L6 inhibitory neurons under three morphological clusters. Cluster 1, 2, 3 are marked in blue, green and red respectively.

cluster 3 neurons had an axon that resided predominantly in L6 and were hence called ‘L6 inhibitors’ (Fig. 3.1.8, Table 3.1.3).

Cluster 1: L1 inhibitors

Results

Parameters	Cluster 1 (N=3)	Cluster 2 (N=15)	Cluster 3 (N=20)	1 vs 2	1 vs 3	2 vs 3
Axonal distribution in L1 (%)	13.42 ± 10.84	0 ± 0	0.11 ± 0.27	< 0.001***	< 0.001***	ns
Axonal distribution in L2 (%)	4.41 ± 0.46	0.04 ± 0.15	0.12 ± 0.3	ns	ns	ns
Axonal distribution in L3 (%)	23 ± 15.35	1.02 ± 2.28	0.35 ± 0.78	< 0.001***	< 0.001***	ns
Axonal distribution in L5 (%)	39.1 ± 17.12	49.17 ± 21.01	3.69 ± 3.24	ns	< 0.001***	< 0.001***
Axonal distribution in L6 (%)	19.49 ± 20.07	47.14 ± 20.89	84.45 ± 13.4	< 0.05*	< 0.001***	< 0.001***
Axonal distribution in WM (%)	0.6 ± 0.95	2.66 ± 3.23	11.28 ± 12.23	ns	ns	< 0.05*
Axon horizontal/vertical	0.8 ± 0.14	1.04 ± 0.19	1.3 ± 0.28	ns	< 0.01**	< 0.01**

Table 3.1.3 Statistical analysis of the axonal properties of L6 inhibitory neurons under three morphological clusters. All data are represented as mean ± standard deviation. The distributions of axon are given by percentages. Tukey test was performed for the significant difference between two clusters. Average values that significantly differ with all other clusters are marked in bold. * $P < 0.05$, ** $P < 0.01$, *** $P < 0.001$.

Cluster 1 consisted only of 3 neurons, i.e. 7.9% of the total number of PFC L6 interneurons. Neurons in this clusters showed a distinct largely vertical axonal projection pattern. The ratio between horizontal and vertical axonal lengths was 0.8 ± 0.14 . The L1 inhibitors showed a significant axonal collateral in L1 (relative axon length: $13.42 \pm 10.84\%$ vs. $0 \pm 0\%$; $0.11 \pm 0.27\%$, $P < 0.001$) and L3 ($23 \pm 15.35\%$ vs. $1.02 \pm 2.28\%$; $0.35 \pm 0.78\%$, $P < 0.001$) compared with the other two clusters, and had only a small axon plexus in L6 ($19.49 \pm 20.07\%$ vs. $47.14 \pm 20.89\%$; $84.45 \pm 13.4\%$, $P < 0.05$; $P < 0.001$) (Fig. 3.1.8, Fig. 3.1.9, Table 3.1.3). This indicates that L1 inhibitors mainly target neurons outside their home layer.

Cluster 2: L5 inhibitors

There were 15 neurons in cluster 2, which constitutes 39.5% of the total population. Most neurons in this cluster had axonal projections towards and in L5, their extent was similar in both horizontal and vertical directions. The ratio between horizontal and vertical axonal lengths was 1.04 ± 0.19 . Neurons near the L5/L6 border showed a preferential innervation of L5, while neurons located close to the border of L6 and the WM had similar axonal length in L5 and L6. All together, L5 inhibitors showed $49.17 \pm 21.01\%$ of the axonal projections in L5 and $47.14 \pm 20.89\%$ of the axonal projections in L6 (Fig. 3.1.8, Fig. 3.1.9, Table 3.1.3).

Cluster 3: L6 inhibitors

Cluster 3 comprised 20 L6 interneurons (52.6%). Neurons in this cluster showed a dominant horizontal rather than vertical axonal projection; the ratio between horizontal and vertical axonal filedspan was 1.3 ± 0.28 . This value was significantly larger than the values in the other two clusters ($P < 0.01$). $84.45 \pm 13.4\%$ of the axon was confined to home layer, which was significantly higher than other clusters ($P < 0.001$). In addition, only very few axonal branches of L6 inhibitors were found in L5 ($3.69 \pm 3.24\%$ vs. $39.1 \pm 17.12\%$; $49.17 \pm 21.01\%$, $P < 0.001$; $P < 0.001$). Furthermore, more than 10% of the L6 inhibitor interneuron axon was located in the WM; this substantially higher compared to L5 inhibitors ($11.28 \pm 12.23\%$ vs. 2.66 ± 3.23 , $P < 0.05$) (Fig. 3.1.8, Fig. 3.1.9, Table 3.1.3). This axonal projection pattern indicates that L6 inhibitors mainly innervate a narrow stratum in their home layer.

Electrophysiological classification

For the analysis of the electrophysiological properties of L6 interneurons, neurons with a series resistance $> 40 \text{ M}\Omega$ or a resting membrane potential more depolarised than -55 mV were excluded. Sometimes the firing frequency of L6 interneurons did not exceed 25-30 Hz even for high current injections; in that case these neurons were also excluded, resulting in a total number of 18 interneurons.

For the electrophysiological classification, we used parameters such as AP halfwidth, AHP amplitude, inter-spike interval, firing frequency and adaptation ratio. After CA, two distinct clusters were separated that displayed significant differences in the above-mentioned parameters; these neurons belong either to the group of FS interneurons or nFS interneurons (Fig. 3.1.10).

Cluster A: nFS interneurons

Three out of 18, i.e. 17% of L6 interneurons belonged to cluster A. The AP halfwidth of these interneurons was much longer than that of the other interneuron class (0.97 ± 0.07 vs. 0.48 ± 0.10 ms, cluster A vs. Cluster B, $P < 0.001$). Neurons in cluster A also showed a significantly larger inter-spike interval (80.9 ± 8.0 vs. 28.6 ± 12.3 ms, $P < 0.001$) and smaller adaptation ratio (0.44 ± 0.20 vs. 0.83 ± 0.14 , $P < 0.001$) compared with neurons in cluster B (Fig. 3.1.11, Table 3.1.4).

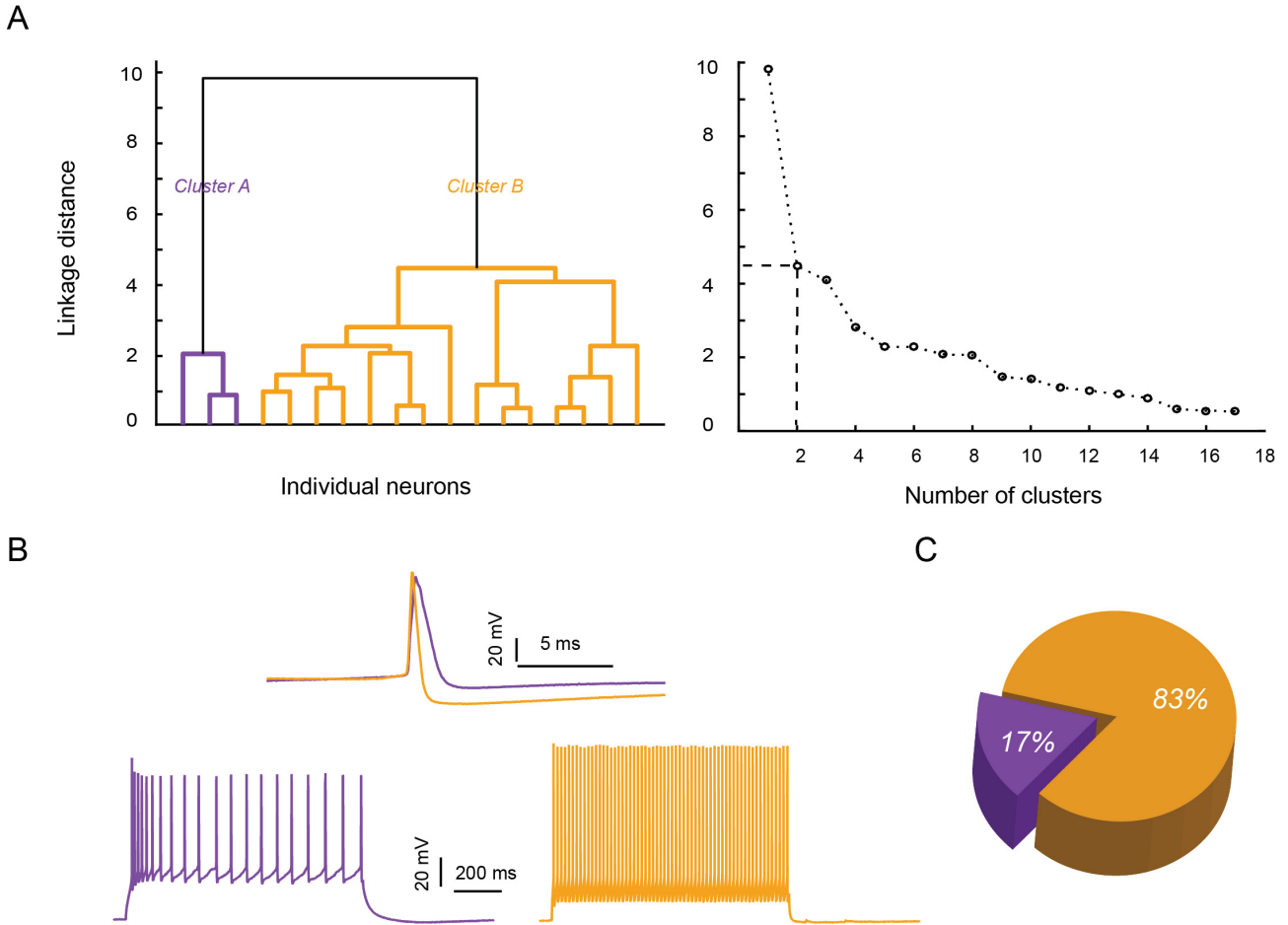


Fig. 3.1.10 Electrophysiological analysis of L6 inhibitory neurons using cluster analysis. (A) Dendrogram from cluster analysis of electrophysiological parameters reveals 2 clusters of L6 interneurons ($n=18$). The Y-axis corresponds to the linkage distance measured by Euclidean distance, and the X-axis shows individual neurons in the left and number of clusters in the right. the Cluster A and cluster B are shown in purple and orange. Dashed line indicate the cut-off position of 2 significant clusters, which was determined by using the Thorndike method. (B) Representative firing pattern and thresholded AP for the two clusters. (C) The percentage of each subcluster is shown in the pie chart.

Cluster B: FS interneurons

Fifteen interneurons were found in cluster B, constituting 83% of the total population. Interneurons in cluster B displayed a higher firing frequency per 100 pA current injection than that of cluster A interneurons (39.4 ± 13.9 vs. 20.5 ± 2.9 Hz / 100 pA, $P < 0.05$), which is a typical characteristic of FS interneurons. Moreover, a significantly larger AHP amplitude were found with interneurons in

Results

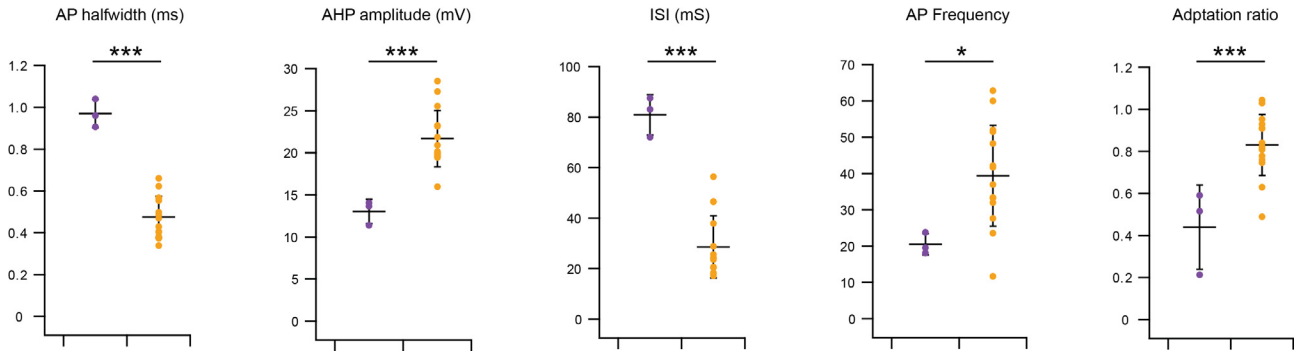


Fig. 3.1.11 Comparison of single AP and firing properties between two clusters of L6 inhibitory neurons. Cluster A and cluster B are shown in purple and orange. All data were shown with mean \pm SD. Tukey's test was performed for the significant difference between groups. * $P < 0.05$, *** $P < 0.001$.

Parameters	Cluster A (n=3)	Cluster B (n=15)	<i>P</i>
Firing Frequency (Hz) / 100 pA	20.5 \pm 2.9	39.4 \pm 13.9	< 0.05*
Adaptation ratio	0.44 \pm 0.20	0.83 \pm 0.14	< 0.001***
AHP amplitude (mV)	13.0 \pm 1.4	21.7 \pm 3.3	< 0.001***
AP half-width (ms)	0.97 \pm 0.07	0.48 \pm 0.10	< 0.001***
ISI average (ms)	80.9 \pm 8.0	28.6 \pm 12.3	< 0.001***

Table 3.1.4 Statistical analysis of the electrophysiological parameters that were used in the cluster analysis of L6 inhibitory neurons. All data are represented as mean \pm standard deviation. Tukey test was performed for the significant difference between two clusters. Significant *p*-values is marked in bold. * $P < 0.05$, ** $P < 0.01$, *** $P < 0.001$.

cluster B (21.7 \pm 3.3 vs. 13.0 \pm 1.4 mV, $P < 0.001$) comparing with the neurons in cluster A (Fig. 3.1.11, Table 3.1.4).

Correlation between morphological and electrophysiological clusters

Three distinct morphological clusters and two different electrophysiological clusters of inhibitory neurons in L6 of rat mPFC were identified quantitatively using cluster analysis. A dataset with a high quality morphological reconstructions may not have a qualified electrophysiological properties. Similarly, the reconstructions with a high truncation that excluded from the dataset, the electrophysiological recordings could be very good. The two dendrograms of morphological and

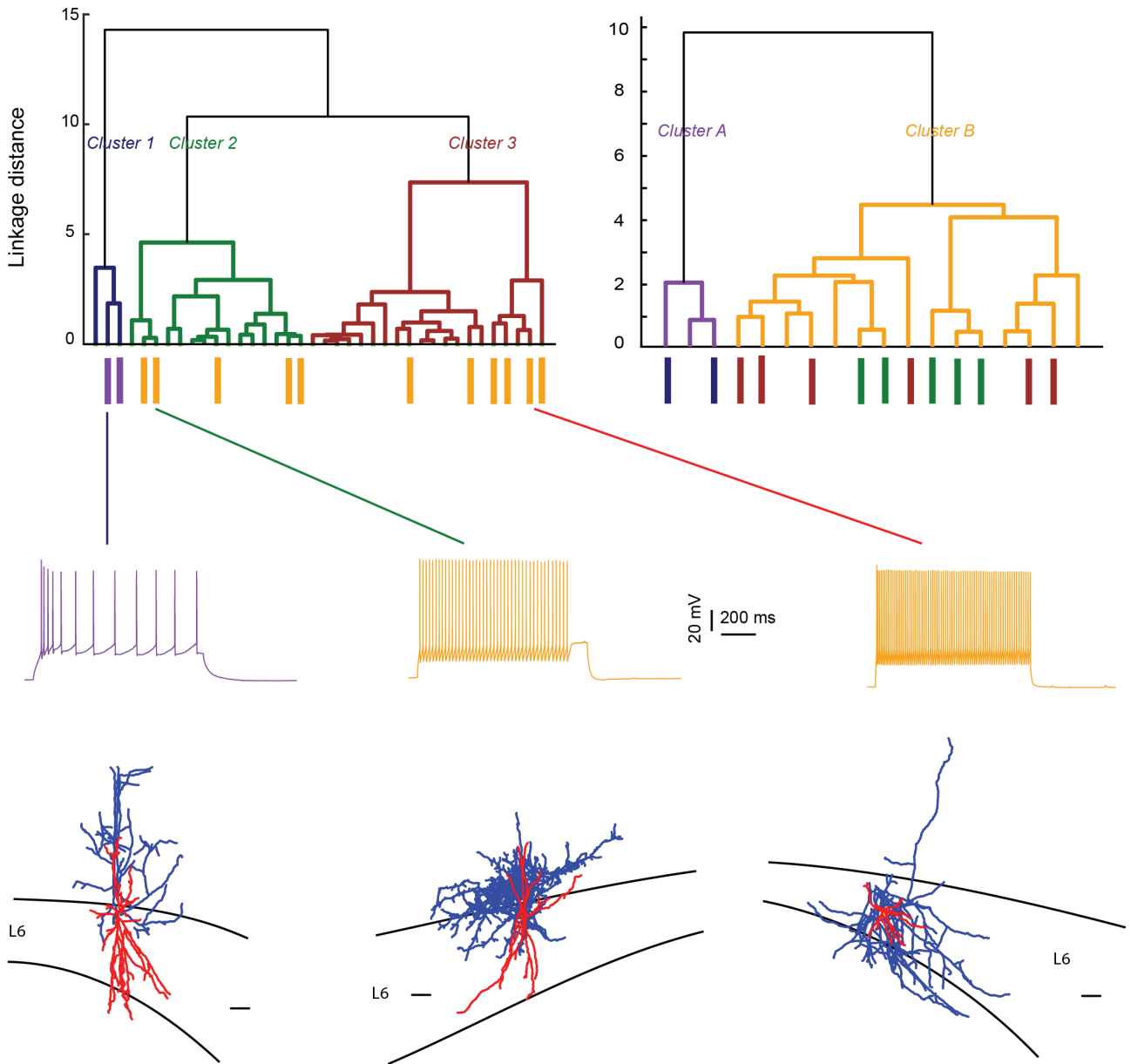


Fig. 3.1.12 Comparison of morphological and electrophysiological clusters of L6 inhibitory neurons. Dendrogram of three morphological clusters was shown in top left and the electrophysiological clusters was placed in top right. The coloured bars beneath each dendrogram represent the corresponding clusters from the other dendrogram. Morphological cluster 3 was having all the 2 types of electrophysiological clusters. Scale bar for reconstruction is 100 μm . Colour code as in Fig. 3.1.8 and Fig. 3.1.10.

electrophysiological CA were shown in Fig. 3.1.12. The coloured bars beneath each dendrogram represent the corresponding clusters from the other dendrogram. For dataset without corresponding morphological or electrophysiological properties no bars are given. There were 14 interneurons included in both morphological and electrophysiological CA.

In the morphological CA, there were only 3 interneurons in cluster 1, the axon of which projected to L1, and for two of those the electrophysiological properties could be analysed; both of them were nFS interneurons, belonging to the electrophysiological cluster A.

Electrophysiological parameters from 5 neurons in morphological cluster 2 were acquired and all of them were classified as FS interneurons. These neurons not only share similar axonal projection pattern that mainly distribute in L5, but also tend to share typical AP and firing properties of FS interneurons.

The L6 inhibitors constituted more than half of the total L6 interneuron population; six of those were also included in the electrophysiological CA. Like L5 inhibitors, all were FS interneurons. Examples were shown in Fig. 3.1.12.

In this study, we found that the morphological and electrophysiological clusters were correlated in morphological clusters. This indicates that L6 interneurons with specific axonal projection patterns might have specific single AP and firing properties. However, this hypothesis needs to be tested further with a larger dataset for each group.

3.2 Monosynaptic connections in L6 of mPFC

Investigation of the neural connectivity and interaction is crucial to understand the circuit dynamics and complexity. Therefore, we performed dual whole-cell recordings between L6 neurons in mPFC with simultaneous biocytin filling to elucidate the functional and morphological characteristics of synaptic connections in this brain region. Previous studies in other brain regions suggested a low connectivity ratio between L6 neurons (Beierlein and Connors 2002; Mercer et al. 2005; West et al. 2006; Lefort et al. 2009; Crandall et al. 2017), so that we used a ‘loose seal’ searching protocol (Methods and materials 2.4.2) to find synaptically coupled neurons.

In total, 159 neurons were recorded as postsynaptic neurons. Among 1450 potential presynaptic neurons, 45 neurons were found to be connected with the recorded postsynaptic neurons, i.e. the connectivity ratio was 3.1% in L6 of mPFC. After re-patching, 23 monosynaptic connections

including 17 excitatory connections and 6 inhibitory connections were recorded in dual whole-cell mode.

The connectivity types were decided by the cell types of presynaptic and postsynaptic neurons, following the same criteria as described in section 3.1 of the Results. The properties of postsynaptic potentials such as peak amplitude, latency, 20-80% rise time, decay time, paired-pulse ratio (PPR), failure rate and coefficient variation (CV) were analysed to characterise these monosynaptic connections.

3.2.1 Synaptic connectivity between L6 excitatory neurons

Using CA based on morphological parameters, excitatory neurons in L6 of mPFC have been classified into two main clusters: upright excitatory neurons (including upright PNs, normal bipolar neurons and multipolar neurons) with a principal dendrite pointing towards the pial surface, and inverted excitatory neurons (including inverted PNs and inverted bipolar neurons, no horizontally oriented PNs were found in paired recordings), the principal dendrite of which points to the WM. Of the 12 excitatory-excitatory (E-E) connections, we were able to determine the connection type of 11 pairs by morphological identification of pre- and postsynaptic neuron type. For one pair, we were unable to recover the morphology of presynaptic neuron; it was therefore excluded from the comparison of different connection types.

In seven out of 11 pairs, i.e. 64% of the E-E connections, the presynaptic neuron was a L6 inverted excitatory neuron. Four of these connections were established between two inverted excitatory neurons (example in Fig. 3.2.1) and three were connections between an inverted and upright neurons (example in Fig. 3.2.2). There were strong connections with a unitary EPSP amplitude of more than 1 mV, as well as weak connections for which the unitary EPSP amplitude was <0.2 mV. The average amplitude of postsynaptic EPSP was 0.79 ± 1.02 mV. The mean PPR of the connections with a presynaptic inverted neuron was 0.93 ± 0.19 and the CV was 0.94 ± 0.36 . The average latency, 20-80% rise time and decay time of postsynaptic EPSP was 1.5 ± 0.7 ms, 1.9 ± 0.6 ms and 58.7 ± 14.0 ms respectively. The failure rate of connections with a presynaptic inverted neuron was $39.5 \pm 19.2\%$ and the mean inter-soma distance between pre- and postsynaptic neuron

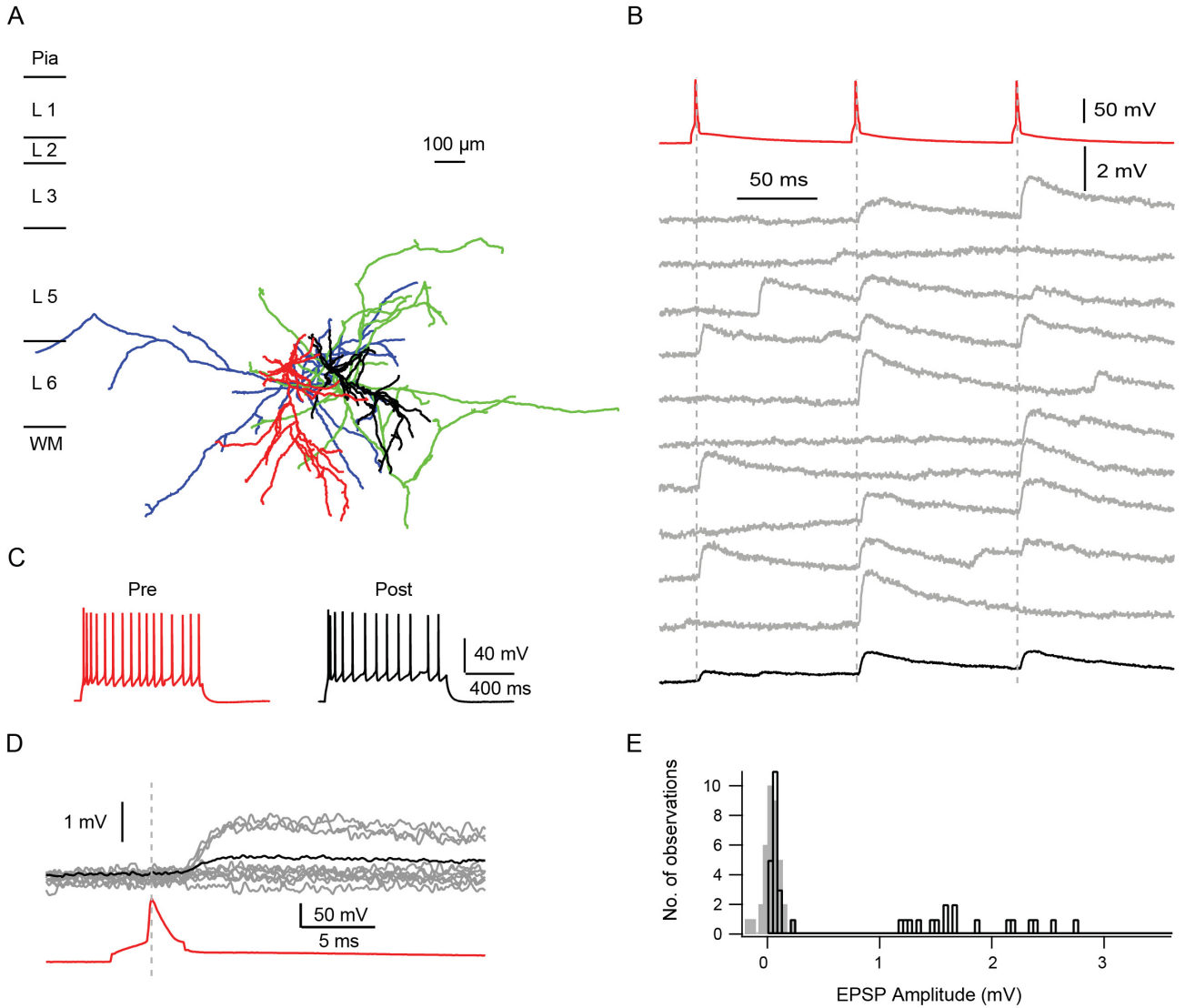


Fig. 3.2.1 A representative L6 Inverted-Inverted excitatory connection. (A) Morphological reconstruction of recorded inverted-inverted PN pair. Presynaptic somatodendritic domain and the axon are shown in red and blue; the postsynaptic somatodendritic domain and the axon are shown in black and green, respectively. (B) Ten consecutive EPSPs (grey, middle) and average (black, bottom) elicited by presynaptic APs (red, top). (C) Firing patterns of the pre- (red) and postsynaptic (black) neurons. (D) A presynaptic AP (red) and 10 consecutive superimposed EPSPs (grey) and their mean EPSP (black) are shown (from the first AP and corresponding EPSP of (B)). (E) Histograms of EPSP amplitude (grey bars for noise).

was $108 \pm 32 \mu\text{m}$. There were no significant differences in the synaptic properties of inverted-inverted excitatory neuron connections and inverted-upright excitatory neuron connections.

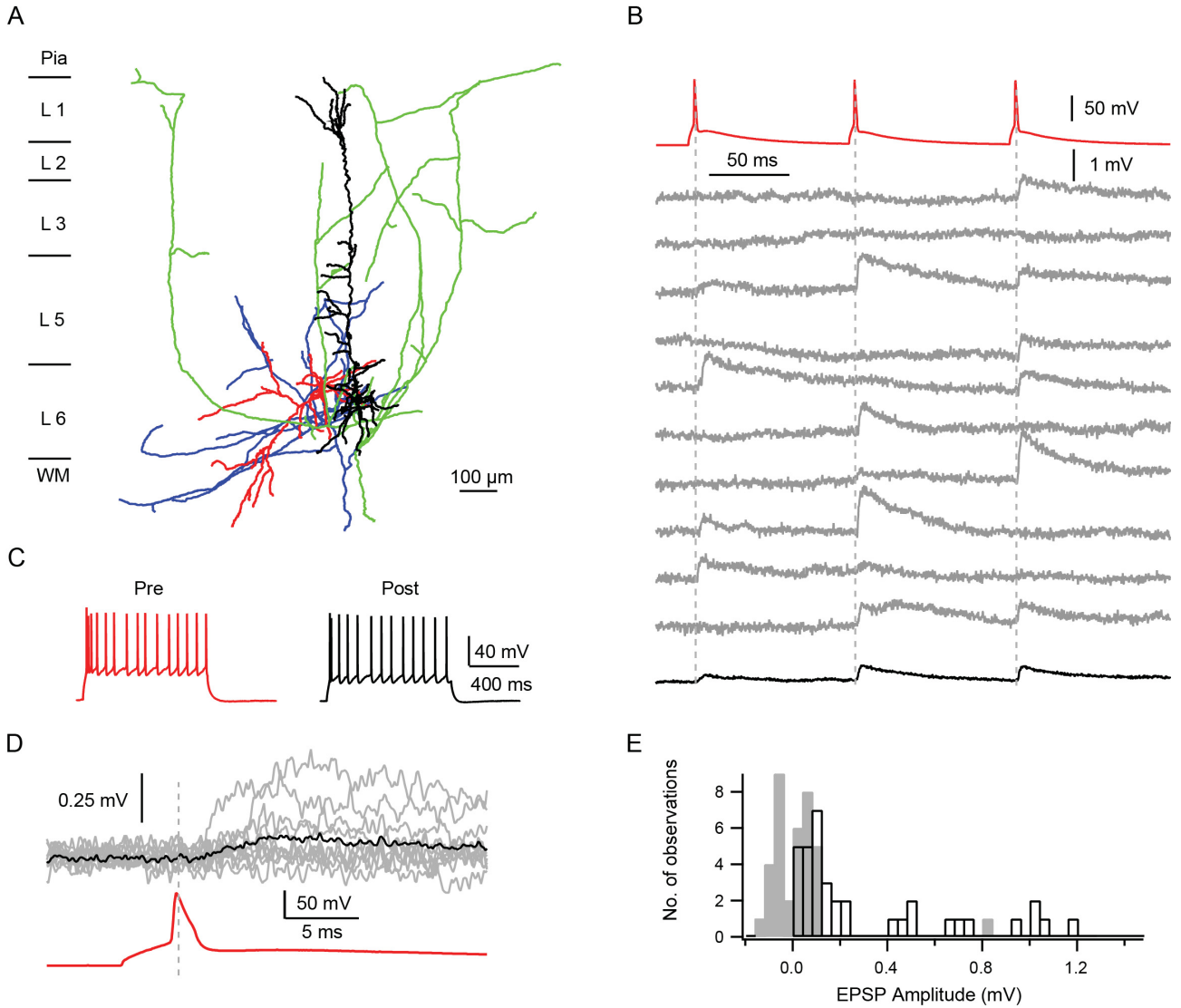


Fig. 3.2.2 A representative L6 Inverted-Upright excitatory connection. (A) Morphological reconstruction of recorded inverted-upright PN pair. Colour code as in Fig. 3.2.1 (B) Ten consecutive EPSPs (grey, middle) and average (black, bottom) elicited by presynaptic APs (red, top). (C) Firing patterns of the pre- (red) and postsynaptic (black) neurons. (D) A presynaptic AP (red) and 10 consecutive superimposed EPSPs (grey) and their mean EPSP (black) are shown (from the first AP and corresponding EPSP of (B)). (E) Histograms of EPSP amplitude (grey bars for noise).

Four connections established by a presynaptic upright L6 excitatory neuron were found, which constitutes 36% of the recorded E-E connections. Unlike connections with a presynaptic inverted excitatory neuron, all presynaptic upright excitatory neurons were synaptically coupled with another postsynaptic upright excitatory neuron (example in 3.2.3). These connections were very weak: the average unitary EPSP amplitude was only 0.09 ± 0.06 mV, which was significantly

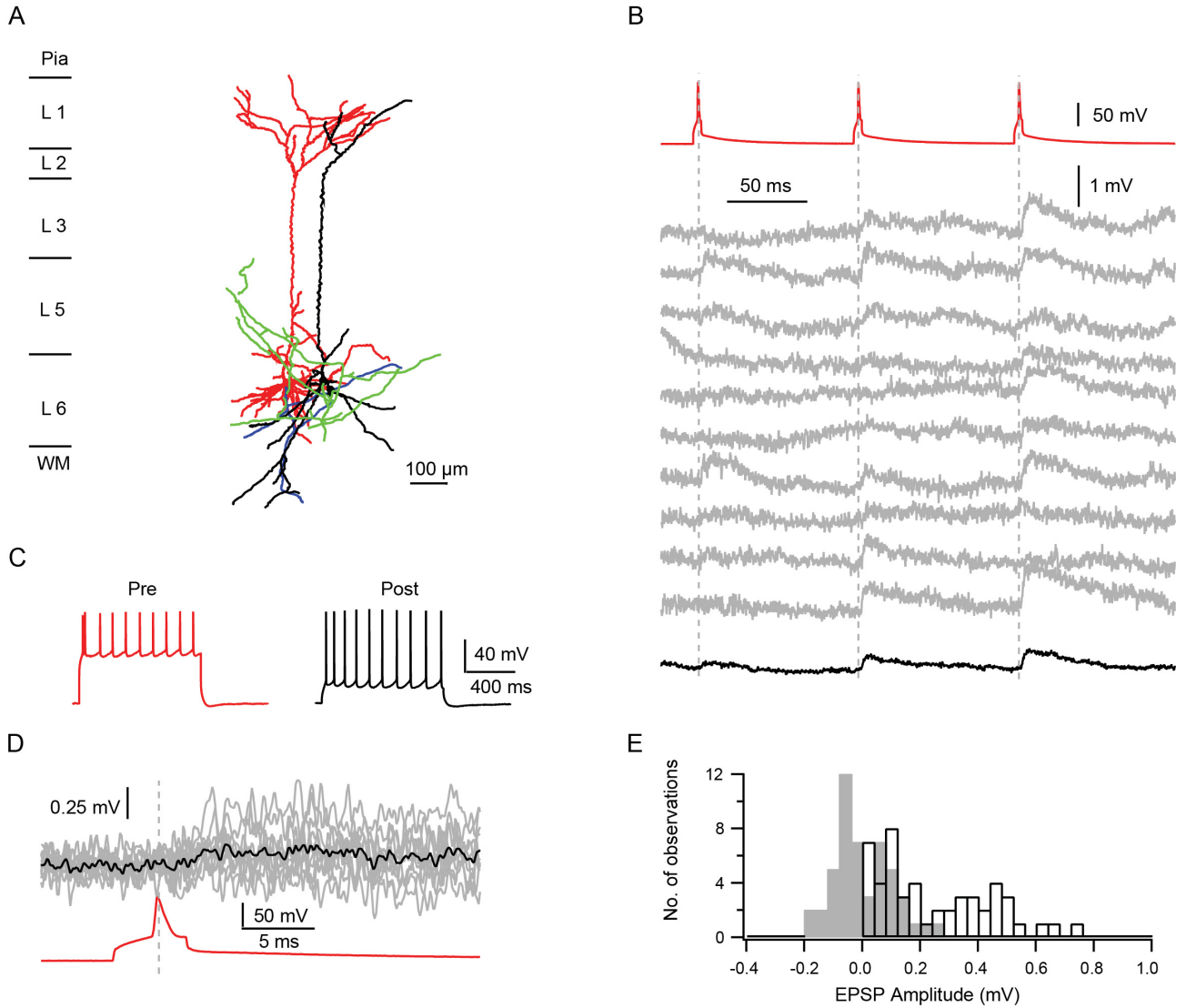
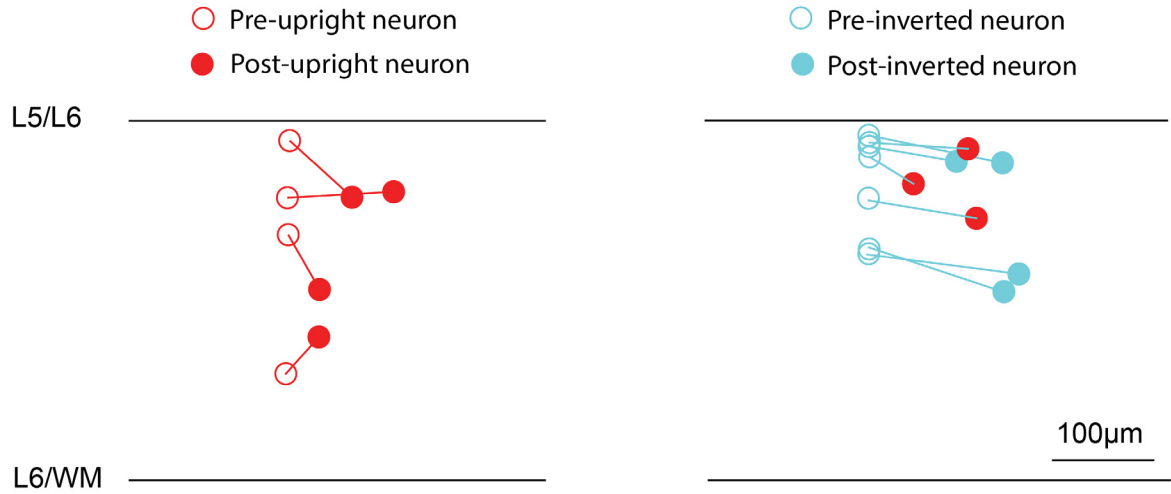


Fig. 3.2.3 A representative L6 Upright-Upright excitatory connection. (A) *Morphological reconstruction of recorded upright-upright PN pair. Colour code as for Figure 3.2.1.* (B) *Ten consecutive EPSPs (grey, middle) and average (black, bottom) elicited by presynaptic APs (red, top).* (C) *Firing patterns of the pre- (red) and postsynaptic (black) neurons.* (D) *A presynaptic AP (red) and 10 consecutive superimposed EPSPs (grey) and their mean EPSP (black) are shown (from the first AP and corresponding EPSP of (B)).* (E) *Histograms of EPSP amplitude (grey bars for noise).*

smaller than that of the connections with a presynaptic inverted excitatory neuron ($P < 0.05$). The mean inter-soma distance was found to be significantly shorter in upright-upright excitatory neuron connections compared to that of connections with a presynaptic inverted neuron ($P < 0.05$) (s. Table 3.2.1, Fig. 3.2.4).

A



B

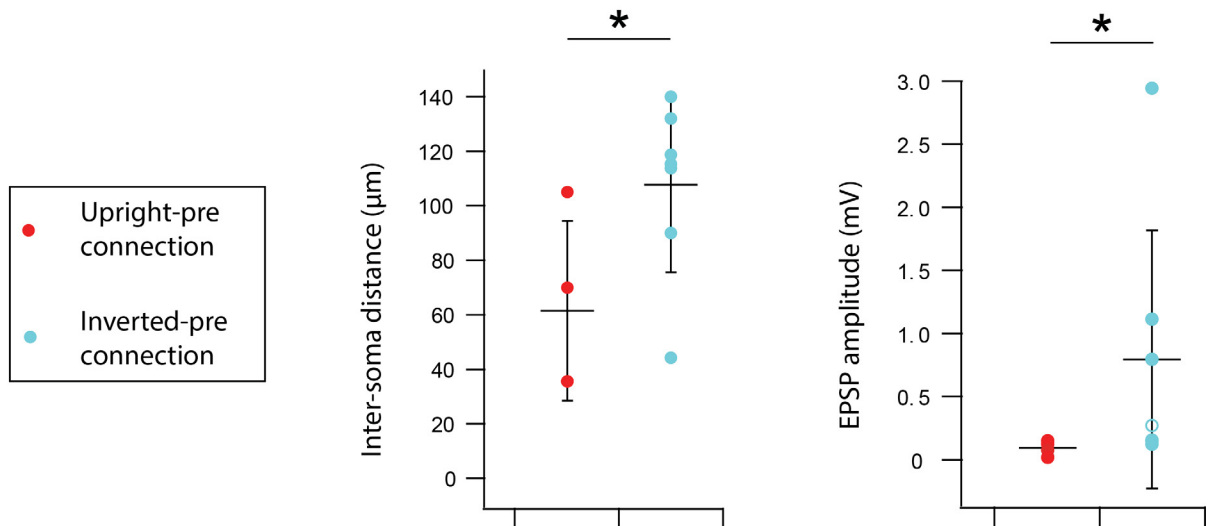


Fig. 3.2.4 Comparison of inter-soma distance and postsynaptic EPSP amplitude between L6 upright-pre and inverted-pre connections. (A) The recording position and inter-soma distance of presynaptic and postsynaptic neurons in individual pair were indicated (left, upright-pre connection; right, inverted-pre connections). The diagram was constructed by aligning the L5/L6 borders. (B) Connections with either an upright presynaptic neuron or an inverted presynaptic neuron showed differences with their inter-soma distance and postsynaptic EPSP amplitude. The medium value of EPSP amplitude from inverted-pre connection is marked with open circle. * $P < 0.05$.

Inverted excitatory neurons constitute 52% of the total population in E-E connections including both presynaptic and postsynaptic neurons. The proportion rises to 64% if only the presynaptic

Results

Parameters	Upright-pre pairs (n=4)	Inverted-pre pairs (n=7)	P
Amplitude (mV)	0.09 ± 0.06	0.79 ± 1.02	< 0.05*
Latency (ms)	0.4, 2.2	1.5 ± 0.7	1.11
20-80% rise time (ms)	2.4, 1.4	1.9 ± 0.6	1.11
Decay time (ms)	25.0	58.5 ± 14.0 (n=6)	0.29
Paired-pulse ratio	4.01 ± 5.69	0.93 ± 0.19	0.32
Failure rate (%)	55.0 ± 13.2	39.5 ± 19.2	0.29
Coefficient of variation	1.01 ± 0.20 (n=3)	0.94 ± 0.36	0.52
Inter-soma distance (µm)	61 ± 33	108 ± 32	< 0.05*

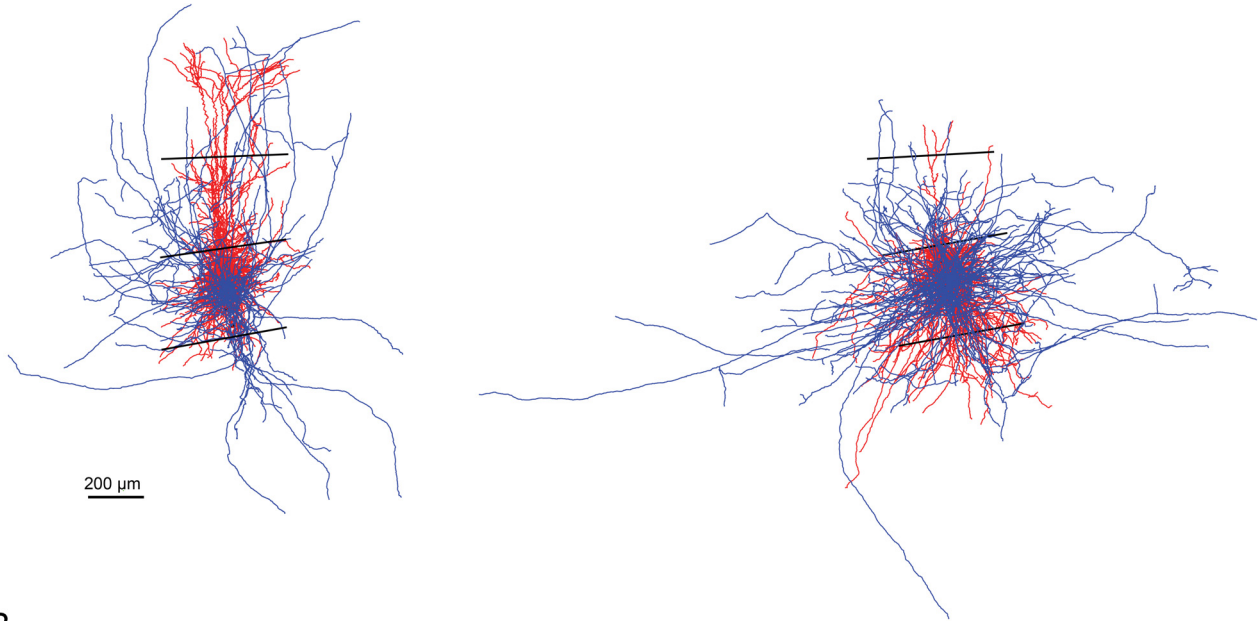
Table 3.2.1 Comparison of EPSP characteristics of L6 upright-pre and inverted-pre excitatory-excitatory connections. All data are represented as mean ± standard deviation. Wilcoxon-Mann-Whitney rank test was performed for the significant difference between two groups. Significant p-values is marked in bold. When the number of experiment is n=1 or 2, only the experiment value are given. *P < 0.05.

neurons are taken into account. Both values were larger than those calculated in 3.1.1. section of the Results. To explore the reason of this as well as the differences found between excitatory neuron connections with either a presynaptic inverted or an upright neuron, we compared the morphological characteristics of axons in these two excitatory neuron types. Axons of 15 upright neurons and 15 inverted excitatory neurons were reconstructed. We found that inverted excitatory

Parameters	Upright neurons (n=15)	Inverted neurons (n=15)	P
Total length of axon (µm)	4519 ± 3159	7223 ± 3853	< 0.05*
Length of axon in L6 (µm)	2239 ± 1319	4553 ± 2463	< 0.01**
Total horizontal field span of axon (µm)	713 ± 306	1083 ± 522	< 0.05*
Total vertical field span of axon (µm)	860 ± 425	776 ± 345	0.55
Horizontal field span of axon in L6(µm)	491 ± 273	906 ± 492	< 0.01**
Field span of axon H/V	0.92 ± 0.42	1.56 ± 0.81	< 0.05*

Table 3.2.2 Comparison of axonal properties between L6 upright and inverted excitatory neuron in pairs. All data are given as mean ± standard deviation. Tukey's test was performed for the significant difference between two groups. Significant p-values is marked in bold. *P < 0.05, **P < 0.01.

A



B

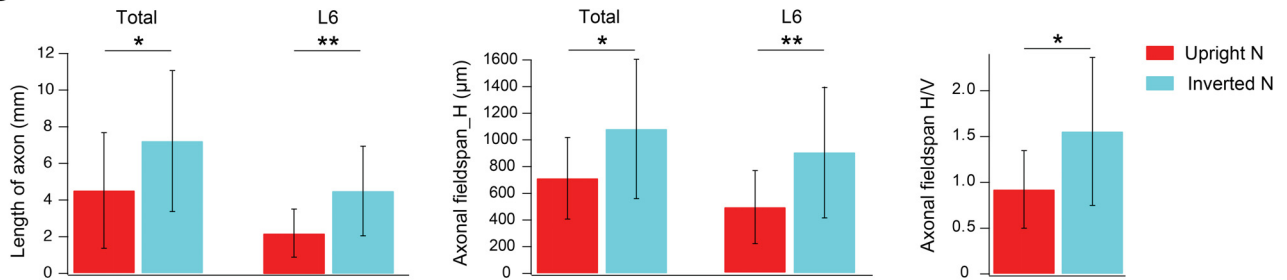


Fig. 3.2.5 Comparison of axonal properties between L6 upright and inverted neuron. (A) Superimposed morphological reconstructions of upright (left, $n=15$) and inverted (right, $n=15$) neurons. The somatodendritic domain and axon are shown in red and blue, respectively; layer borders of L3/L5, L5/L6 and L6/WM are indicated with black lines from top to bottom. With increasing distance from the cell body, axon truncations are more severe. (B) Inverted excitatory neurons show a significant difference in length of axon (total and in L6), horizontal field span of axon (total and in L6) and ratio between horizontal and vertical fieldspan of axon. * $P < 0.05$, ** $P < 0.01$.

neurons had a significantly larger axon length than upright neurons (7223 ± 3853 vs. 4519 ± 3159 μm , $P < 0.05$). The length of the axon located in L6 was also found to be larger for inverted excitatory neurons (4553 ± 2463 vs. 2239 ± 1319 μm , $P < 0.01$). Moreover, by calculating the axonal field span, we showed that that inverted excitatory neurons had a larger horizontal field span in L6 compared to upright excitatory neurons (906 ± 492 vs. 491 ± 273 μm , $P < 0.01$). The ratio between the horizontal field span and vertical field span of axons was also significantly different

between inverted and upright excitatory neurons ($P < 0.05$). For upright excitatory neurons this ratio was 0.92 ± 0.42 but 1.56 ± 0.81 for inverted excitatory neurons, indicating that inverted excitatory neurons have a dominant horizontal axonal projections (Fig. 3.2.5, Table 3.2.2).

3.2.2 Synaptic connectivity between L6 excitatory and inhibitory neurons

In summary, eleven monosynaptic connections were recorded in whole-cell mode between L6 excitatory neurons and inhibitory neurons, of which two were reciprocal synaptic connections. Five monosynaptic excitatory connections from excitatory neurons to inhibitory neurons and six monosynaptic inhibitory connections from inhibitory neurons to excitatory neurons were obtained, respectively. Excitatory neurons were morphologically classified as upright and inverted excitatory neurons (Results 3.1.1), while inhibitory neurons were identified electrophysiologically either as FS or nFS interneurons (Results 3.1.2).

Excitatory connections from L6 excitatory neurons to inhibitory neurons

Four out of five excitatory-inhibitory (E-I) connections had a presynaptic upright excitatory neuron and 3 of them formed excitatory synapses with FS interneuron (example in Fig. 3.2.6 A-D). The mean inter-soma distance between pre- and postsynaptic neurons was $96 \pm 51 \mu\text{m}$ in upright excitatory neuron-FS connections. The average postsynaptic EPSP amplitude was $0.32 \pm 0.41 \text{ mV}$,

Parameters	Upright-FS (n=3)	Upright-nFS (n=1)	Inverted-FS (n=1)
Amplitude (mV)	0.32 ± 0.41	0.02	2.57
Latency (ms)	1.3 ± 1.3	2.1	0.2
20-80% rise time (ms)	0.6 ± 0.2	0.3	1.1
Decay time (ms)	9.2, 6.9 (n=2)	-	14.2
Paired-pulse ratio	2.69 ± 0.70	3.48	0.72
Failure rate (%)	54.1 ± 32.7	84.0	0.0
Coefficient of variation	1.20 ± 0.33	1.47	0.47
Inter-soma distance (μm)	96 ± 51	64	50

Table 3.2.3 EPSP characteristics of L6 excitatory-inhibitory neuron connections. *All data are given as mean \pm standard deviation. When the number of experiment is n=1 or 2, only individual values are given.*

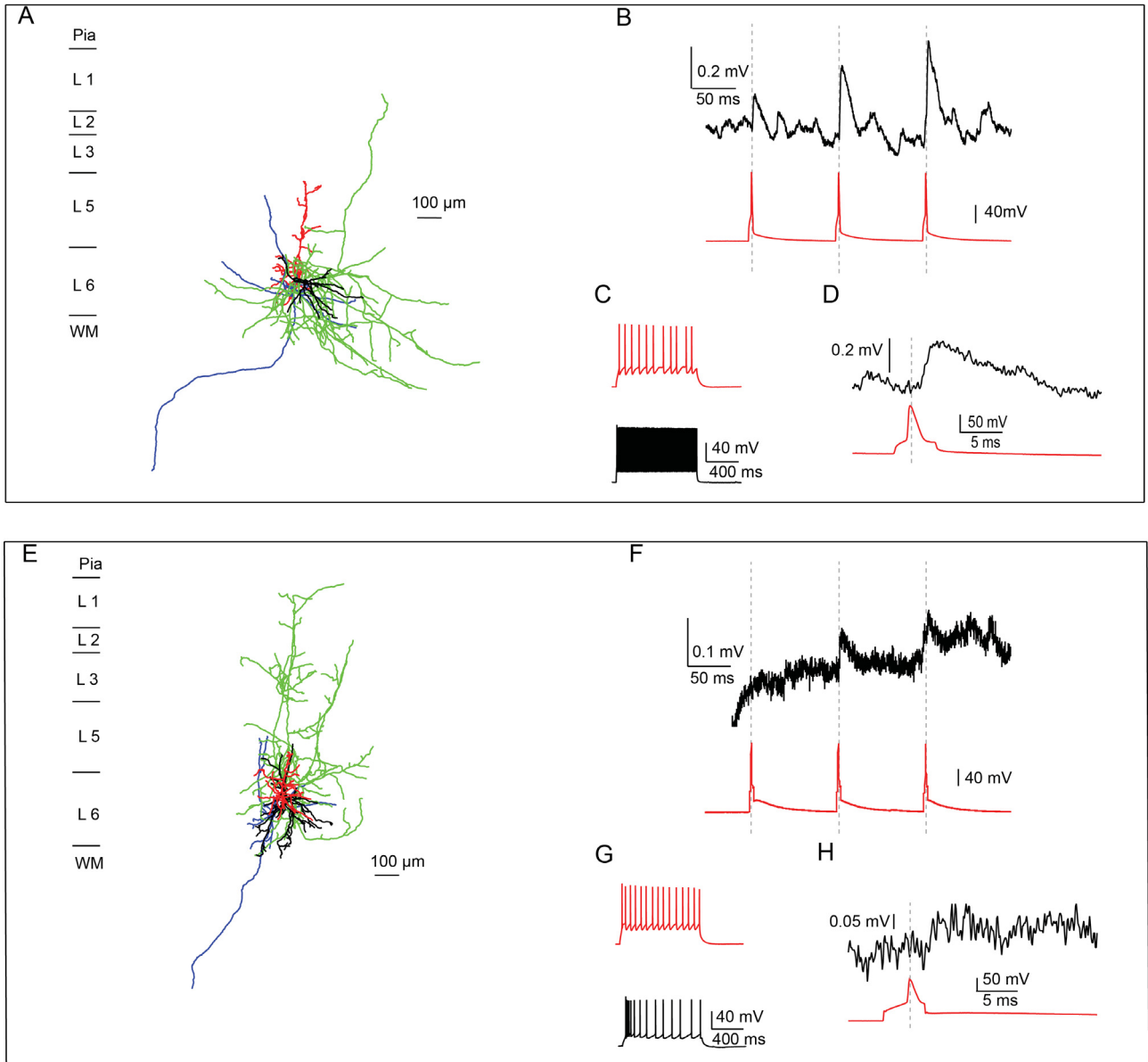


Fig. 3.2.6 Examples of L6 upright PN-interneurons connection. (A-D) A representative upright PN-FS excitatory connections. (E-H) A representative upright PN-nFS excitatory connections. (A&E). Morphological reconstruction of the recorded neuron pair. Colour code as in Fig. 3.2.1. (B&F). Average EPSPs (black, top) of corresponding connections elicited by presynaptic APs (red, bottom), which showed short-term plasticity. (C&G). Firing patterns of the pre- (red) and postsynaptic (black) neurons. (D&H). A presynaptic AP (red) and mean first EPSP (black) are shown.

while the 20-80% rise time and latency of EPSP was 0.6 ± 0.2 ms and 1.3 ± 1.3 ms respectively, with a decay time of 8.1 ± 1.7 ms. The mean failure rate was $54.1 \pm 32.7\%$ and the CV 1.20 ± 0.33 .

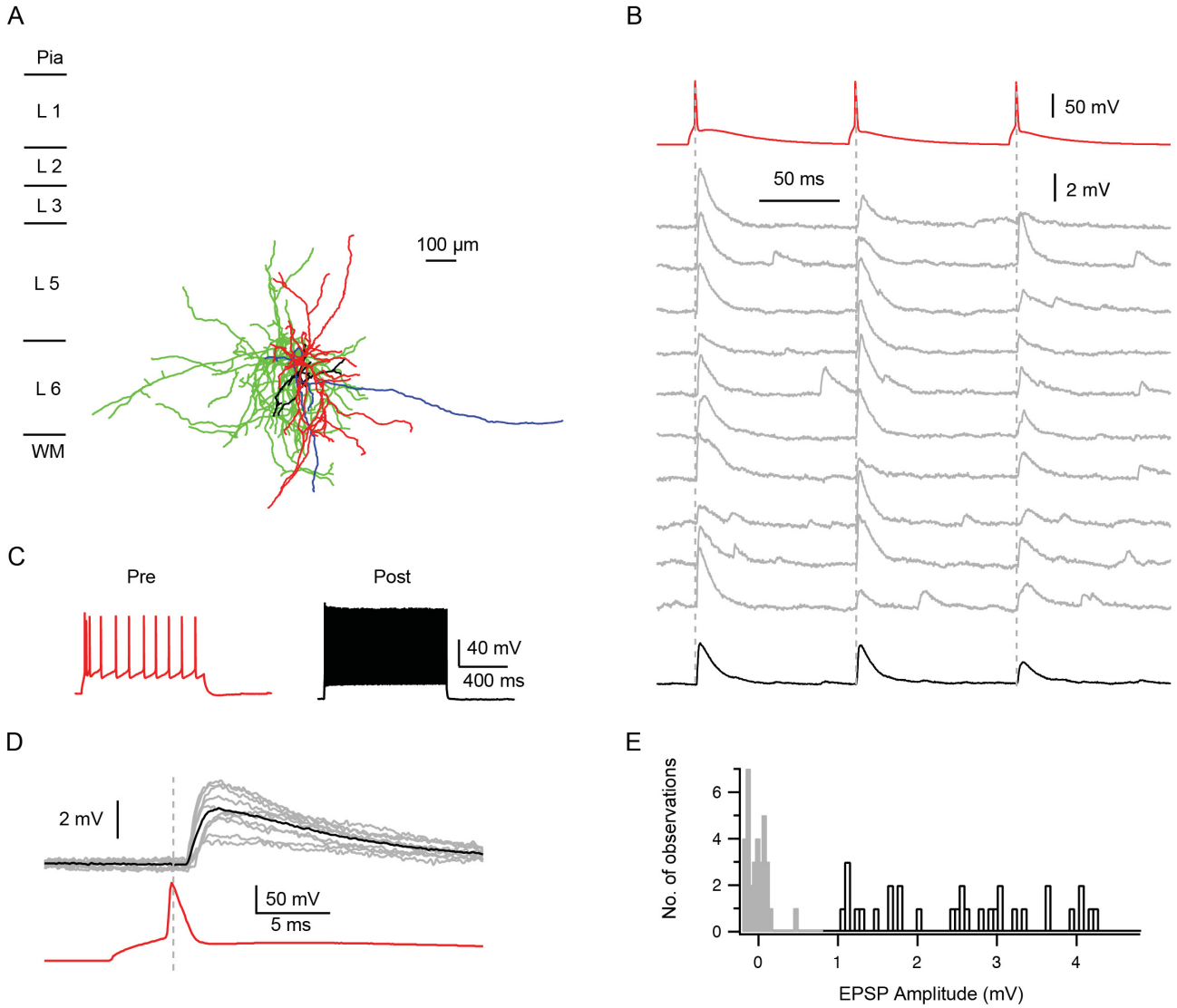


Fig. 3.2.7 A representative L6 inverted excitatory neuron -FS excitatory connection. (A) Morphological reconstruction of recorded inverted excitatory neuron-FS neuron pair. Colour code as in Fig. 3.2.1. (B) Ten consecutive EPSPs (grey, middle) and average (black, bottom) elicited by presynaptic APs (red, top). (C) Firing patterns of the pre- (red) and postsynaptic (black) neurons. (D) A presynaptic AP (red) and 10 consecutive superimposed EPSPs (grey) and their mean EPSP (black) are shown (from the first AP and corresponding EPSP of (B)). (E) Histograms of EPSP amplitude (grey bars for noise).

All the upright excitatory neuron-FS connections showed paired pulse facilitation with a mean PPR of 2.69 ± 0.70 (Fig. 3.2.6 B).

Only one upright PN-nFS connection was recorded in this study (example in Fig. 3.2.6 E-H). The postsynaptic EPSPs displayed short-term facilitation (PPR: 3.48) as did upright PN-FS connection

Results

(Fig. 3.2.6 F). The synaptic efficacy of this pair was very low with a high failure rate of 84% and a small average unitary EPSP amplitude of 0.02 mV. The inter-soma distance between the presynaptic excitatory neuron and the postsynaptic nFS neuron was 64 μm . The 20-80% rise time and latency of the postsynaptic EPSP was 0.3 ms and 2.1 ms. Due to the small EPSP amplitude, we were not able to determine the EPSP time course for this synaptic connection (Table 3.2.3).

Apart from the upright excitatory neuron-interneuron connections, one E-I connections with a presynaptic inverted L6 neuron was also found (example in Fig. 3.2.7). The presynaptic inverted excitatory neuron established synaptic contacts with a postsynaptic FS interneuron. The efficacy of this pair was very high: the postsynaptic neuron responded to every presynaptic AP (0% failure rate) and the average unitary EPSP amplitude was 2.57 mV, with a small CV of 0.47. Moreover, unlike the upright excitatory-interneuron E-I connections, this inverted excitatory neuron-FS connection displayed an obvious paired pulse depression (Fig. 3.2.7 B), with a PPR of 0.72. The inter-soma distance between the pre- and postsynaptic neuron was 50 μm . The 20-80% rise time, latency and decay time of postsynaptic EPSP was 1.1 ms, 0.2 ms and 14.2 ms respectively (Table 3.2.3).

Inhibitory connections from L6 inhibitory neurons to excitatory neurons

Parameters	FS-Upright (n=5)	FS-Inverted (n=1)
Amplitude (mV)	0.41 \pm 0.32	0.33
Latency (ms)	0.9 \pm 0.3	3.8
20-80% rise time (ms)	3.3 \pm 1.7	8.3
Decay time (ms)	44.6 \pm 26.7	66.0
Paired-pulse ratio	1.24 \pm 0.44	0.80
Failure rate (%)	31.5 \pm 17.8	27.0
Coefficient of variation	0.63 \pm 0.15	0.51
Inter-soma distance (μm)	86 \pm 54	249

Table 3.2.4 IPSP characteristics of L6 inhibitory-excitatory neuron connections. *All data are represented as mean \pm standard deviation. When the number of experiment is n=1 or 2, only the experiment value are given.*

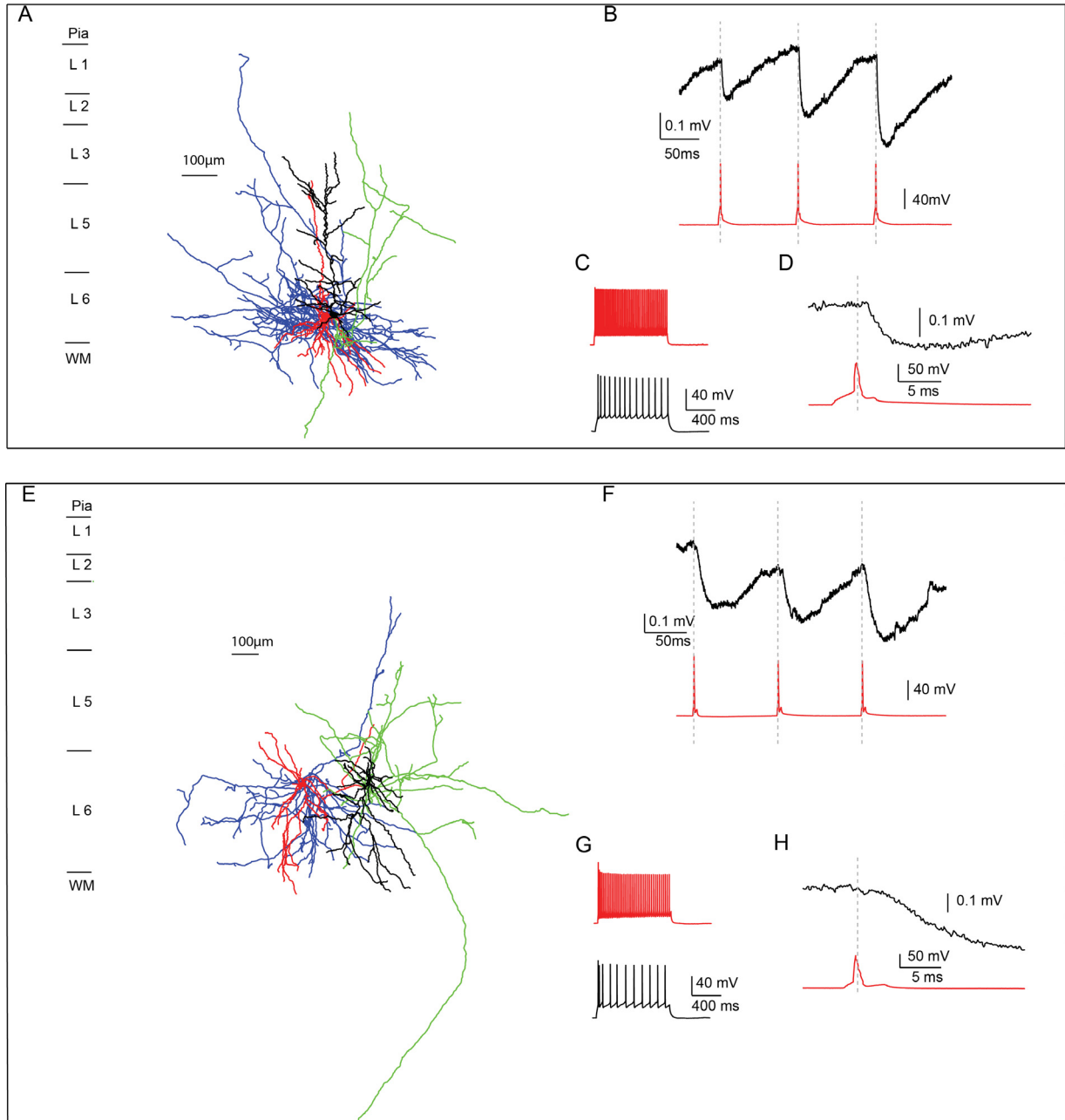


Fig. 3.2.8 Examples of L6 inhibitory FS-excitatory neuron connections. (A-D) *A representative an inhibitory FS-upright excitatory neuron connection.* (E-H) *A representative inhibitory FS-inverted excitatory neuron connection.* (A&E). *Morphological reconstruction of corresponding pair. Colour code as in Fig. 3.2.1.* (B&F). *Average IPSPs (black, top) of corresponding connections elicited by presynaptic APs (red, bottom), which showed short-term plasticity.* (C&G). *Firing patterns of the pre- (red) and postsynaptic (black) neurons.* (D&H). *A presynaptic AP (red) and mean first IPSP (black) are shown.*

Of the six inhibitory-excitatory (I-E) connections, all the presynaptic neurons were found to be FS interneuron and most of them were forming synapses with upright excitatory neuron (5 out of 6) (example in Fig. 3.2.8 A-D); the mean inter-soma distance for these connections was $86 \pm 54 \mu\text{m}$.

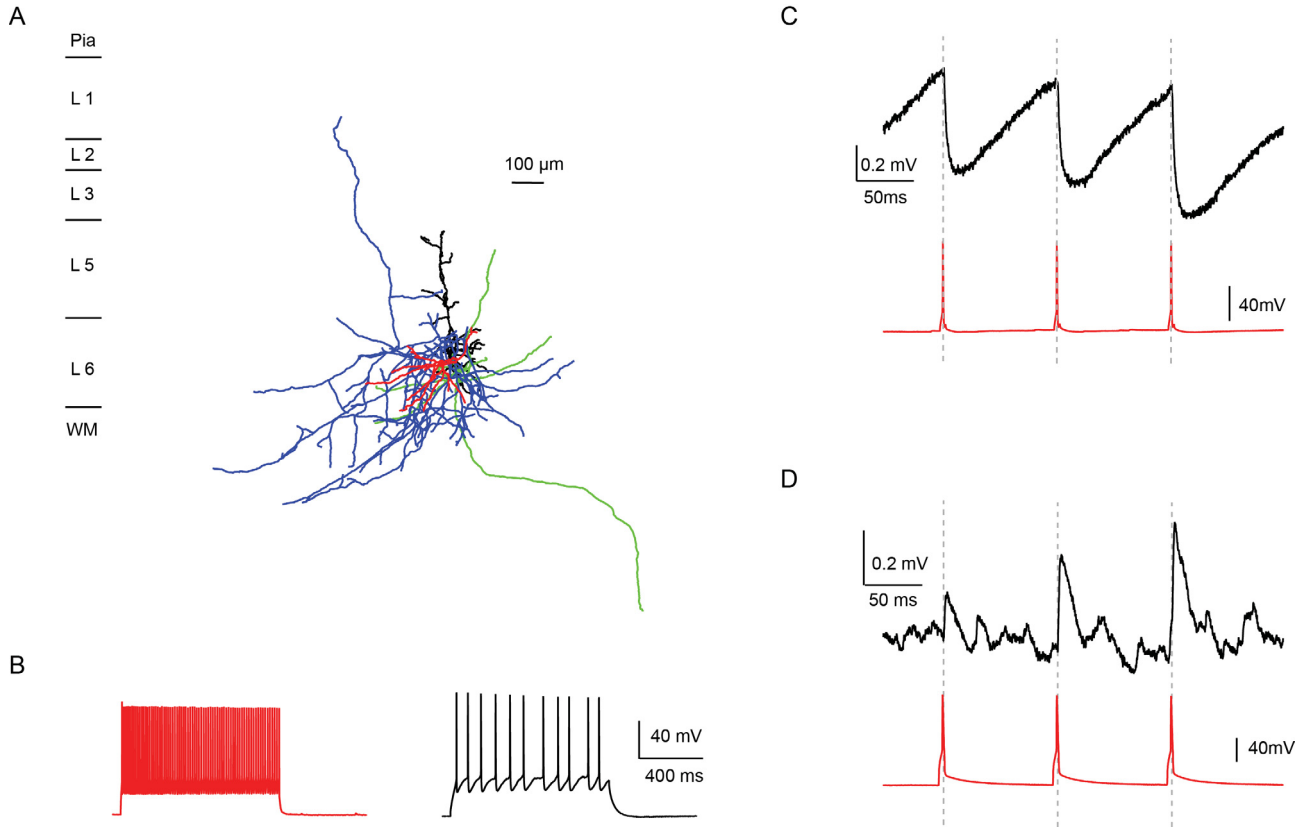


Fig. 3.2.9 Examples of a L6 reciprocal connection. (A). Morphological reconstruction of recorded reciprocal pair. Colour code as in Fig. 3.2.1. (B). Firing patterns of the FS interneuron (red) and Upright excitatory (black) neurons. (C). Average IPSPs (black, top) of postsynaptic excitatory neuron elicited by presynaptic APs (red, bottom). (D). Average EPSPs (black, top) of postsynaptic interneuron elicited by presynaptic APs (red, bottom).

They showed an average failure rate of $31.5 \pm 17.8\%$ and a CV of 0.63 ± 0.15 . The average amplitude, latency, 20-80% rise time and decay time of the postsynaptic unitary IPSP was 0.41 ± 0.32 mV, 0.9 ± 0.3 ms, 3.3 ± 1.7 ms and 44.6 ± 26.7 ms respectively. The mean PPR was calculated as 1.24 ± 0.44 (Table 3.2.4).

Only one FS-inverted excitatory neuron pair was recorded in whole-cell mode (example in Fig. 3.2.8 E-H). The amplitude of postsynaptic IPSP was 0.33 mV with a decay time of 66.0 ms. The failure rate was 27.0% and the CV was 0.51. The inter-soma distance between pre- and post-synaptic neurons was 249 μm . The 20-80% rise time and latency of the postsynaptic IPSP were 8.3 ms and 3.8 ms respectively, which might due to a distal location of the synaptic contacts.

Two reciprocal connections were found in this study and they were both connections between upright excitatory neurons and FS interneurons (example in Fig. 3.2.9).

3.3 Adenosine effects on excitatory neurons and microcircuits of mPFC

To investigate the effect of adenosine on single neuronal activity in the deep layers of mPFC, 103 excitatory neurons (including upright PNs, bipolar neurons, multipolar neurons, inverted PNs, horizontally oriented PNs and inverted bipolar neurons) located in L5 and L6 of mPFC were recorded in whole-cell mode using different pharmacological protocols. Neurons for which the series resistance was $>50 \text{ M}\Omega$ or changed by more than 25% during the experiment were excluded from the analysis. Adenosine was also applied during dual whole-cell recordings of 17 synaptically coupled neurons to study the impact of adenosine on synaptic transmission in L6 of mPFC.

Adenosine and the specific agonists and antagonists of adenosine receptors were bath-applied for 5-20 min and the membrane and synaptic properties of L6 neurons were measured before, during and after adenosine application. After the electrophysiological recordings, slices were fixed and processed for biocytin staining; neurons were subsequently reconstructed to analyse their morphology.

	Control	100 μM Adenosine	Wash out	<i>P</i>
L5 PNs (n=17)				
RMP (mV)	-62.5 ± 3.0 (n=36)	-65.9 ± 3.7 (n=36) / -65.1 ± 4.2 (n=22)	-61.2 ± 4.4 (n=22)	< 0.001 / < 0.001
Input resistance ($\text{M}\Omega$)	182 ± 66	174 ± 0.65	225 ± 129	0.42 / < 0.01
Time constant (ms)	36.7 ± 10.5	28.7 ± 5.6	43.3 ± 14.6	< 0.01 / < 0.001
Rheobase (pA)	85 ± 30	125 ± 66	95 ± 53	< 0.01 / < 0.05

Table 3.3.1 Adenosine (100 μM) modulation of passive properties of PNs in L5 of mPFC. *All data are given as mean \pm standard deviation. The number of cells for the calculation of the RMP is higher than for the other passive properties due to an uninterrupted continuous recording of the RMP in a subset of experiments. Two values of RMP were measured at the stable phase immediately after applying adenosine and before wash out, and were compared with control condition and wash out phase respectively. Paired t-tests was performed for the significant difference between two groups. Significant p-values is marked in bold. * $P < 0.05$, ** $P < 0.01$, *** $P < 0.001$.*

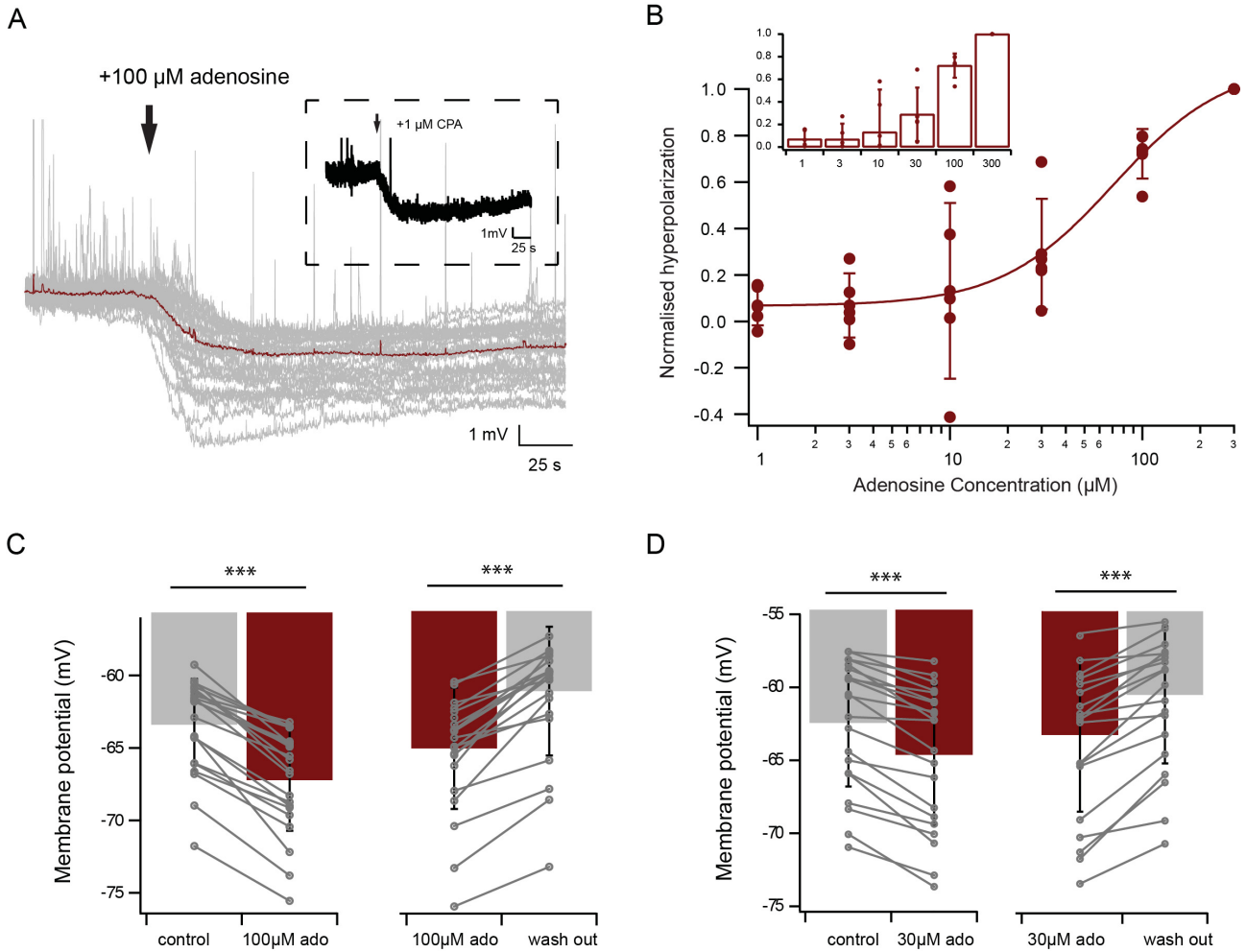


Fig. 3.3.1 Adenosine hyperpolarises the membrane potential of L5 pyramidal cells. (A) Example traces of the RMP during bath application of 100 μM adenosine (start at arrow). The average response is shown in dark red (n=36). Inset shows an example trace of RMP during application of 1 μM AA_1R agonist CPA. (B) Normalised dose-response curve and average responses (inset, normalised) for adenosine concentrations from 1 to 300 μM (n=5). (C) Average response of the RMP during application of 100 μM adenosine (n=36) and wash out phase (n=22). (D) Average response of the RMP during application of 30 μM adenosine (n=21) and wash out phase (n=21). Paired *t*-tests were performed to determine significant differences between two groups. * $P < 0.05$, ** $P < 0.01$, *** $P < 0.001$.

3.3.1 Adenosine modulates single neuron activities in L5 and L6

Effect of adenosine on the single neuron activities in L5

To investigate how adenosine modulates neuronal activity in the deep layers of mPFC, adenosine as well as the agonists and antagonists of its receptor subtypes were bath-applied during recordings from L5 PN. Bath application of 100 μM adenosine hyperpolarised the resting membrane potential (RMP) by on average 3.4 ± 1.6 mV [RMP: -62.5 ± 3.0 mV (control) vs. -65.9 ± 3.7 mV

(adenosine), $n=36$, paired t-test, $P < 0.001$]. This effect could be mimicked by bath application of $1 \mu\text{M}$ CPA, a specific $A_1\text{AR}$ agonist (Fig. 3.3.1A, Table 3.3.1). The size of the hyperpolarisation was dependent on the adenosine concentration ($\text{EC}_{50} 71.0 \pm 3.4 \mu\text{M}$, $n=5$, Fig. 3.3.1B). Already bath application of $30 \mu\text{M}$ adenosine hyperpolarised the RMP significantly from $-62.4 \pm 4.4 \text{ mV}$ to $-64.6 \pm 4.8 \text{ mV}$ ($n=21$, paired t-test, $P < 0.001$, Fig. 3.3.1D, Table 3.3.2).

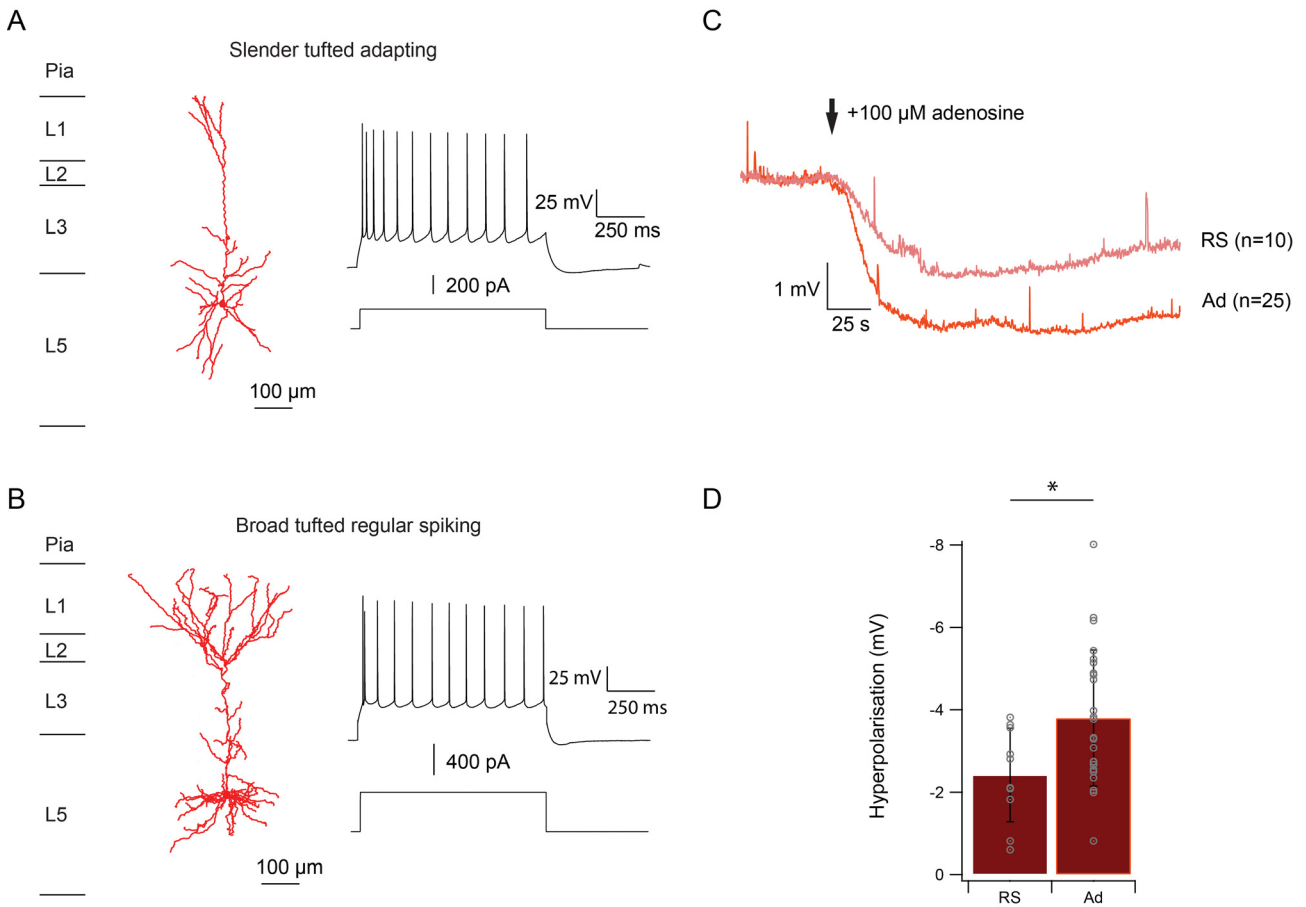


Fig. 3.3.2 Response size depends on the subtype of L5 PNs. (A) An example morphological reconstruction of soma and dendrites and electrophysiological profile of slender tufted adapting neuron. The AP firing response is shown when minimally 10 APs were elicited with corresponding current steps below. (B) An example morphological reconstruction of soma and dendrites and electrophysiological profile of broad tufted regular spiking neuron. (C) Average traces of the RMP during application of $100 \mu\text{M}$ adenosine (start at arrow) for the 2 subtypes of L5 PNs. (D) Adenosine-induced ($100 \mu\text{M}$) hyperpolarisation of the RMP for the two subtypes of L5 PNs. Tukey's test was performed for the significant difference between two groups. $*P < 0.05$.

Results

Adenosine application affected the passive membrane properties of L5 PN: Bath application of adenosine decreased the membrane time constant (36.7 ± 10.5 ms vs. 28.7 ± 5.6 ms, 100 μ M adenosine, $n=17$, paired t-test, $P < 0.01$) and input resistance (151 ± 92 M Ω vs. 118 ± 61 M Ω , 30 μ M adenosine, $n=20$, paired t-test, $P < 0.01$), probably by increasing the open probability of potassium channels. The rheobase current was significantly increased following adenosine application (100 μ M adenosine, 85 ± 30 pA vs. 125 ± 66 pA, $n=17$, paired t-test, $P < 0.01$, and 30 μ M adenosine, 149 ± 82 pA vs. 208 ± 106 pA, $n=20$, paired t-test, $P < 0.001$), suggesting that adenosine causes a reduction of cellular excitability (Table 3.3.1, Table 3.3.2).

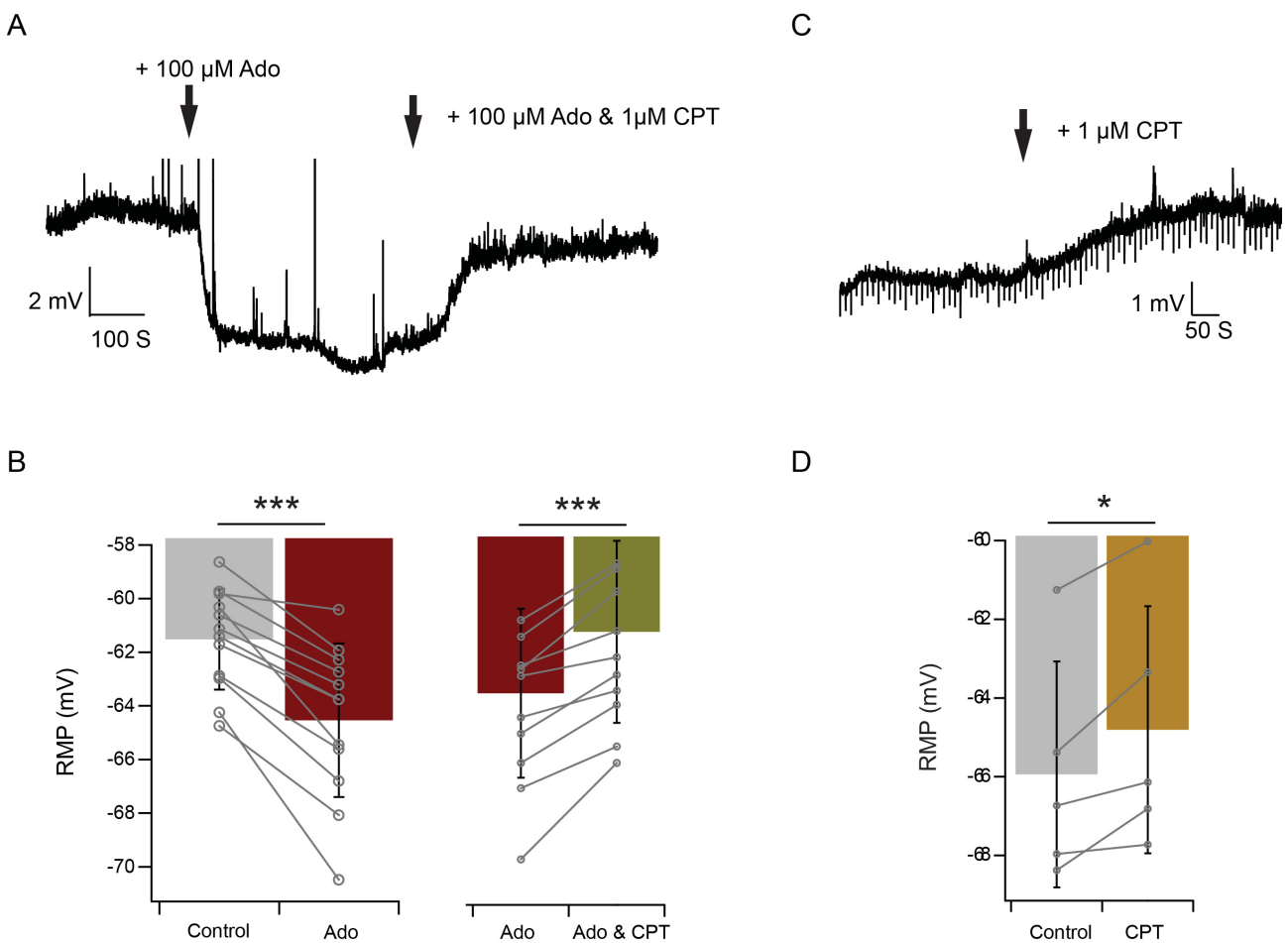


Fig. 3.3.3 Effects of AA₁R antagonist CPT to the membrane potential of L5 pyramidal cells.

(A) A voltage recording during bath application of adenosine and CPT. (B) Adenosine-induced (100 μ M) hyperpolarisation of the RMP and the change of RMP during co-applying adenosine and CPT (1 μ M) ($n=12$). (C) Voltage recording during bath application of CPT alone. (D) CPT-induced (1 μ M) depolarisation of RMP ($n=5$). Paired t-tests were performed to test for significant differences between the two groups. * $P < 0.05$, *** $P < 0.001$.

Results

	Control	30 μ M Adenosine	Wash out	P
L5 PNs (n=20)				
RMP (mV) (n=21)	-62.4 \pm 4.4	-64.6 \pm 4.8 / -62.9 \pm 5.1	-60.2 \pm 4.5	< 0.001 / < 0.001
Input resistance (M Ω)	151 \pm 92	118 \pm 61	127 \pm 69	< 0.01 / 0.07
Time constant (ms)	22.6 \pm 8.2	22.1 \pm 9.7	36.3 \pm 15.5	0.67 / < 0.001
Rheobase (pA)	149 \pm 82	208 \pm 106	155 \pm 86	< 0.001 / < 0.001
L6 excitatory neurons (n=5)				
RMP (mV)	-67.5 \pm 7.8 (n=20)	-71.0 \pm 7.4 (n=20) / -70.5 \pm 6.9 (n=6)	-67.4 \pm 7.6 (n=6)	< 0.001 / < 0.01
Input resistance (M Ω)	427 \pm 111	477 \pm 148	560 \pm 112	0.20 / < 0.05
Time constant (ms)	27.9 \pm 4.2	28.6 \pm 5.0	37.0 \pm 3.4	0.83 / 0.06
Rheobase (pA)	62 \pm 41	78 \pm 59	48 \pm 31	0.14 / 0.08

Table 3.3.2 Adenosine (30 μ M) modulation of passive properties of excitatory neurons in L5 and L6 of mPFC. All data are given as mean \pm standard deviation. The number of cells for calculating the resting membrane potential (RMP) is higher than for the passive properties to allow an uninterrupted continuous recording of the RMP in a subset of experiments. Two values of RMP were measured during the stable phase immediately after applying adenosine and before wash out, and were compared with control condition and wash out phase respectively. paired t-tests was performed for the significant difference between two groups. Significant p-values are marked in bold. * $P < 0.05$, ** $P < 0.01$, *** $P < 0.001$.

L5 PNs of mPFC were classified into two distinct subtypes according to their electrophysiological and morphological properties: Broad tufted neurons that respond to current injection with a regular spiking (RS), and slender tufted neurons that showed an adapting (Ad) firing pattern (Fig. 3.3.2 A&B). The size of adenosine-induced hyperpolarisation was dependent on the PN subtype. Compared with broad tufted RS pyramidal cells (n=10), slender tufted Ad pyramidal cells (n=25) showed a larger hyperpolarising response following bath application of 100 μ M adenosine (difference -3.8 \pm 1.7 mV vs. -2.4 \pm 1.1 mV, tukey's test, $P < 0.05$, Fig. 3.3.2 C&D). Thus, PNs in L5 of mPFC displayed a heterogeneous responsiveness to adenosine, with slender-tufted Ad neurons being more sensitive to adenosine modulation than broad-tufted RS neurons.

Results

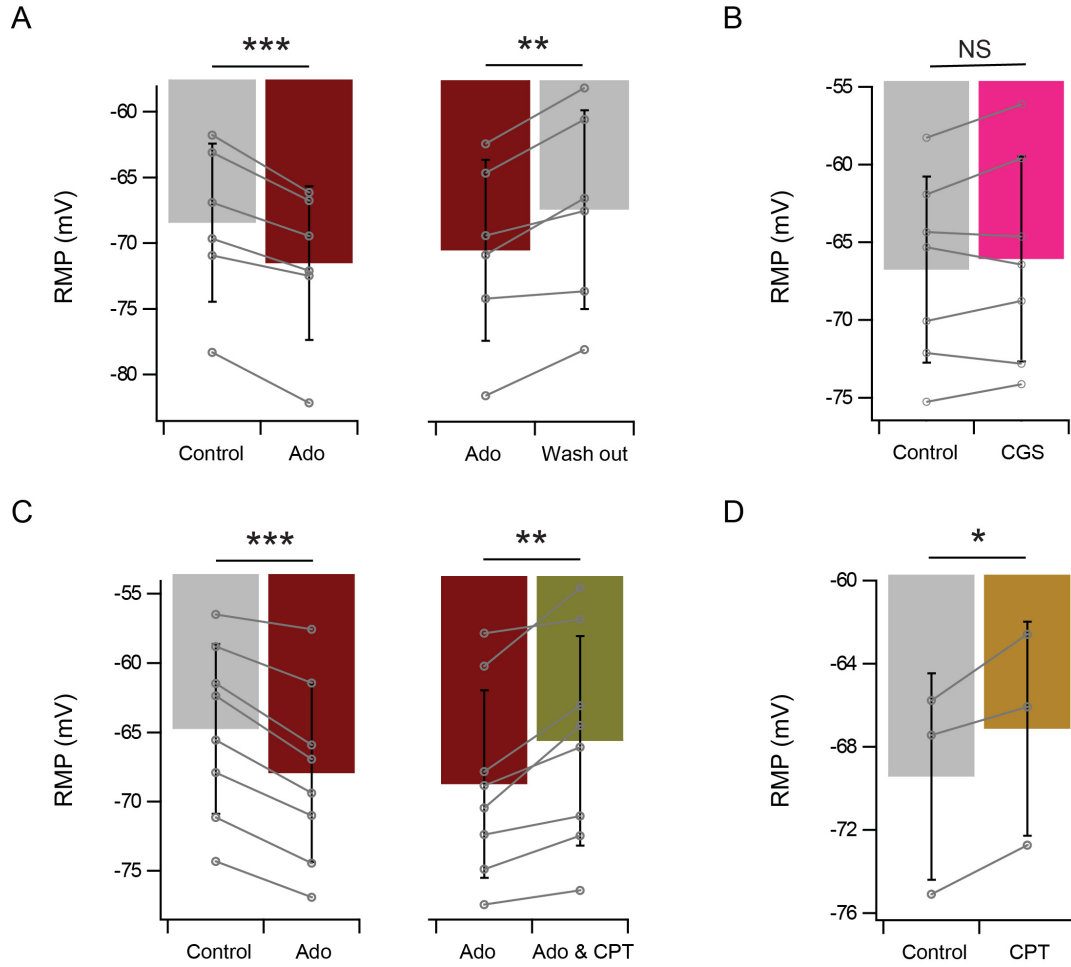


Fig. 3.3.4 Adenosine hyperpolarises the membrane potential of L6 excitatory neurons through A_1 ARs. (A) Average response ($n = 6$) of the RMP during application of 30 μ M adenosine. (B) Average response ($n = 7$) change of the RMP during application of 30 nM of the A_{2A} AR agonist CGS21680. (C) Average response ($n = 8$) of the RMP during application of 30 μ M adenosine, followed by co-application of 1 μ M the A_1 AR antagonist CPT. (D) Average response ($n = 3$) of the RMP during application of 1 μ M CPT. Paired t -tests was performed for the significant difference between two groups. * $P < 0.05$, ** $P < 0.01$, *** $P < 0.001$.

In addition, bath application of the A_1 AR antagonist CPT reversed the adenosine-induced hyperpolarisation to baseline level [RMP: -61.5 ± 1.9 mV (control) vs. -64.5 ± 2.9 mV (100 μ M adenosine), $n=12$, $P < 0.001$, and -63.5 ± 3.1 mV (100 μ M adenosine) vs. -61.3 ± 3.3 mV (100 μ M adenosine + 1 μ M CPT), $n=12$, $P < 0.001$, Fig. 3.3.3 A&B]. Interestingly, a significant depolarisation of the RMP was observed when CPT was bath applied alone [RMP: -65.9 ± 2.9 mV (control) vs. -64.8 ± 3.1 mV (1 μ M CPT), $n=5$, paired t -test, $P < 0.05$, Fig. 3.3.3 C&D] suggesting a tonic effect of adenosine.

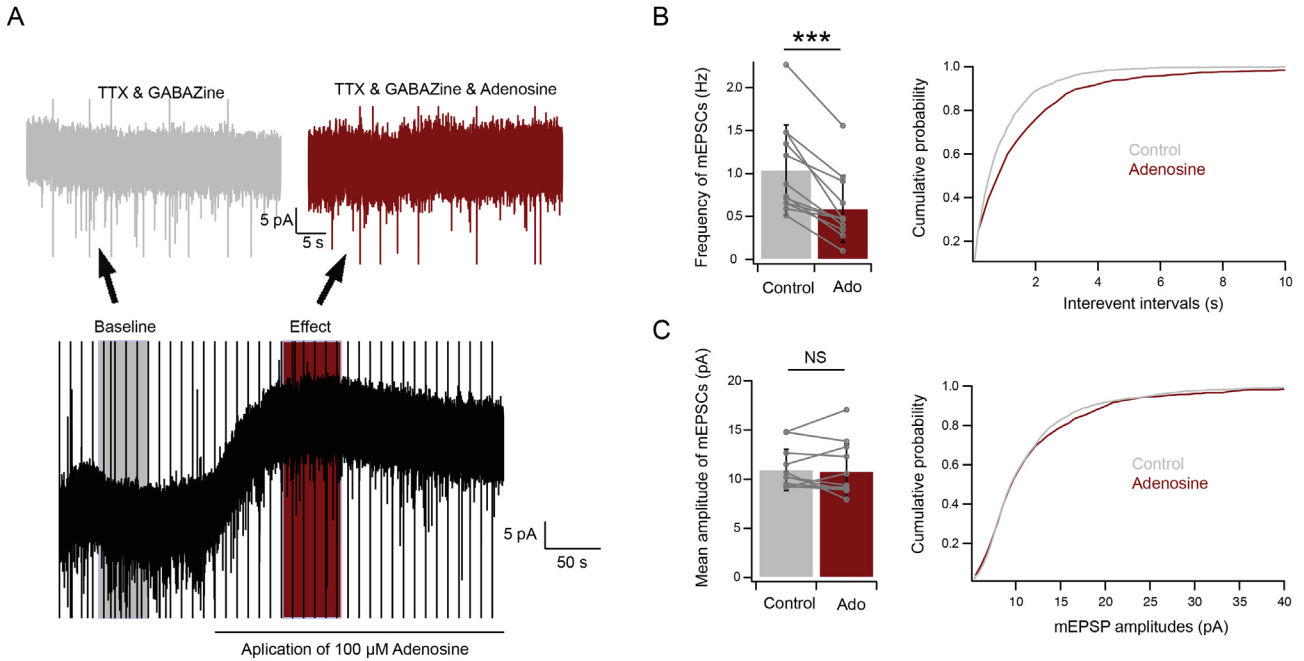


Fig. 3.3.5 Adenosine modulates miniature spontaneous synaptic activity of L6 excitatory neurons. (A) An example voltage-clamp recording of spontaneous activity during bath application of TTX (0.5 μ M), Gabazine (10 μ M) and adenosine (100 μ M). (B) An increase of the inter-event interval (IEI, right, 1114 samples for control and 626 samples for adenosine from 12 cells) and a decrease of mEPSC frequency (left, $n=12$) were observed during application of adenosine (100 μ M). (C) No significant difference in the mEPSC amplitudes was found during adenosine application (1126 samples for control and 637 samples for adenosine from 12 cells). Paired t -tests were performed for the significant difference between two groups. *** $P < 0.001$.

Adenosine effects on single neuron activity in L6

Similar experiments with adenosine and specific agonist and antagonist of the adenosine receptor subtypes were made with L6 excitatory neurons of mPFC. Bath application of 30 μ M adenosine hyperpolarised L6 excitatory neurons with an average amplitude of 3.4 ± 1.4 mV [RMP: -67.5 ± 7.8 mV (control) vs. -71.0 ± 7.4 mV (adenosine), $n=20$, paired t -test, $P < 0.001$, Table 3.3.2]. ‘Upright’ and ‘inverted’ excitatory neurons showed similar responses to adenosine [hyperpolarisation: 3.9 ± 1.5 mV (upright neurons, $n=10$) vs. 3.2 ± 1.2 mV (inverted neurons, $n=8$), Tukey’s test, $P=0.34$]. No significant difference of the RMP was found following bath application of 30 nM CGS21680, a specific A_{2A} AR agonist [RMP: -66.8 ± 6.0 mV (control) vs. -66.1 ± 6.4 mV (CGS21680), $n=7$, paired t -test, $P=0.24$, Fig. 3.3.4B]. Co-application of adenosine and CPT resulted in a return of the adenosine-induced hyperpolarisation to baseline [RMP: -64.8 ± 6.1 mV (control) vs. -67.9 ± 6.4

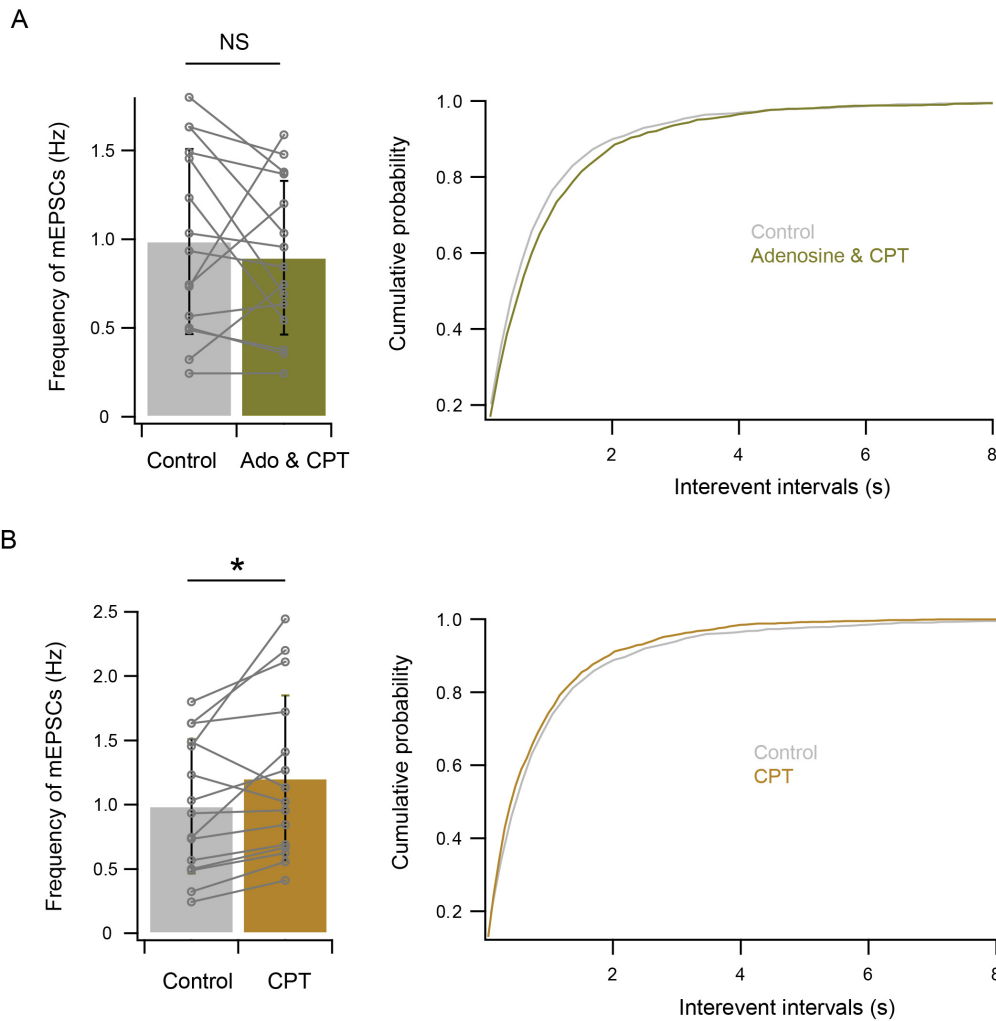


Fig. 3.3.6 Effects of adenosine A₁ receptor antagonist CPT to the miniature spontaneous synaptic activity of L6 excitatory neurons. (A) Adenosine-induced decrease of mEPSC frequency was recovered to the control level during co-applying adenosine (100 μ M) and CPT (1 μ M) ($n=15$). (B) A decrease of IEI (right, 1318 samples for control and 1447 samples for CPT from 15 cells) and an increase of mEPSC frequency (left, $n=15$) were observed during application of CPT (1 μ M) alone. Paired t -tests was performed for the significant difference between two groups. * $P < 0.05$.

mV (30 μ M adenosine), $n=8$, paired t -test, $P < 0.001$, and -67.5 ± 6.3 mV (30 μ M adenosine) vs. -64.6 ± 7.0 mV (30 μ M adenosine + 1 μ M CPT), $n=12$, paired t -test, $P < 0.01$, Fig.3.3.4C]. Bath application of CPT alone resulted in a depolarisation of the RMP in all tested L6 excitatory neurons of mPFC [RMP: -69.4 ± 5.0 mV (control) vs. -67.1 ± 5.2 mV (1 μ M CPT), $n=3$, paired t -test, $P < 0.05$, Fig. 3.3.4D].

Results

To test the presynaptic effect of adenosine, spontaneous postsynaptic activity of L6 excitatory neurons was recorded in voltage-clamp mode. In the presence of 0.5 μM TTX and 10 μM gabazine in the bath, miniature excitatory postsynaptic currents (mEPSCs) were recorded under control conditions and in the presence of adenosine. Bath application of 100 μM adenosine significantly reduced the frequency of mEPSCs from 1.0 ± 0.5 to 0.6 ± 0.4 ($n=12$, paired t-test, $P < 0.001$, Fig. 3.3.5A&B), which is reflected in an increase of inter-event interval from 0.9 ± 1.1 s to 1.6 ± 2.4 s (1114 events for control and 626 events for adenosine from 12 cells, Tukey's test, $P < 0.001$, Fig. 3.3.5B). No significant change in the amplitude of mEPSCs was observed [10.9 ± 2.1 pA (control) vs. 10.8 ± 2.8 pA (adenosine), $n=12$, paired t-test, $P = 0.70$, Fig. 3.3.5C], suggesting that adenosine modulates excitatory synaptic transmission largely via a presynaptic mechanism.

Co-application of 100 μM adenosine and 1 μM CPT completely blocked the adenosine-induced decrease of the mEPSCs frequency [0.99 ± 0.52 (control) vs. 0.90 ± 0.43 (adenosine + CPT), $n=15$, $P = 0.43$, Fig. 3.3.6A], indicating that adenosine inhibits neurotransmitter release at excitatory synapses by activating $A_1\text{ARs}$. Furthermore, an increase of mEPSCs frequency was found when CPT was applied without adenosine [1.0 ± 0.5 (control) vs. 1.2 ± 0.7 (1 μM CPT), $n=15$, $P < 0.05$, Fig. 3.3.6B], suggesting the existence of endogenous adenosine tone under the recording conditions.

n=9	Control	30 μM Adenosine	30 μM Adenosine & 1 μM CPT	P
EPSP amplitude (mV)	0.72 ± 0.60	0.17 ± 0.15	0.51 ± 0.52	< 0.01 / 0.06
Norm. EPSP amplitude	1	0.27 ± 0.18	0.68 ± 0.18	< 0.001 / < 0.01
Paired-pulse ratio (n=8)	0.87 ± 0.32	1.36 ± 0.58	0.94 ± 1.75 (n=7)	< 0.05 / 0.22
Coefficient variation	0.83 ± 0.48	1.21 ± 0.30	0.87 ± 0.28 (n=8)	< 0.05 / < 0.05
Failure rate (%)	24.9 ± 21.9	64.9 ± 14.2	26.5 ± 13.2 (n=8)	< 0.001 / < 0.001
Latency (ms) (n=6)	1.3 ± 0.5	1.4 ± 0.6	1.6 ± 0.5 (n=4)	0.34 / 0.86
20-80% rise time (ms) (n=7)	1.3 ± 0.4	1.4 ± 0.7	1.5 ± 0.6 (n=6)	0.43 / 0.77
Decay time (ms) (n=6)	39.1 ± 24.3	38.6 ± 40.1	52.0 ± 33.7 (n=5)	0.97 / 0.33

Table 3.3.3 EPSP properties of L6 excitatory connections under control, 30 μM adenosine and 30 μM adenosine & 1 μM CPT conditions. All data are given as mean \pm standard deviation. Paired t-tests were performed to determine whether the two groups were statistically significant different. P-values for significance are marked in bold. * $P < 0.05$, ** $P < 0.01$, *** $P < 0.001$.

3.3.2 Adenosine modulates excitatory synaptic transmission in L6

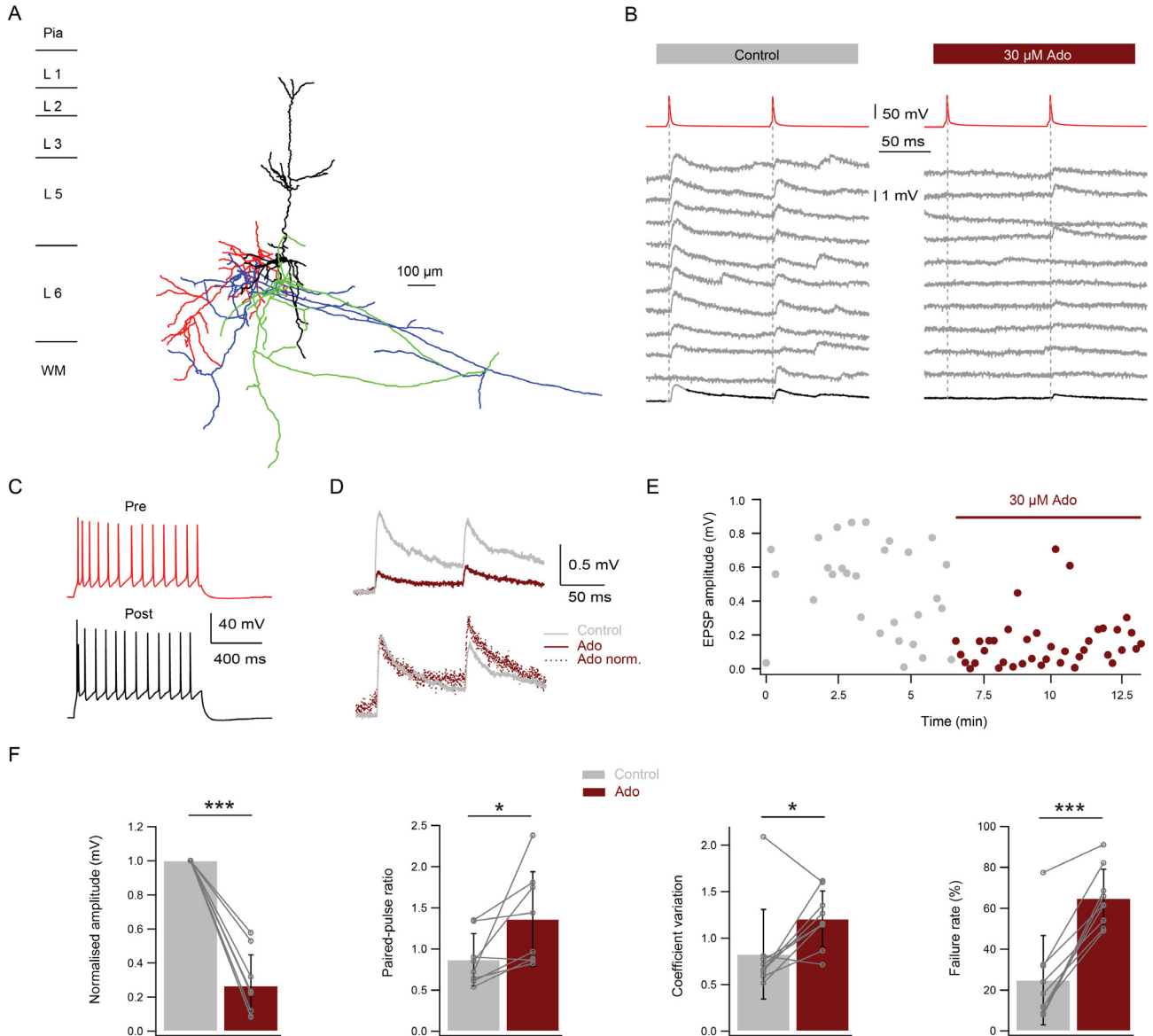


Fig. 3.3.7 Adenosine suppresses synaptic transmission of excitatory connections in L6 of mPFC. (A-E) Example recordings from an excitatory (inverted PN-upright PN) connection under control and adenosine (30 μ M) condition. (A) Morphological reconstruction of the recorded inverted PN-upright PN pair. Colour code as in Fig. 3.2.1. (B) Ten consecutive EPSPs (grey, middle) and average (black, bottom) elicited by presynaptic APs (red, top) under control and adenosine conditions. (C) Firing patterns of the pre- (red) and postsynaptic (black) neurons. (D) Overlay of average EPSPs. (E) Time course of EPSP amplitude change during application of adenosine. (F) Summary data ($n=9$, for PPR, $n=8$) of adenosine-induced changes in EPSP properties. Paired t -test, * $P < 0.05$, *** $P < 0.001$.

Results

	Control	10 μ M Adenosine	<i>P</i>
Inv.-pre connections (n=4)			
EPSP amplitude (mV)	0.87 \pm 0.86	0.49 \pm 0.51	0.15
Norm. EPSP amplitude	1	0.59 \pm 0.25	< 0.05
Paired-pulse ratio	0.74 \pm 0.31	0.83 \pm 0.09	0.54
Coefficient variation	0.72 \pm 0.27	0.84 \pm 0.03	0.38
Failure rate (%)	25.8 \pm 26.5	42.7 \pm 20.0	0.12
Upr.-pre connections (n=4)			
EPSP amplitude (mV)	0.16 \pm 0.12	0.02 \pm 0.02	0.09
Norm. EPSP amplitude (mV)	1	0.18 \pm 0.04	< 0.001
Paired-pulse ratio	1.49 \pm 0.57	3.1 \pm 3.37	0.36
Coefficient variation	1.06 \pm 0.30	0.96 \pm 0.07	0.55
Failure rate (%)	59.1 \pm 17.0	83.4 \pm 4.0	0.07

Table 3.3.4 EPSP properties of excitatory connections with different presynaptic neurons under control and 10 μ M adenosine conditions. *All data are given as mean \pm standard deviation. Paired t-tests were performed for the significant difference between two groups. Significant p-values is marked in bold. * $P < 0.05$, *** $P < 0.001$.*

Paired recordings were made from synaptically coupled L6 neurons in mPFC. For excitatory connections, the postsynaptic mean EPSP amplitude decreased from 0.72 ± 0.60 mV to 0.17 ± 0.15 mV (n=9, paired t-test, $P < 0.01$) while the paired-pulse ratio (PPR) increased from 0.87 ± 0.32 to 1.36 ± 0.58 (n=8, paired t-test, $P < 0.05$) following bath application of adenosine (30 μ M). Furthermore, the CV increased from 0.83 ± 0.48 to 1.21 ± 0.30 (n=9, paired t-test, $P < 0.05$) and the failure rate increased from 24.9 ± 21.9 % to 64.9 ± 14.2 % (n=9, paired t-test, $P < 0.001$). No significant changes in EPSP latency, 20-80% rise time and decay time were found, indicating that adenosine suppresses synaptic transmission of excitatory connections mainly via a presynaptic mechanism (Table 3.3.3, Fig.3.3.7).

Inverted and upright excitatory neurons display distinct characteristics with respect to their passive and active electrical properties, axonal projection pattern and neuronal connectivity. Although the connections established by an inverted excitatory neuron and an upright excitatory neuron showed no significant difference in their response to adenosine (30 μ M), we found that these two types of

Results

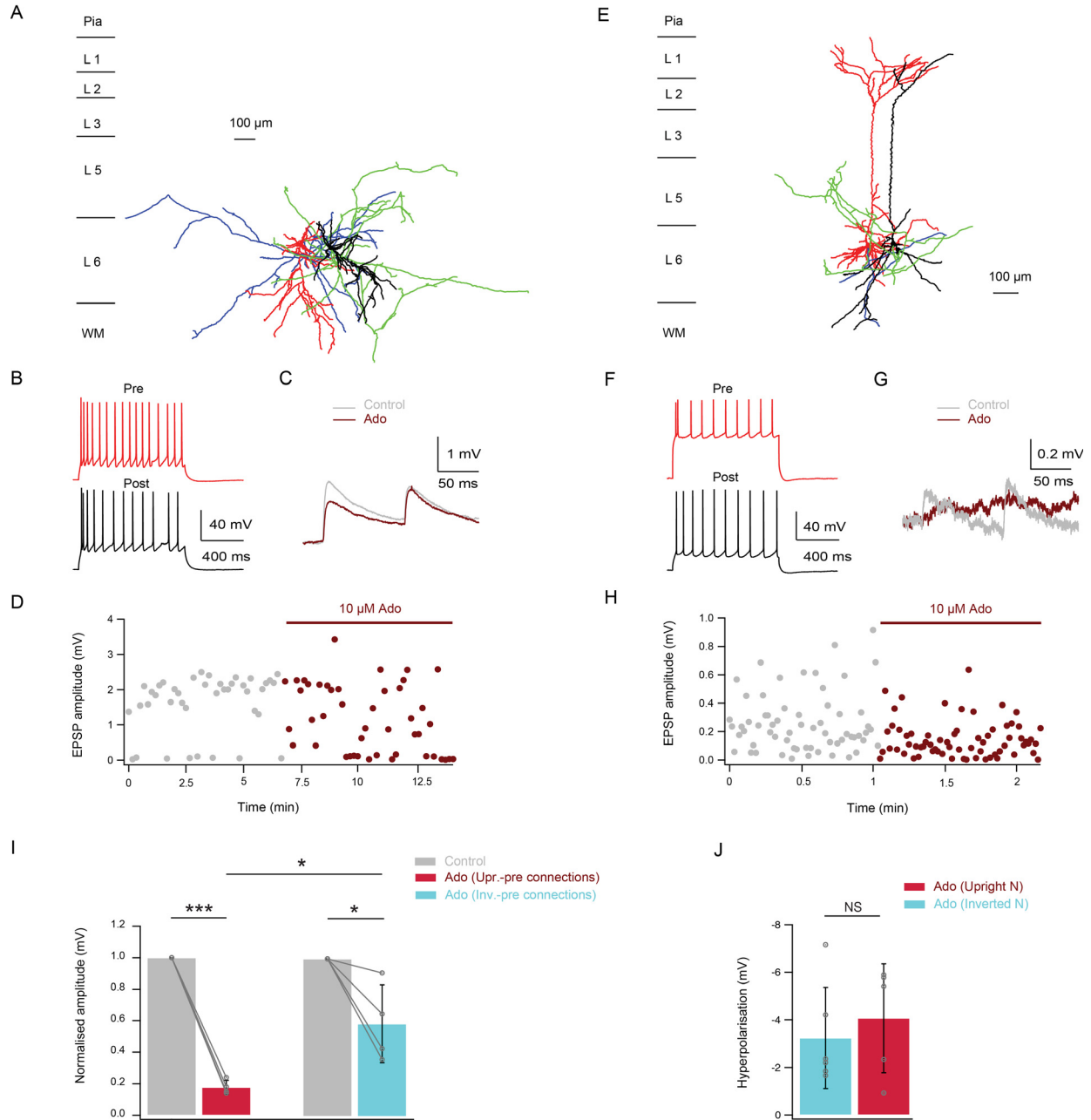


Fig. 3.3.8 Excitatory connections with different types of presynaptic neurons showed different sensitivities to a low concentration of adenosine. (A-D) Example recordings from an inverted-inverted PN connection under control and adenosine (10 µM) condition. (E-H) Example recordings from an upright PN-upright PN connection under control and adenosine (10 µM) condition. (A&E) Morphological reconstruction of recorded pair. Colour code as in Fig. 3.2.1. (B&F) Firing patterns of the pre- and postsynaptic neurons. (C&G) Overlay of average EPSPs. (D&H) Time course of EPSP amplitude change during application of adenosine. (I) Summary data ($n=4$ for each type) of adenosine-induced changes in EPSP amplitude. Paired t -test and Tukey's test were performed to determine significant differences between control and adenosine conditions, and between the two connection types. (J) Adenosine-induced (10 µM) hyperpolarisation of the RMP with two neuron types (inverted excitatory neurons, $n=6$, upright excitatory neurons, $n=5$). Tukey's test, $*P < 0.05$, $***P < 0.001$.

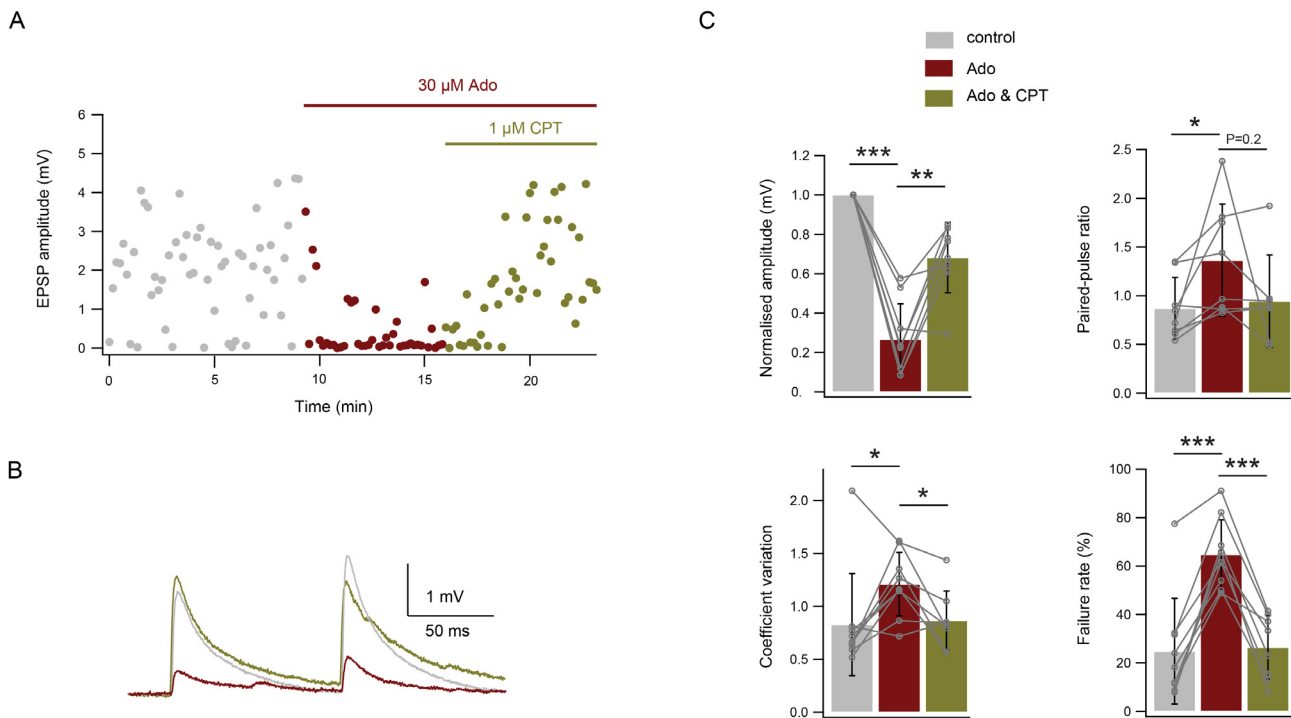


Fig. 3.3.9 Adenosine modulates synaptic transmission of excitatory connections in L6 of mPFC through A₁ARs. (A) Time course of EPSP amplitude change from an excitatory connection during application of adenosine (30 μ M) and A₁AR antagonist CPT (1 μ M). (B) Overlay of average EPSPs under control, adenosine and adenosine&CPT condition. (C) Summary data ($n=9$ for adenosine and $n=8$ for adenosine&CPT, for PPR, $n=8$ and $n=7$) of EPSP properties under control, adenosine and adenosine&CPT condition. Paired t -test, * $P < 0.05$, ** $P < 0.01$, *** $P < 0.001$.

connections reacted differently to a low concentration of adenosine. Bath application of 10 μ M adenosine decreased the amplitude of the unitary EPSP at connections with a presynaptic inverted excitatory neuron to $59 \pm 25\%$ of control level ($n=4$, paired t -test, $P < 0.05$). The amplitude of postsynaptic EPSP at connections with a presynaptic upright excitatory neuron was reduced to $18 \pm 4\%$ of control level ($n=4$, paired t -test, $P < 0.001$) after applying the same adenosine concentration, which was significantly lower compared with the connections established by a inverted excitatory neuron ($n=4$, Tukey's test, $P < 0.05$, Fig. 3.3.8, Table 3.3.3). The postsynaptic membrane potential was measured simultaneously and no difference in the size of adenosine-induced hyperpolarisation was found between these two neuron types (Fig. 3.3.8). These findings suggest that the presynaptic terminals of upright excitatory neurons are more sensitive to low concentration of adenosine compared to those of inverted excitatory neurons.

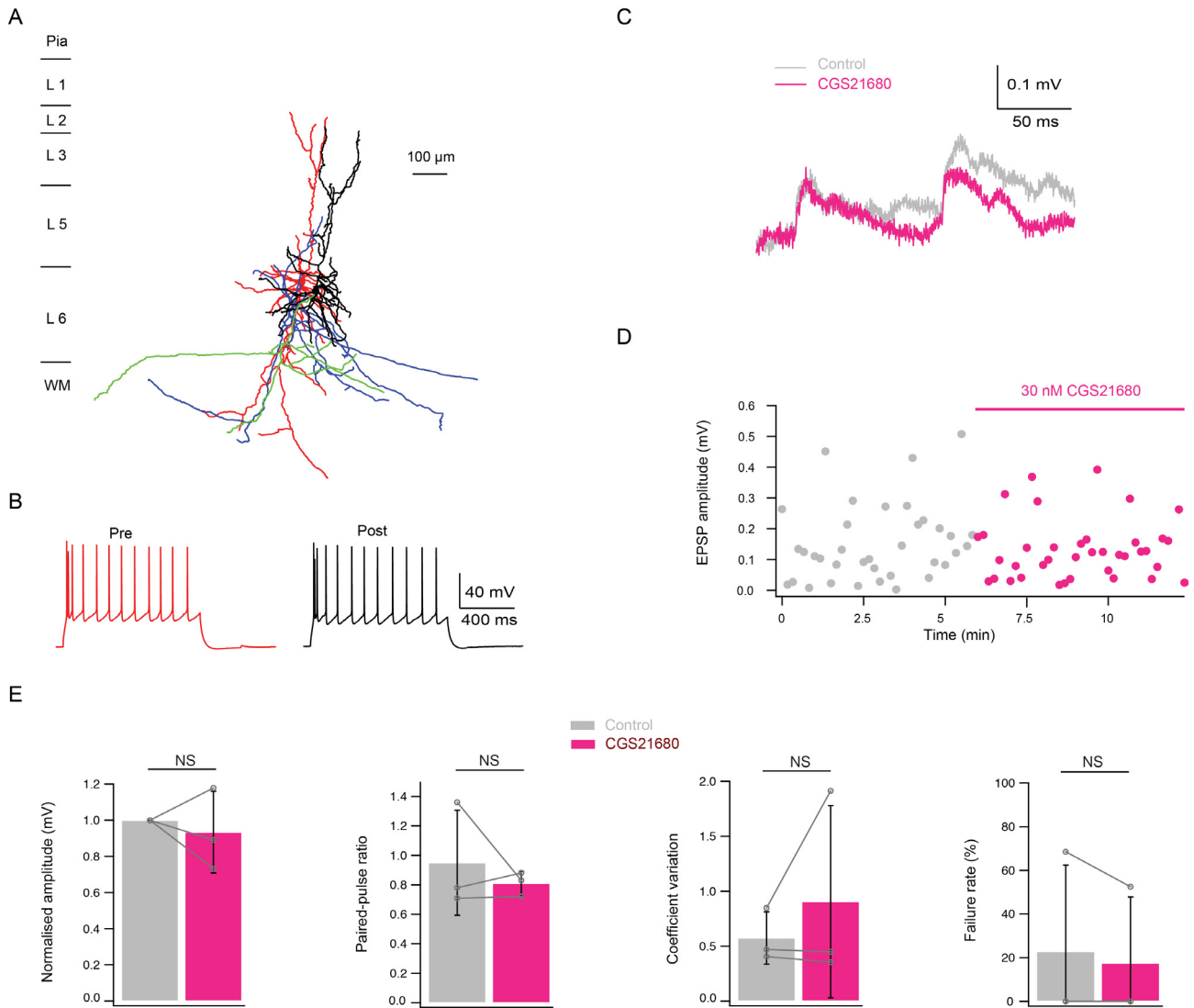


Fig. 3.3.10 Effect of CGS21680 on the excitatory connectivity. (A-D) Example recordings from an excitatory (inverted bipolar neuron-upright PN) connection under control conditions and in the presence of the A_2A AR agonist CGS21680 (30 nM). (A) Morphology of the recorded E-E neuron pair. Colour code as in Fig. 3.2.1. (B) Firing patterns of the pre- (red) and postsynaptic (black) neurons. (C) Overlay of the average unitary EPSPs under control and CGS21680 (30 nM) condition. (D) Time course of EPSP amplitude change during application of CGS21680. (E) Summary data of CGS21680-induced changes in EPSP properties. Paired t-test.

Single cell recordings had shown that adenosine changed the membrane properties through activation of A_1 ARs. To investigate whether the adenosine effect on synaptic transmission is induced by A_1 AR activation, CPT (1 μ M) was co-applied with adenosine (30 μ M) after adenosine had been applied alone. The effect of adenosine on excitatory connections was blocked and recovered from $27 \pm 18\%$ to $68 \pm 18\%$ of the control level ($n=9$, paired t-test, $P < 0.01$). Co-

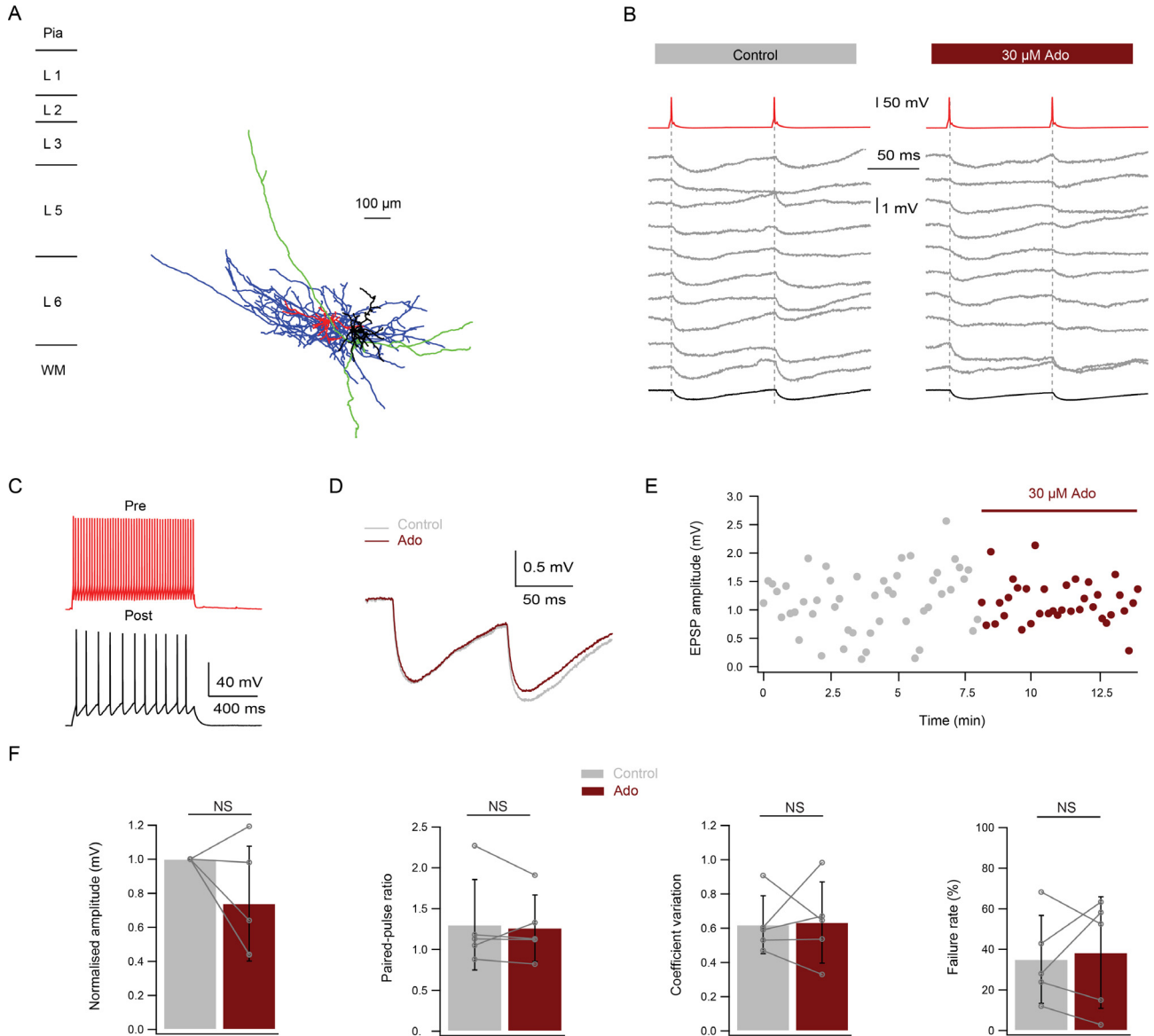


Fig. 3.3.11 Effect of adenosine on the inhibitory connectivity. (A-E) Example recordings from an inhibitory (FS-upright PN) connection under control and adenosine (30 μ M) condition. (A) Morphological reconstruction of the recorded FS-upright PN pair. Colour code as in Fig. 3.2.1. (B) Ten consecutive IPSPs (grey, middle) and average (black, bottom) elicited by presynaptic APs (red, top) under control and adenosine conditions. (C) Firing patterns of the pre- (red) and postsynaptic (black) neurons. (D) Overlay of the average IPSPs. (E) The time course of the IPSP changed during application of adenosine. (F) Summary data of adenosine-induced changes in IPSP properties. Paired *t*-test, *n*=5.

application of adenosine and CPT also blocked the adenosine-induced changes on other EPSP properties [CV: 0.83 ± 0.48 (control, *n*=9) vs. 1.21 ± 0.30 (30 μ M adenosine, *n*=9) vs. 0.87 ± 0.28 (30 μ M adenosine and 1 μ M CPT, *n*=8), paired *t*-test, *P* < 0.05; Failure rate: $24.9 \pm 21.9\%$ (control,

Results

n=9) vs. $64.9 \pm 14.2\%$ (30 μ M adenosine, n=9) vs. $26.5 \pm 13.2\%$ (30 μ M adenosine and 1 μ M CPT, n=8), Table 3.3.3, Fig. 3.3.9]. This suggests that adenosine decreases the neurotransmitter release probability via activation of presynaptic A₁ARs.

To investigate whether A_{2A}ARs also participate in the adenosine-induced effects on synaptic transmission, 30 nM of the specific A_{2A}AR agonist CGS21680 was bath-applied during recordings of excitatory connections. Synaptic properties related to the release probability at excitatory connections were not changed by CGS21680 (Fig. 3.3.10). Single cell recordings revealed no change of postsynaptic resting membrane potential following bath application of CGS21680. Taken together, these results indicate a low A_{2A}AR expression in L6 of mPFC.

The effect of adenosine was also tested during recordings of inhibitory connections between a (presynaptic) inhibitory neurons and excitatory neurons. No significant differences in the unitary IPSP amplitude [0.51 ± 0.40 mV (control) vs. 0.39 ± 0.42 (30 μ M adenosine), paired t-test, $P=0.16$, Fig. 3.3.11] and other synaptic properties were found, indicating that adenosine does not affect inhibitory synaptic transmission at these connections.

4. Discussion

4.1 Classification of excitatory neurons in L6 of mPFC

L6 excitatory neurons show a high degree of morphological diversity in all neocortical areas including the mPFC (Yang et al. 1996; Zhang and Deschenes 1997; Kumar and Ohana 2008; Thomson 2010; Marx and Feldmeyer 2013; van Aerde and Feldmeyer 2013). However, only few studies have attempted a quantitative classification of L6 neurons and none focussed exclusively on the classification of excitatory neurons in L6 of mPFC. In this study, we performed an unsupervised CA based on neuronal dendritic morphology, which classified the excitatory neurons in L6 of mPFC in an objective and quantitative way. Following morphological reconstructions, neurons were grouped into two major categories: upright excitatory neurons with their primary or apical dendrites spanning superficial layers and terminating in L5 to L1 and inverted/horizontally oriented neurons, which had principal dendrites pointing towards the WM or oriented sideways. Upright excitatory neurons were further subdivided into six subgroups including broad tufted PNs, slender tufted PNs, untufted PNs, short PNs, multipolar neurons and normal bipolar neurons. Inverted excitatory neurons were further classified into two subgroups: inverted/horizontally oriented PNs and inverted bipolar neurons. Because the classification of excitatory neurons was mainly based on the properties of their principal dendrites, we had to name a dendrite of multipolar neurons ‘principal dendrite’, which in this case, was the dendrite projecting towards superficial layers. For bipolar neurons, we have defined the ‘principal dendrite’ and ‘secondary dendrite’ basing on their morphological appearance (Fig. 3.1.3). We classified them into two subgroups i.e. ‘normal bipolar neurons’ and ‘inverted bipolar neurons’ respectively. Nevertheless, by further subdividing the two main clusters into eight subclusters, multipolar and bipolar neurons were then easily distinguished from other subgroups of PNs.

In the cerebral cortex the incidence of inverted PNs is only 1% of rat (Parnavelas et al. 1977) and this fraction changes through species and area (up to 8.5%) (Globus and Scheibel 1967; Qi et al. 1999; Mendizabal-Zubiaga et al. 2007). They are most numerous in L5 and L6 in all studied species (Mendizabal-Zubiaga et al. 2007) and the percentage of inverted PNs in L6B of rat somatosensory cortex was found to be around 10% (Marx and Feldmeyer 2013). In our study, the cluster 2 - ‘inverted excitatory neurons’ include the inverted PNs, horizontally oriented PNs and bipolar inverted neurons. With the 79 mPFC L6 excitatory neurons, they consists of 31 neurons, i.e. 39% of

the total population. Inverted PNs represent 32% of the total number in the classification with exclusion of 5 bipolar inverted neurons and one horizontally oriented PN. Some neurons used for CA are from the paired recordings experiments; it appears that inverted excitatory neurons and upright excitatory neurons show different preference in forming synaptic connections. After omitting all the presynaptic neurons, about 31% of 71 randomly patched neurons are inverted PNs. This high incidence of inverted PNs in mPFC suggests that they might play an important role in the L6 microcircuitry of mPFC.

In addition to differences in morphology, upright excitatory neurons and inverted excitatory neurons in somatosensory cortex also display distinct passive and active physiological properties, such as resting membrane potential, input resistance, action potential threshold and half width (Steger et al. 2013). These electrophysiological differences were observed also in mPFC when comparing the electrophysiological properties of the two morphological clusters. Although all the excitatory neurons in L6 are unique with their high cellular input resistance resulting in a high excitability (van Aerde and Feldmeyer 2013), inverted excitatory neurons have more a depolarised resting membrane potential and AP threshold, larger membrane input resistance and time constant, longer AP halfwidth, smaller rheobase and average ISI compared to upright excitatory neurons. Differences between inverted excitatory neurons and upright excitatory neurons in resting membrane potential and input resistance suggest a potential difference in the distribution of ion channels that determine intrinsic electrophysiological properties, such as the potassium leak channel (Lesage 2003). Differences in AP threshold and AP halfwidth may result from a difference in ion channels contributing to action potential initiation and repolarisation such as voltage-gated sodium channel and potassium channel types, which will also affect the AP firing frequency (Miller et al. 2008). The dendritic arborisation of the different L6 excitatory neuron types may explain how a neuron integrates incoming signals and therefore affect the AP firing properties. It has been found that in some cases, neurons with different dendritic domains also display distinct firing pattern (Mainen and Sejnowski 1996; Gullledge et al. 2005; van Aerde and Feldmeyer 2013). However, here we did not find a correlation between dendritic morphology and electrophysiological firing pattern with L6 excitatory neurons. Our findings regarding the morphological and intrinsic physiological properties indicate that inverted excitatory neurons are a unique class of neurons, which could therefore play a special role in the L6 microcircuitry of mPFC.

4.2 Classification of inhibitory neurons in L6 of mPFC

GABAergic interneurons in mPFC play an important role in diverse higher order cognitive functions (Lu et al. 1994; Sohal et al. 2009; Gaykema et al. 2014). The heterogeneity of interneurons, with respect to morphology, electrophysiology and expression of molecular markers has been characterised in detail in different cortical layers and areas (Cauli et al. 1997; Markram et al. 2004; Ascoli et al. 2008; Helmstaedter et al. 2009; Rudy et al. 2011; DeFelipe et al. 2013; Koelbl et al. 2015; Tremblay et al. 2016; Arzt et al. 2017; Emmenegger et al. 2018; Feldmeyer et al. 2018). However, the structural and functional properties of mPFC interneurons are less well known.

The axonal and dendritic characteristics are largely stable parameters and therefore eminently suitable for classifying interneurons. However, the intrinsic electrical excitability can be predicted only in part by the dendritic geometry (Mainen and Sejnowski 1996; Helmstaedter et al. 2009). Morphological parameters of axons are considered to be the most functionally relevant and meaningful neuronal properties, as they define the innervation domains and enable a reliable prediction of synaptic connectivity. The axonal projection pattern provides information about the potential connectivity and density of synaptic contacts, which cannot be acquired using other methods (Lubke et al. 2003; Helmstaedter et al. 2009; Feldmeyer D 2010; Qi et al. 2015; Emmenegger et al. 2018). In this study, an unsupervised CA based on the axonal projection patterns was performed, resulting in three clusters that showed distinct functionally relevant projection patterns.

Our data showed that L6 interneurons have the potential to differentially innervate neurons from various cortical layers. L1 inhibitors vertically project their axons and show a high axonal distribution in L1-L3 (41%). They are referred to as Martinotti-like cells, which have been described in L6 and form innervation to L1 (Ferrer et al. 1986; Prieto and Winer 1999; Wang et al. 2004; Arzt et al. 2017). The fraction of these neuron type has been estimated as 16.5% in the somatosensory cortex (Wang et al. 2004). We found three mPFC L1 inhibitors (Martinotti-like neurons) in our unbiased sample of 38 L6 interneurons (7.9%), a percentage similar to reported in a recent study on L6 interneurons in somatosensory cortex (Arzt et al. 2017). However, the potential truncation of the L1 projecting, tufted axons during the slice preparation cannot be excluded, so that

the incidence of the projections in the superficial layers and the vertically projecting Martinotti-like neurons may therefore be underestimated.

Apart from L1 inhibitors, most L6 interneurons have their innervated targets in L5 and L6 reflecting from more than 80% innervation domain of the axons. It should be noted that neurons of the same cluster often display rather heterogeneous axonal domains. In general, 49% of the axon of L5 inhibitors resides in L5. However, depending on the location of the cell body, the axonal distributions in L6 ranged from 5% to 81% (average 47%). The axon of L6 inhibitors is mainly located in L6 (84%) with some collaterals in the WM (11%) and only a few in L5 (4%); these interneurons also have a large horizontal axonal field span indicating that they provide intralaminar inhibition.

In mPFC, L6 interneurons also show a large diversity in their electrophysiological properties. As we have only 18 neurons that matched our criteria for a full electrophysiological analysis, it is difficult to categorise them taking all the electrophysiological parameters into account. We used only single AP properties and firing properties that we considered to be most relevant for performing a CA based on the electrophysiology of L6 interneurons. Two clusters of L6 interneurons were acquired and we named them FS and nFS interneurons. Our data indicates that L1 inhibitors in the morphological CA are all nFS, while L5 inhibitors and L6 inhibitors are all FS interneurons. This suggests that the correlation between morphology and intrinsic neuronal physiology of interneurons may exist in this area. However, considering that only less than half of the L5 inhibitors and L6 inhibitors have the qualified electrophysiological data, nFS interneurons may also exist in these 2 morphological clusters.

In line with studies in somatosensory cortex (Katzel et al. 2011; Arzt et al. 2017), our results on the L6 interneuron classification suggest that inhibitory interneurons in L6 of mPFC predominately innervate L6 and L5, while connections to neurons in more superficial layers are very sparse.

4.3 Monosynaptic connections in L6 of mPFC

The connectivity ratio between L6 neurons was estimated to be about ~6.5% in rat barrel cortex (Yang and Feldmeyer, unpublished observations), which is remarkably lower than that found for

neurons in superficial layers (Beierlein and Connors 2002; Mercer et al. 2005; West et al. 2006; Crandall et al. 2017). In this study, the connectivity ratio was found to be only 3.1% and thus considerably lower than that reported for somatosensory cortex.

The strength of a connection is related to the number of synaptic contacts, the quantal size and the synaptic release probability, which is reflected in the unitary PSP amplitude, paired pulse behaviour, failure rate and CV (Branco and Staras 2009). The short-term plasticity of synaptic connections can be characterised by the paired pulse behaviour, i.e. the change in PSP amplitude during consecutive stimulation at a fixed interval (e.g., 100 ms). Previous studies in rat somatosensory cortex have shown that PPR, CV and failure rate are inversely related to the unitary PSP amplitude and paired pulse facilitation, small PSP amplitude, high failure rate and large CV normally signify a low release probability (e.g. Feldmeyer et al. 1999; Feldmeyer et al. 2002; Qi and Feldmeyer 2016). Despite of the difference in connections types, the connections we found in L6 of mPFC generally follow this rule as well.

Although connections between excitatory neurons provide the majority of intracortical and extracortical projections, most E-E connection are very weak (Thomson and Deuchars 1997; Reyes and Sakmann 1999; Thomson et al. 2002). With our 12 E-E connections in L6 of mPFC, more than half of them showed a postsynaptic unitary EPSP < 0.2 mV, indicating a low release probability. The mean EPSP amplitude of the weakest connection we were able to detect was lower than 20 μ V. We were able to determine the morphology of 10 E-E connections and found that homologous connections (i.e. those between similar neuron types) are more frequent than heterologous ones. Similar results were found in L4 of rat somatosensory cortex (Feldmeyer et al. 1999; Feldmeyer 2012). Two pairs were established from inverted excitatory neurons to upright excitatory neurons and 4 of them are connections between inverted excitatory neurons. Unlike inverted excitatory neurons, upright excitatory neurons were found to form synaptic connections with upright excitatory neurons only ($n=4$), and their connectivity ratio was low while we found both weak and strong connections with a presynaptic inverted neuron. A recent study has shown that as postsynaptic neurons, inverted excitatory neurons and upright excitatory neurons displayed no differences in the EPSP properties such as amplitude, latency and rise time (Steger et al. 2018). In contrast, we found that inverted-pre connections had significantly larger mean unitary EPSP

amplitudes than upright-pre connections. Morphological reconstructions of the axons of these two cell types may explain this phenomenon because inverted excitatory neurons have a larger axonal field span and density within L6, so that the probability of forming synaptic contacts with other L6 neurons is higher.

In contrast to the high fraction of inverted excitatory neurons in the E-E connections (six out of ten connections have a presynaptic inverted excitatory neurons), of five E-I connections, we had found only 1 connection with a presynaptic inverted excitatory neuron. This implies that inverted excitatory neurons are the primary neuronal type to form excitatory intralaminar synaptic connections, but with only network between excitatory neurons. However, considering the small sample size, this needs to be confirmed in the future work. In only one E-I connections established by an upright neuron the postsynaptic neuron was an L6 nFS interneuron. This upright PN-nFS connection was weak and unreliable with an extremely small EPSP amplitude (0.02 mV) and a high failure rate of 84%, which is probably due to a low neurotransmitter release probability.

Short-term plasticity are resulting from a combination of synaptic properties, such as vesicle depletion and accumulation of calcium in the presynaptic terminal and the desensitisation of neurotransmitter receptors at the postsynaptic site (Zucker and Regehr 2002; Thomson 2003; Abbott and Regehr 2004; Regehr 2012). Previous studies on the unitary synapses established by excitatory neurons onto interneurons have hypothesised that short-term plasticity of those excitatory synapses depend on the postsynaptic neuron type (Thomson 1997; Markram et al. 1998). Connections established by upright excitatory neurons displayed short-term facilitation, irrespective whether the postsynaptic neuron is FS interneuron or nFS interneuron. Conversely, the only pair between a presynaptic inverted neuron and a FS interneuron showed short-term depression. The exact mechanism behind this short-term plasticity is still unclear. Upright excitatory neurons and inverted excitatory neurons may interact differently with interneurons at the synaptic site and induce structural or/and functional changes resulting in a different short-term plasticity.

It has been described above that most of the FS interneurons have a local innervation domain, whereas nFS interneurons often possess axonal collaterals that project to superficial layers. This is in line with our findings on L6 inhibitory connections. We acquired six inhibitory connections and

all of them were formed by presynaptic FS interneurons. Taking all connection types into account, we had found only two reciprocal connections and they were both connections between a FS interneurons and an upright excitatory neuron, which may due to their high incidence (39% for upright excitatory neuron and 44% for FS interneurons) in E-I and I-E connections.

Our findings regarding monosynaptic connections in L6 of mPFC provide a first insight into the complex organisation of the local L6 microcircuitry and reveal distinct synaptic and network features of different types of synaptic connections.

4.4 Adenosine modulation on cortical microcircuitry of mPFC

The classic view is that cellular excitability of the PNs is suppressed in the presence of elevated concentrations of adenosine acting via G_i -coupled A_1ARs . Activation of these receptors leads to the opening of K_{ir} channels (Gerber et al. 1989; Luscher et al. 1997; van Aerde et al. 2013; Qi et al. 2017) and/or blocking of HCN channels (Rainnie et al. 1994). Adenosine did not affect the membrane properties of inhibitory neurons, indicating no or very low expression of A_1ARs (Rivkees et al. 1995; Ochiishi et al. 1999; Qi et al. 2017). A previous study on the effects of adenosine in prefrontal cortex indicated that instead of exerting a general inhibitory tone on the cortical network, adenosine is modulating different PN types in a specific and distinct way (van Aerde et al. 2013).

For L5 of mPFC, a number of studies had described a differential responsiveness of PN subtypes to neuromodulators such as serotonin, dopamine, adrenaline and acetylcholine (Beique et al. 2007; Dembrow et al. 2010; Avesar and Gullledge 2012; Gee et al. 2012; Seong and Carter 2012). In general, slender tufted L5 PNs are characterised by adaptive firing pattern, high membrane input resistance, low voltage sags and axonal projections to the contralateral cortex and striatum. Broad tufted PNs on the other hand display regular spiking firing pattern, low membrane input resistance, large voltage sags and axonal projections to the thalamus or brainstem (Wang et al. 2006; Otsuka and Kawaguchi 2008; Dembrow et al. 2010; Avesar and Gullledge 2012). Here we found that slender tufted L5 PNs are more sensitive to adenosine than broad tufted PNs, reflecting a larger hyperpolarisation during adenosine application (van Aerde et al. 2013). This indicates that slender

tufted PN are more readily down regulated during high cortical activity and energy consumption and moreover, these two subtypes of L5 PNs may play different roles during adenosine signalling.

The heterogeneity of the adenosine responsiveness was not observed with the subtypes of excitatory neurons in L6 of mPFC. However, apart from examining changes in basic membrane properties during adenosine application, we also performed an analysis of the miniature spontaneous activity in L6 excitatory neurons of the mPFC. Adenosine dramatically decreased the frequency of mEPSCs via the activation of A₁ARs, whereas no changes of mEPSP amplitude was observed. Synaptic inputs onto L6 excitatory neurons are originating from the thalamus or from interlaminar and intralaminar areas. Our finding suggests adenosine exerts its inhibitory effect via adenosine receptors at the presynaptic terminals and reduces the neurotransmitter release probability in those cortical and subcortical areas (Fontanez and Porter 2006; Kerr et al. 2013).

Combinations of both presynaptic (e.g. PPR, CV and failure rate) and postsynaptic (e.g. rise time, latency and decay time) properties are characteristic of different synapse types in the neocortex (Feldmeyer et al. 1999; Silver et al. 2003). Our paired recording data on the excitatory connections show that adenosine induced an increase of the PPR, CV and failure rate, whereas the properties associated with the postsynaptic site remain largely unchanged. This suggests that adenosine suppressed synaptic transmission of excitatory connections mainly by decreasing presynaptic neurotransmitter release. In some but not all the inhibitory connections, we found that adenosine also induced a minor suppression onto the postsynaptic IPSP amplitude. However, this reduction of the IPSP amplitude immediately recovered and returned to the baseline level when the membrane potential of the postsynaptic neurons was clamped to the value before adenosine application. Inhibition of GABAergic synapses by adenosine were found in hippocampus and cortices of immature or juvenile rat (Jeong et al. 2003; Kirmse et al. 2008; Kruglikov and Rudy 2008). Our results suggest that instead of a direct suppression of presynaptic GABA release, the inhibition of GABAergic transmission by adenosine is more likely due to a shunting effect induced by the changes of postsynaptic membrane properties (Takigawa and Alzheimer 2002; Ilie et al. 2012; Qi et al. 2017).

Discussion

Adenosine suppresses synaptic transmission between excitatory neurons via both pre- and postsynaptic A₁ARs, but these effects are induced by activation/deactivation of different ion channel types. It has been shown that block of K_{ir} channels removes the adenosine-induced membrane hyperpolarisation but not the inhibition of synaptic transmission (Qi et al. 2017). This indicates that K_{ir} channels are only involved in the postsynaptic effect of adenosine (Luscher et al. 1997; van Aerde et al. 2013). The inhibition of synaptic transmission by adenosine via A₁ARs most likely results from the reduction of presynaptic neurotransmitter release, which results from a reduction in calcium influx through presynaptic voltage-dependent calcium channels (Wu and Saggau 1994, 1997). The effect of adenosine was concentration dependent and the low EC₅₀ suggests that the presynaptic release probability and hence presynaptic calcium channels are more sensitive to adenosine than K_{ir} channels (van Aerde et al. 2013; Qi et al. 2017). Applying low (10 μ M) concentrations of adenosine to E-E synaptic connections revealed a difference in the magnitude of adenosine-mediated suppression between inverted-pre and upright-pre connections. Connections with an upright presynaptic neuron are more sensitive to adenosine compared to those with an inverted presynaptic neuron. This may result from difference in the presynaptic calcium channel types and/or the G protein signalling cascades in the presynaptic terminals of two subtypes of connections (Wu and Saggau 1994).

In addition, by applying the A₁AR antagonist CPT the presence of endogenous extracellular adenosine was uncovered in the mPFC slice preparation. In the presence of CPT alone the membrane potential became more depolarised and the spontaneous mEPSC frequency increased through a block of the tonic adenosine effect. The endogenous adenosine concentration was estimated to be 1-2 μ M, suggesting that the tonic modulation is only small and mainly affects synaptic release (Kerr et al. 2013; Qi et al. 2017).

Previous studies on A_{2A}ARs in the hippocampus have shown that these receptors enhance excitatory synaptic transmission (Rebola et al. 2003; Rombo et al. 2015). A study in rat visual cortex demonstrated a modulation of inhibitory transmission via A_{2A}ARs, which requires the activation of A₁ receptors (Zhang et al. 2015). However, we did not find any significant changes neither on the postsynaptic membrane properties nor the synaptic properties during application of the A_{2A}AR

Discussion

agonist. This suggests a very low if any $A_{2A}ARs$ expression on both pre- and postsynaptic sites in L6 of mPFC.

Summary

Layer 6 of medial prefrontal cortex (mPFC) is a largely unexplored area with a very heterogeneous cellular composition. Classification of excitatory and inhibitory neurons is crucial for understanding neural circuit dynamics. The characterisation of synaptic connectivity allows an insight of how mPFC microcircuitry processes and integrates complex information.

In this study, single and dual whole-cell patch-clamp recordings with simultaneous biocytin-fillings were made from L6 excitatory, inhibitory and synaptically coupled neurons. Quantitative classifications were performed with excitatory neurons and inhibitory neurons by using principal component analysis and unsupervised cluster analysis. Two main clusters of L6 excitatory neurons were identified based on their dendritic morphology: (1) upright excitatory neurons with their primary or apical dendrites spanning superficial layers and terminating in L5 to L1 and (2) inverted/horizontally oriented excitatory neurons, which had primary dendrites pointing towards the white matter or oriented sideways. L6 interneurons were classified into three major categories that showed distinct axonal projection pattern: L1 inhibitors showed axonal projections similar to Martinotti-like cells extending to layer 1, L5 inhibitors displayed translaminar projections mostly to layer 5 and in layer 6, whereas L6 inhibitors were confined to layer 6. Moreover, our data suggested a correlation between morphological properties and intrinsic physiological properties with both excitatory and inhibitory L6 neurons.

By using pair recordings, an extremely low connectivity ratio in L6 of mPFC (3.1%) was calculated and interestingly, we found that inverted excitatory neurons performed a higher preference in forming synaptic connections with other excitatory neurons compared with upright neurons. In general, our findings revealed different synaptic features of different types of synaptic connections in L6 of rat mPFC, providing a first insight into the complex organisation of the local L6 microcircuitry.

The neuromodulator adenosine is considered to be a key regulator of sleep homeostasis by exerting a negative control on the arousal centre of the brain. Although the effects of adenosine on cortical and subcortical areas have been previously described, the effect of adenosine on neuronal network activity at the cellular level in mPFC remains unknown. Here, we showed that adenosine suppresses

Summary

synaptic transmission of excitatory connections mainly by decreasing presynaptic neurotransmitter release. This inhibitory effect of adenosine is blocked by the specific A1 receptor antagonist, CPT, indicated that adenosine modulates synaptic transmission of excitatory connections through activation of adenosine A1 receptors. Moreover, the connections with different presynaptic neuron types showed varied sensitivity to adenosine, suggesting a functional difference between these neuron types.

Zusammenfassung

Die Lamina 6 (L6) des medialen präfrontalen Cortex (mPFC) ist eine weitgehend unerforschte corticale Schicht, deren Neuronpopulation sehr heterogen ist. Um die Dynamik neuronaler Schaltkreise zu verstehen, ist eine Klassifizierung der exzitatorischen wie auch inhibitorischen Neuronentypen unerlässlich. Die Charakterisierung der neuronaler Konnektivität erlaubt es, Einsichten darüber zu gewinnen, wie die neuronaler Schaltkreise des mPFC komplexe Informationen verarbeiten und integrieren.

Im Rahmen der vorliegenden Arbeit wurden Patch-clamp Ableitungen mit simultanen Biocytinfüllungen von einzelnen Neuronen bzw. exzitatorischen oder inhibitorischen synaptischen Verbindungen durchgeführt. Mittels einer Hauptkomponenten-Analyse und anschließender unbewachter Cluster-Analyse wurde eine quantitative Klassifizierung der exzitatorischen und inhibitorischen Neurone durch geführt. Basierend auf der Morphologie der Dendriten wurden zwei Hauptgruppen von L6 exzitatorischen Neuronen identifiziert: (1) aufrechte Pyramidenzellen mit apikalen bzw. Primär-Dendriten die in Richtung der Pia projizierten und in L5 bis L1 endeten und (2) invertierte/horizontal orientierte Neurone, deren Primärdendrit in Richtung auf die weiße Substanz verlief oder horizontal orientiert war. Basierend auf ihrer atonalen Projektion konnten L6 Interneurone in drei Hauptkategorien eingeteilt werden. L1 Inhibitoren besaßen ein Axon, das die L1 innovierte, ähnlich wie die sogenannten Martinotti-Zellen. L5 Inhibitoren zeigten eine transaminare atonale Projektion in L5 während das Axon von L6 Inhibitoren weitgehend auf die L6 beschränkt war. Die Daten wiesen zudem darauf hin, dass die morphologischen und intrinsischen elektrophysiologischen Eigenschaften sowohl der exzitatorischen als auch der inhibitorischen L6 Neurone korrelierten.

Paarableitungen zeigten, dass die synaptische Konnektivität von L6 Neuronen gering (3.1%) war; dabei erwies sich, dass im Vergleich zu aufrechten Pyramidenzellen invertierte Neurone häufiger synaptische Kontakten mit anderen exzitatorischen L6 Neuronen ausbildeten. Zusammenfassend konnten wir die unterschiedlichen Eigenschaften verschiedener synaptischer Verbindungen in L6 des mPFC, so daß diese Daten eine erste Übersicht über die komplexe Organisation der lokalen neuronaler Schaltkreise in der kortikalen Schicht geben.

Summary

Der Neuromodulator Adenosin wird als Regulator der Schlaf-Homöostase angesehen, der eine negative Kontrolle über die Wachzentren des Hirns ausübt. Auch wenn die Effekte von Adenosine sowohl in einigen kortikalen und subkortikalen Arealen bekannt sind, so ist dessen Wirkung auf die Aktivität des neuronaler Netzwerkes des mPFC auf zellulärem Niveau weitgehend unbekannt. Hier konnten wir zeigen, dass Adenosin die exzitatorische synaptische Transmission hauptsächlich durch Verminderung der präsynaptischen Neurotransmitterfreisetzung hemmt. Dieser inhibitorische Adenosin-Effekt konnte durch den spezifischen Antagonisten des Adenosin A1 Rezeptoren CPT gehemmt werden. Die Adenosin-Modulation der synaptischen Transmission exzitatorischer Verbindungen wird somit durch Adenosin A1 Rezeptoren vermittelt. Darüber hinaus zeigte sich, dass verschiedene präsynaptische Neurone eine unterschiedliche Adenosin-Sensitivität aufwiesen, was auf eine Neuron-Typ spezifische funktionelle Unterschiede hindeutet.

References

- Abbott LF, Regehr WG. 2004. Synaptic computation. *Nature*. 431:796-803.
- Alexander GE, DeLong MR, Strick PL. 1986. Parallel organization of functionally segregated circuits linking basal ganglia and cortex. *Annual review of neuroscience*. 9:357-381.
- Amaral DG, Price JL. 1984. Amygdalo-cortical projections in the monkey (*Macaca fascicularis*). *The Journal of comparative neurology*. 230:465-496.
- Arrigoni E, Chamberlin NL, Saper CB, McCarley RW. 2006. Adenosine inhibits basal forebrain cholinergic and noncholinergic neurons in vitro. *Neuroscience*. 140:403-413.
- Arrigoni E, Rainnie DG, McCarley RW, Greene RW. 2001. Adenosine-mediated presynaptic modulation of glutamatergic transmission in the laterodorsal tegmentum. *The Journal of neuroscience : the official journal of the Society for Neuroscience*. 21:1076-1085.
- Arzt M, Sakmann B, Meyer HS. 2017. Anatomical Correlates of Local, Translaminar, and Transcolumnar Inhibition by Layer 6 GABAergic Interneurons in Somatosensory Cortex. *Cerebral cortex*. 1-12.
- Ascoli GA, Alonso-Nanclares L, Anderson SA, Barrionuevo G, Benavides-Piccione R, Burkhalter A, Buzsaki G, Cauli B, Defelipe J, Fairen A, Feldmeyer D, Fishell G, Fregnac Y, Freund TF, Gardner D, Gardner EP, Goldberg JH, Helmstaedter M, Hestrin S, Karube F, Kisvarday ZF, Lambolez B, Lewis DA, Marin O, Markram H, Munoz A, Packer A, Petersen CC, Rockland KS, Rossier J, Rudy B, Somogyi P, Staiger JF, Tamas G, Thomson AM, Toledo-Rodriguez M, Wang Y, West DC, Yuste R. 2008. Petilla terminology: nomenclature of features of GABAergic interneurons of the cerebral cortex. *Nature reviews Neuroscience*. 9:557-568.
- Avesar D, Gullledge AT. 2012. Selective serotonergic excitation of callosal projection neurons. *Front Neural Circuits*. 6:12.
- Bannon NM, Zhang P, Ilin V, Chistiakova M, Volgushev M. 2014. Modulation of synaptic transmission by adenosine in layer 2/3 of the rat visual cortex in vitro. *Neuroscience*. 260:171-184.
- Barbas H, De Olmos J. 1990. Projections from the amygdala to basoventral and mediodorsal prefrontal regions in the rhesus monkey. *The Journal of comparative neurology*. 300:549-571.
- Barbas H, Pandya DN. 1989. Architecture and intrinsic connections of the prefrontal cortex in the rhesus monkey. *The Journal of comparative neurology*. 286:353-375.
- Basheer R, Bauer A, Elmenhorst D, Ramesh V, McCarley RW. 2007. Sleep deprivation upregulates A1 adenosine receptors in the rat basal forebrain. *Neuroreport*. 18:1895-1899.
- Basheer R, Strecker RE, Thakkar MM, McCarley RW. 2004. Adenosine and sleep-wake regulation. *Prog Neurobiol*. 73:379-396.
- Bates JF, Goldman-Rakic PS. 1993. Prefrontal connections of medial motor areas in the rhesus monkey. *The Journal of comparative neurology*. 336:211-228.
- Bauer A, Holschbach MH, Meyer PT, Boy C, Herzog H, Olsson RA, Coenen HH, Zilles K. 2003. In vivo imaging of adenosine A1 receptors in the human brain with [¹⁸F]CPFPX and positron emission tomography. *Neuroimage*. 19:1760-1769.
- Bauer A, Langen KJ, Bidmon H, Holschbach MH, Weber S, Olsson RA, Coenen HH, Zilles K. 2005. ¹⁸F-CPFPX PET identifies changes in cerebral A1 adenosine receptor density caused by glioma invasion. *J Nucl Med*. 46:450-454.
- Baumgartner G. 2009. Organization and function of the neocortex. *Neuro-Ophthalmology*. 3:1-14.

References

- Beierlein M, Connors BW. 2002. Short-term dynamics of thalamocortical and intracortical synapses onto layer 6 neurons in neocortex. *Journal of neurophysiology*. 88:1924-1932.
- Beique JC, Imad M, Mladenovic L, Gingrich JA, Andrade R. 2007. Mechanism of the 5-hydroxytryptamine 2A receptor-mediated facilitation of synaptic activity in prefrontal cortex. *Proceedings of the National Academy of Sciences of the United States of America*. 104:9870-9875.
- Berridge CW, Arnsten AFT. 2015. Catecholamine mechanisms in the prefrontal cortex: proven strategies for enhancing higher cognitive function. *Current Opinion in Behavioral Sciences*. 4:33-40.
- Bicks LK, Koike H, Akbarian S, Morishita H. 2015. Prefrontal Cortex and Social Cognition in Mouse and Man. *Front Psychol*. 6:1805.
- Boison D, Singer P, Shen HY, Feldon J, Yee BK. 2012. Adenosine hypothesis of schizophrenia--opportunities for pharmacotherapy. *Neuropharmacology*. 62:1527-1543.
- Bontempi B, Laurent-Demir C, Destrade C, Jaffard R. 1999. Time-dependent reorganization of brain circuitry underlying long-term memory storage. *Nature*. 400:671-675.
- Botvinick MM, Cohen JD, Carter CS. 2004. Conflict monitoring and anterior cingulate cortex: an update. *Trends in cognitive sciences*. 8:539-546.
- Brambilla D, Chapman D, Greene R. 2005. Adenosine Mediation of Presynaptic Feedback Inhibition of Glutamate Release. *Neuron*. 46:275-283.
- Branco T, Staras K. 2009. The probability of neurotransmitter release: variability and feedback control at single synapses. *Nat Rev Neurosci*. 10:373-383.
- Brodmann K, Gary LJ. 2006. Brodmann's localisation in the cerebral cortex : the principles of comparative localisation in the cerebral cortex based on cytoarchitectonics. New York, NY: Springer.
- Brown SP, Hestrin S. 2009. Intracortical circuits of pyramidal neurons reflect their long-range axonal targets. *Nature*. 457:1133-1136.
- Burkhalter A. 1989. Intrinsic connections of rat primary visual cortex: laminar organization of axonal projections. *The Journal of comparative neurology*. 279:171-186.
- Cauli B, Audinat E, Lambolez B, Angulo MC, Ropert N, Tsuzuki K, Hestrin S, Rossier J. 1997. Molecular and physiological diversity of cortical nonpyramidal cells. *The Journal of neuroscience : the official journal of the Society for Neuroscience*. 17:3894-3906.
- Cauli B, Zhou X, Tricoire L, Toussay X, Staiger JF. 2014. Revisiting enigmatic cortical calretinin-expressing interneurons. *Front Neuroanat*. 8:52.
- Clowry GJ. 2015. An enhanced role and expanded developmental origins for gamma-aminobutyric acidergic interneurons in the human cerebral cortex. *J Anat*. 227:384-393.
- Cotel F, Fletcher LN, Kalita-de Croft S, Apergis-Schoute J, Williams SR. 2017. Cell Class-Dependent Intracortical Connectivity and Output Dynamics of Layer 6 Projection Neurons of the Rat Primary Visual Cortex. *Cereb Cortex*. 1-11.
- Crandall SR, Patrick SL, Cruikshank SJ, Connors BW. 2017. Infrabarrels Are Layer 6 Circuit Modules in the Barrel Cortex that Link Long-Range Inputs and Outputs. *Cell Rep*. 21:3065-3078.
- Damasio AR, Graff-Radford NR, Eslinger PJ, Damasio H, Kassell N. 1985. Amnesia following basal forebrain lesions. *Archives of neurology*. 42:263-271.
- Davis M, Barad M, Otto M, Southwick S. 2006. Combining pharmacotherapy with cognitive behavioral therapy: traditional and new approaches. *Journal of traumatic stress*. 19:571-581.

References

- DeFelipe J, Lopez-Cruz PL, Benavides-Piccione R, Bielza C, Larranaga P, Anderson S, Burkhalter A, Cauli B, Fairen A, Feldmeyer D, Fishell G, Fitzpatrick D, Freund TF, Gonzalez-Burgos G, Hestrin S, Hill S, Hof PR, Huang J, Jones EG, Kawaguchi Y, Kisvarday Z, Kubota Y, Lewis DA, Marin O, Markram H, McBain CJ, Meyer HS, Monyer H, Nelson SB, Rockland K, Rossier J, Rubenstein JL, Rudy B, Scanziani M, Shepherd GM, Sherwood CC, Staiger JF, Tamas G, Thomson A, Wang Y, Yuste R, Ascoli GA. 2013. New insights into the classification and nomenclature of cortical GABAergic interneurons. *Nature reviews Neuroscience*. 14:202-216.
- Dembrow NC, Chitwood RA, Johnston D. 2010. Projection-specific neuromodulation of medial prefrontal cortex neurons. *The Journal of neuroscience : the official journal of the Society for Neuroscience*. 30:16922-16937.
- Dunwiddie TV, Diao L, Kim HO, Jiang JL, Jacobson KA. 1997. Activation of hippocampal adenosine A3 receptors produces a desensitization of A1 receptor-mediated responses in rat hippocampus. *The Journal of neuroscience : the official journal of the Society for Neuroscience*. 17:607-614.
- Dunwiddie TV, Masino SA. 2001. The role and regulation of adenosine in the central nervous system. *Annual review of neuroscience*. 24:31-55.
- Elmenhorst D, Basheer R, McCarley RW, Bauer A. 2009. Sleep deprivation increases A(1) adenosine receptor density in the rat brain. *Brain research*. 1258:53-58.
- Elmenhorst D, Meyer PT, Winz OH, Matusch A, Ermert J, Coenen HH, Basheer R, Haas HL, Zilles K, Bauer A. 2007. Sleep deprivation increases A1 adenosine receptor binding in the human brain: a positron emission tomography study. *The Journal of neuroscience : the official journal of the Society for Neuroscience*. 27:2410-2415.
- Emmenegger V, Qi G, Wang H, Feldmeyer D. 2018. Morphological and Functional Characterization of Non-fast-Spiking GABAergic Interneurons in Layer 4 Microcircuitry of Rat Barrel Cortex. *Cerebral cortex*.
- Euston DR, Gruber AJ, McNaughton BL. 2012. The role of medial prefrontal cortex in memory and decision making. *Neuron*. 76:1057-1070.
- Feldmeyer D. 2012. Excitatory neuronal connectivity in the barrel cortex. *Front Neuroanat*. 6:24.
- Feldmeyer D, Egger V, Lubke J, Sakmann B. 1999. Reliable synaptic connections between pairs of excitatory layer 4 neurones within a single 'barrel' of developing rat somatosensory cortex. *The Journal of physiology*. 521 Pt 1:169-190.
- Feldmeyer D LbJ. 2010. New Aspects of Axonal Structure and Function. *New Aspects of Axonal Structure and Function*. 1-237.
- Feldmeyer D, Lubke J, Silver RA, Sakmann B. 2002. Synaptic connections between layer 4 spiny neurone-layer 2/3 pyramidal cell pairs in juvenile rat barrel cortex: physiology and anatomy of interlaminar signalling within a cortical column. *The Journal of physiology*. 538:803-822.
- Feldmeyer D, Qi G, Emmenegger V, Staiger JF. 2018. Inhibitory interneurons and their circuit motifs in the many layers of the barrel cortex. *Neuroscience*. 368:132-151.
- Feldmeyer D, Radnikow G. 2016. Paired Recordings from Synaptically Coupled Neurones in Acute Neocortical Slices. In: Korngreen A, editor. *Advanced patch-clamp analysis for neuroscientists* New York: Springer Science+Business Media p 171-191.
- Feoktistov I, Biaggioni I. 1997. Adenosine A2B receptors. *Pharmacological reviews*. 49:381-402.

References

- Ferrer I, Fabregues I, Condom E. 1986. A Golgi study of the sixth layer of the cerebral cortex. I. The lissencephalic brain of Rodentia, Lagomorpha, Insectivora and Chiroptera. *J Anat.* 145:217-234.
- Fontanez DE, Porter JT. 2006. Adenosine A1 receptors decrease thalamic excitation of inhibitory and excitatory neurons in the barrel cortex. *Neuroscience.* 137:1177-1184.
- Frankland PW, Bontempi B, Talton LE, Kaczmarek L, Silva AJ. 2004. The involvement of the anterior cingulate cortex in remote contextual fear memory. *Science.* 304:881-883.
- Fredholm BB. 2007. Adenosine, an endogenous distress signal, modulates tissue damage and repair. *Cell Death Differ.* 14:1315-1323.
- Fredholm BB, Cunha RA, Svenningsson P. 2003. Pharmacology of adenosine A2A receptors and therapeutic applications. *Current topics in medicinal chemistry.* 3:413-426.
- Fuster JM. 2001. The prefrontal cortex--an update: time is of the essence. *Neuron.* 30:319-333.
- Gass JT, Chandler LJ. 2013. The Plasticity of Extinction: Contribution of the Prefrontal Cortex in Treating Addiction through Inhibitory Learning. *Frontiers in psychiatry.* 4:46.
- Gaykema RP, Nguyen XM, Boehret JM, Lambeth PS, Joy-Gaba J, Warthen DM, Scott MM. 2014. Characterization of excitatory and inhibitory neuron activation in the mouse medial prefrontal cortex following palatable food ingestion and food driven exploratory behavior. *Front Neuroanat.* 8:60.
- Gee S, Ellwood I, Patel T, Luongo F, Deisseroth K, Sohal VS. 2012. Synaptic activity unmasks dopamine D2 receptor modulation of a specific class of layer V pyramidal neurons in prefrontal cortex. *The Journal of neuroscience : the official journal of the Society for Neuroscience.* 32:4959-4971.
- Gerber U, Greene RW, Haas HL, Stevens DR. 1989. Characterization of inhibition mediated by adenosine in the hippocampus of the rat in vitro. *The Journal of physiology.* 417:567-578.
- Gerwins P, Fredholm BB. 1992. Stimulation of adenosine A1 receptors and bradykinin receptors, which act via different G proteins, synergistically raises inositol 1,4,5-trisphosphate and intracellular free calcium in DDT1 MF-2 smooth muscle cells. *Proceedings of the National Academy of Sciences of the United States of America.* 89:7330-7334.
- Gilbert CD. 1983. Microcircuitry of the visual cortex. *Annual review of neuroscience.* 6:217-247.
- Globus A, Scheibel AB. 1967. Pattern and field in cortical structure: the rabbit. *The Journal of comparative neurology.* 131:155-172.
- Goldman PS, Nauta WJ. 1976. Autoradiographic demonstration of a projection from prefrontal association cortex to the superior colliculus in the rhesus monkey. *Brain research.* 116:145-149.
- Goldman-Rakic PS, Schwartz ML. 1982. Interdigitation of contralateral and ipsilateral columnar projections to frontal association cortex in primates. *Science.* 216:755-757.
- Goldman-Rakic PS, Selemon LD, Schwartz ML. 1984. Dual pathways connecting the dorsolateral prefrontal cortex with the hippocampal formation and parahippocampal cortex in the rhesus monkey. *Neuroscience.* 12:719-743.
- Gulledge AT, Kampa BM, Stuart GJ. 2005. Synaptic integration in dendritic trees. *J Neurobiol.* 64:75-90.
- Helmstaedter M, Sakmann B, Feldmeyer D. 2009. Neuronal correlates of local, lateral, and translaminar inhibition with reference to cortical columns. *Cerebral cortex.* 19:926-937.

References

- Helmstaedter M, Sakmann B, Feldmeyer D. 2009. The relation between dendritic geometry, electrical excitability, and axonal projections of L2/3 interneurons in rat barrel cortex. *Cerebral cortex*. 19:938-950.
- Herculano-Houzel S. 2009. The human brain in numbers: a linearly scaled-up primate brain. *Front Hum Neurosci*. 3:31.
- Holroyd CB, Coles MG, Nieuwenhuis S. 2002. Medial prefrontal cortex and error potentials. *Science*. 296:1610-1611 author reply 1610-1611.
- Hoover WB, Vertes RP. 2007. Anatomical analysis of afferent projections to the medial prefrontal cortex in the rat. *Brain Struct Funct*. 212:149-179.
- Ilie A, Raimondo JV, Akerman CJ. 2012. Adenosine release during seizures attenuates GABAA receptor-mediated depolarization. *The Journal of neuroscience : the official journal of the Society for Neuroscience*. 32:5321-5332.
- Jacobson KA, Gao ZG. 2006. Adenosine receptors as therapeutic targets. *Nature reviews Drug discovery*. 5:247-264.
- Jeong HJ, Jang IS, Nabekura J, Akaike N. 2003. Adenosine A1 receptor-mediated presynaptic inhibition of GABAergic transmission in immature rat hippocampal CA1 neurons. *Journal of neurophysiology*. 89:1214-1222.
- Jiang X, Shen S, Cadwell CR, Berens P, Sinz F, Ecker AS, Patel S, Tolias AS. 2015. Principles of connectivity among morphologically defined cell types in adult neocortex. *Science*. 350:aac9462.
- Jiang X, Wang G, Lee AJ, Stornetta RL, Zhu JJ. 2013. The organization of two new cortical interneuronal circuits. *Nature neuroscience*. 16:210-218.
- Katzel D, Zemelman BV, Buettner C, Wolfel M, Miesenböck G. 2011. The columnar and laminar organization of inhibitory connections to neocortical excitatory cells. *Nature neuroscience*. 14:100-U135.
- Kaufmann WE, Moser HW. 2000. Dendritic anomalies in disorders associated with mental retardation. *Cerebral cortex*. 10:981-991.
- Kawaguchi Y, Kubota Y. 1993. Correlation of physiological subgroupings of nonpyramidal cells with parvalbumin- and calbindinD28k-immunoreactive neurons in layer V of rat frontal cortex. *J Neurophysiol*. 70:387-396.
- Kawaguchi Y, Kubota Y. 1996. Physiological and morphological identification of somatostatin- or vasoactive intestinal polypeptide-containing cells among GABAergic cell subtypes in rat frontal cortex. *The Journal of neuroscience : the official journal of the Society for Neuroscience*. 16:2701-2715.
- Kawaguchi Y, Kubota Y. 1997. GABAergic cell subtypes and their synaptic connections in rat frontal cortex. *Cerebral cortex*. 7:476-486.
- Kerr MI, Wall MJ, Richardson MJ. 2013. Adenosine A1 receptor activation mediates the developmental shift at layer 5 pyramidal cell synapses and is a determinant of mature synaptic strength. *The Journal of physiology*. 591:3371-3380.
- Kirmse K, Dvornik A, Grantyn R, Kirischuk S. 2008. Developmental downregulation of excitatory GABAergic transmission in neocortical layer I via presynaptic adenosine A(1) receptors. *Cerebral cortex*. 18:424-432.
- Klausberger T, Somogyi P. 2008. Neuronal diversity and temporal dynamics: the unity of hippocampal circuit operations. *Science*. 321:53-57.

References

- Koelbl C, Helmstaedter M, Lubke J, Feldmeyer D. 2015. A barrel-related interneuron in layer 4 of rat somatosensory cortex with a high intrabarrel connectivity. *Cerebral cortex*. 25:713-725.
- Kruglikov I, Rudy B. 2008. Perisomatic GABA release and thalamocortical integration onto neocortical excitatory cells are regulated by neuromodulators. *Neuron*. 58:911-924.
- Kumar P, Ohana O. 2008. Inter- and intralaminar subcircuits of excitatory and inhibitory neurons in layer 6a of the rat barrel cortex. *Journal of neurophysiology*. 100:1909-1922.
- Latini S, Pedata F. 2001. Adenosine in the central nervous system: release mechanisms and extracellular concentrations. *Journal of neurochemistry*. 79:463-484.
- Lee AJ, Wang G, Jiang X, Johnson SM, Hoang ET, Lante F, Stornetta RL, Beenhakker MP, Shen Y, Julius Zhu J. 2015. Canonical Organization of Layer 1 Neuron-Led Cortical Inhibitory and Disinhibitory Interneuronal Circuits. *Cerebral cortex*. 25:2114-2126.
- Lefort S, Tómm C, Floyd Sarria JC, Petersen CC. 2009. The excitatory neuronal network of the C2 barrel column in mouse primary somatosensory cortex. *Neuron*. 61:301-316.
- Lesage F. 2003. Pharmacology of neuronal background potassium channels. *Neuropharmacology*. 44:1-7.
- Lewis DA, Fish KN, Arion D, Gonzalez-Burgos G. 2011. Perisomatic inhibition and cortical circuit dysfunction in schizophrenia. *Curr Opin Neurobiol*. 21:866-872.
- Lin AS, Uhde TW, Slate SO, McCann UD. 1997. Effects of intravenous caffeine administered to healthy males during sleep. *Depression and anxiety*. 5:21-28.
- Lodato S, Arlotta P. 2015. Generating neuronal diversity in the mammalian cerebral cortex. *Annu Rev Cell Dev Biol*. 31:699-720.
- Lopes LV, Cunha RA, Ribeiro JA. 1999. Cross talk between A(1) and A(2A) adenosine receptors in the hippocampus and cortex of young adult and old rats. *Journal of neurophysiology*. 82:3196-3203.
- Lu MT, Preston JB, Strick PL. 1994. Interconnections between the prefrontal cortex and the premotor areas in the frontal lobe. *The Journal of comparative neurology*. 341:375-392.
- Lubke J, Roth A, Feldmeyer D, Sakmann B. 2003. Morphometric analysis of the columnar innervation domain of neurons connecting layer 4 and layer 2/3 of juvenile rat barrel cortex. *Cerebral cortex*. 13:1051-1063.
- Lui JH, Hansen DV, Kriegstein AR. 2011. Development and evolution of the human neocortex. *Cell*. 146:18-36.
- Luna B, Minshew NJ, Garver KE, Lazar NA, Thulborn KR, Eddy WF, Sweeney JA. 2002. Neocortical system abnormalities in autism: an fMRI study of spatial working memory. *Neurology*. 59:834-840.
- Luscher C, Jan LY, Stoffel M, Malenka RC, Nicoll RA. 1997. G protein-coupled inwardly rectifying K⁺ channels (GIRKs) mediate postsynaptic but not presynaptic transmitter actions in hippocampal neurons. *Neuron*. 19:687-695.
- Macek TA, Schaffhauser H, Conn PJ. 1998. Protein kinase C and A3 adenosine receptor activation inhibit presynaptic metabotropic glutamate receptor (mGluR) function and uncouple mGluRs from GTP-binding proteins. *The Journal of neuroscience : the official journal of the Society for Neuroscience*. 18:6138-6146.
- Mainen ZF, Sejnowski TJ. 1996. Influence of dendritic structure on firing pattern in model neocortical neurons. *Nature*. 382:363-366.

References

- Manzoni OJ, Manabe T, Nicoll RA. 1994. Release of adenosine by activation of NMDA receptors in the hippocampus. *Science*. 265:2098-2101.
- Markram H, Toledo-Rodriguez M, Wang Y, Gupta A, Silberberg G, Wu C. 2004. Interneurons of the neocortical inhibitory system. *Nature reviews Neuroscience*. 5:793-807.
- Markram H, Wang Y, Tsodyks M. 1998. Differential signaling via the same axon of neocortical pyramidal neurons. *Proceedings of the National Academy of Sciences of the United States of America*. 95:5323-5328.
- Marx M, Feldmeyer D. 2013. Morphology and physiology of excitatory neurons in layer 6b of the somatosensory rat barrel cortex. *Cerebral cortex*. 23:2803-2817.
- Marx M, Gunter RH, Hucko W, Radnikow G, Feldmeyer D. 2012. Improved biocytin labeling and neuronal 3D reconstruction. *Nature protocols*. 7:394-407.
- McBain CJ, Fisahn A. 2001. Interneurons unbound. *Nature reviews Neuroscience*. 2:11-23.
- Megias M, Emri Z, Freund TF, Gulyas AI. 2001. Total number and distribution of inhibitory and excitatory synapses on hippocampal CA1 pyramidal cells. *Neuroscience*. 102:527-540.
- Mendizabal-Zubiaga JL, Reblet C, Bueno-Lopez JL. 2007. The underside of the cerebral cortex: layer V/VI spiny inverted neurons. *J Anat*. 211:223-236.
- Mercer A, West DC, Morris OT, Kirchhecker S, Kerkhoff JE, Thomson AM. 2005. Excitatory connections made by presynaptic cortico-cortical pyramidal cells in layer 6 of the neocortex. *Cerebral cortex*. 15:1485-1496.
- Meyer HS, Schwarz D, Wimmer VC, Schmitt AC, Kerr JN, Sakmann B, Helmstaedter M. 2011. Inhibitory interneurons in a cortical column form hot zones of inhibition in layers 2 and 5A. *Proceedings of the National Academy of Sciences of the United States of America*. 108:16807-16812.
- Meyer HS, Wimmer VC, Oberlaender M, de Kock CP, Sakmann B, Helmstaedter M. 2010. Number and laminar distribution of neurons in a thalamocortical projection column of rat vibrissa cortex. *Cereb Cortex*. 20:2277-2286.
- Meyer PT, Elmenhorst D, Matusch A, Winz O, Zilles K, Bauer A. 2006. A1 adenosine receptor PET using [18F]CPFPX: displacement studies in humans. *Neuroimage*. 32:1100-1105.
- Miller EK, Cohen JD. 2001. An integrative theory of prefrontal cortex function. *Annual review of neuroscience*. 24:167-202.
- Miller MN, Okaty BW, Nelson SB. 2008. Region-specific spike-frequency acceleration in layer 5 pyramidal neurons mediated by Kv1 subunits. *The Journal of neuroscience : the official journal of the Society for Neuroscience*. 28:13716-13726.
- Molnar Z, Cheung AF. 2006. Towards the classification of subpopulations of layer V pyramidal projection neurons. *Neurosci Res*. 55:105-115.
- Monyer H, Markram H. 2004. Interneuron Diversity series: Molecular and genetic tools to study GABAergic interneuron diversity and function. *Trends Neurosci*. 27:90-97.
- Mountcastle VB. 1957. Modality and topographic properties of single neurons of cat's somatic sensory cortex. *J Neurophysiol*. 20:408-434.
- Mueller SG, Laxer KD, Barakos J, Cheong I, Garcia P, Weiner MW. 2009. Widespread neocortical abnormalities in temporal lobe epilepsy with and without mesial sclerosis. *Neuroimage*. 46:353-359.
- Murray EA, Wise SP, Graham KS. 2017. The evolution of memory systems : ancestors, anatomy, and adaptations. Oxford, United Kingdom ; New York, NY: Oxford University Press.

References

- Muzur A, Pace-Schott EF, Hobson JA. 2002. The prefrontal cortex in sleep. *Trends in cognitive sciences*. 6:475-481.
- Narayanan RT, Udvary D, Oberlaender M. 2017. Cell Type-Specific Structural Organization of the Six Layers in Rat Barrel Cortex. *Front Neuroanat*. 11:91.
- Nieuwenhuys R, Donkelaar HJt, Nicholson C. 1998. The central nervous system of vertebrates. Berlin ; New York: Springer.
- Ochiishi T, Chen L, Yukawa A, Saitoh Y, Sekino Y, Arai T, Nakata H, Miyamoto H. 1999. Cellular localization of adenosine A1 receptors in rat forebrain: immunohistochemical analysis using adenosine A1 receptor-specific monoclonal antibody. *The Journal of comparative neurology*. 411:301-316.
- Olah ME, Stiles GL. 1995. Adenosine receptor subtypes: characterization and therapeutic regulation. *Annual review of pharmacology and toxicology*. 35:581-606.
- Otsuka T, Kawaguchi Y. 2008. Firing-pattern-dependent specificity of cortical excitatory feed-forward subnetworks. *The Journal of neuroscience : the official journal of the Society for Neuroscience*. 28:11186-11195.
- Pandya DN, Yeterian EH. 1990. Prefrontal cortex in relation to other cortical areas in rhesus monkey: architecture and connections. *Progress in brain research*. 85:63-94.
- Parnavelas JG, Lieberman AR, Webster KE. 1977. Organization of neurons in the visual cortex, area 17, of the rat. *J Anat*. 124:305-322.
- Petersen CC, Sakmann B. 2000. The excitatory neuronal network of rat layer 4 barrel cortex. *The Journal of neuroscience : the official journal of the Society for Neuroscience*. 20:7579-7586.
- Petrides M, Pandya DN. 1984. Projections to the frontal cortex from the posterior parietal region in the rhesus monkey. *The Journal of comparative neurology*. 228:105-116.
- Petrides M, Pandya DN. 1999. Dorsolateral prefrontal cortex: comparative cytoarchitectonic analysis in the human and the macaque brain and corticocortical connection patterns. *The European journal of neuroscience*. 11:1011-1036.
- Pichon F, Nikonenko I, Kraftsik R, Welker E. 2012. Intracortical connectivity of layer VI pyramidal neurons in the somatosensory cortex of normal and barrelless mice. *The European journal of neuroscience*. 35:855-869.
- Porkka-Heiskanen T, Strecker RE, Thakkar M, Bjorkum AA, Greene RW, McCarley RW. 1997. Adenosine: a mediator of the sleep-inducing effects of prolonged wakefulness. *Science*. 276:1265-1268.
- Porrino LJ, Crane AM, Goldman-Rakic PS. 1981. Direct and indirect pathways from the amygdala to the frontal lobe in rhesus monkeys. *The Journal of comparative neurology*. 198:121-136.
- Portas CM, Thakkar M, Rainnie DG, Greene RW, McCarley RW. 1997. Role of adenosine in behavioral state modulation: a microdialysis study in the freely moving cat. *Neuroscience*. 79:225-235.
- Porter JT, Cauli B, Staiger JF, Lambolez B, Rossier J, Audinat E. 1998. Properties of bipolar VIPergic interneurons and their excitation by pyramidal neurons in the rat neocortex. *The European journal of neuroscience*. 10:3617-3628.
- Posner MI, Rothbart MK, Sheese BE, Tang Y. 2007. The anterior cingulate gyrus and the mechanism of self-regulation. *Cogn Affect Behav Neurosci*. 7:391-395.

References

- Poulsen SA, Quinn RJ. 1998. Adenosine receptors: new opportunities for future drugs. *Bioorganic & medicinal chemistry*. 6:619-641.
- Prieto JJ, Winer JA. 1999. Layer VI in cat primary auditory cortex: Golgi study and sublaminal origins of projection neurons. *The Journal of comparative neurology*. 404:332-358.
- Prince DA, Stevens CF. 1992. Adenosine decreases neurotransmitter release at central synapses. *Proceedings of the National Academy of Sciences of the United States of America*. 89:8586-8590.
- Qi G, Feldmeyer D. 2016. Dendritic Target Region-Specific Formation of Synapses Between Excitatory Layer 4 Neurons and Layer 6 Pyramidal Cells. *Cerebral cortex*. 26:1569-1579.
- Qi G, Radnikow G, Feldmeyer D. 2015. Electrophysiological and morphological characterization of neuronal microcircuits in acute brain slices using paired patch-clamp recordings. *J Vis Exp*. 52358.
- Qi G, van Aerde K, Abel T, Feldmeyer D. 2017. Adenosine Differentially Modulates Synaptic Transmission of Excitatory and Inhibitory Microcircuits in Layer 4 of Rat Barrel Cortex. *Cerebral cortex*. 27:4411-4422.
- Qi HX, Jain N, Preuss TM, Kass JH. 1999. Inverted pyramidal neurons in chimpanzee sensorimotor cortex are revealed by immunostaining with monoclonal antibody SMI-32. *Somatosens Mot Res*. 16:49-56.
- Radnikow G, Feldmeyer D. 2018. Layer- and Cell Type-Specific Modulation of Excitatory Neuronal Activity in the Neocortex. *Front Neuroanat*. 12:1.
- Rainnie DG, Grunze HC, McCarley RW, Greene RW. 1994. Adenosine inhibition of mesopontine cholinergic neurons: implications for EEG arousal. *Science*. 263:689-692.
- Rebola N, Pinheiro PC, Oliveira CR, Malva JO, Cunha RA. 2003. Subcellular localization of adenosine A(1) receptors in nerve terminals and synapses of the rat hippocampus. *Brain research*. 987:49-58.
- Regehr WG. 2012. Short-term presynaptic plasticity. *Cold Spring Harb Perspect Biol*. 4:a005702.
- Reyes A, Sakmann B. 1999. Developmental switch in the short-term modification of unitary EPSPs evoked in layer 2/3 and layer 5 pyramidal neurons of rat neocortex. *The Journal of neuroscience : the official journal of the Society for Neuroscience*. 19:3827-3835.
- Rivkees SA, Price SL, Zhou FC. 1995. Immunohistochemical detection of A1 adenosine receptors in rat brain with emphasis on localization in the hippocampal formation, cerebral cortex, cerebellum, and basal ganglia. *Brain research*. 677:193-203.
- Rockland KS. 2017. What do we know about laminar connectivity? *Neuroimage*.
- Rogel A, Bromberg Y, Sperling O, Zoref-Shani E. 2005. Phospholipase C is involved in the adenosine-activated signal transduction pathway conferring protection against iodoacetic acid-induced injury in primary rat neuronal cultures. *Neuroscience letters*. 373:218-221.
- Rombo DM, Newton K, Nissen W, Badurek S, Horn JM, Minichiello L, Jefferys JG, Sebastiao AM, Lamsa KP. 2015. Synaptic mechanisms of adenosine A2A receptor-mediated hyperexcitability in the hippocampus. *Hippocampus*. 25:566-580.
- Rudy B, Fishell G, Lee S, Hjerling-Leffler J. 2011. Three groups of interneurons account for nearly 100% of neocortical GABAergic neurons. *Dev Neurobiol*. 71:45-61.
- Rushworth MF, Noonan MP, Boorman ED, Walton ME, Behrens TE. 2011. Frontal cortex and reward-guided learning and decision-making. *Neuron*. 70:1054-1069.
- Sachdeva S, Gupta M. 2013. Adenosine and its receptors as therapeutic targets: An overview. *Saudi Pharm J*. 21:245-253.

References

- Scanziani M, Capogna M, Gahwiler BH, Thompson SM. 1992. Presynaptic inhibition of miniature excitatory synaptic currents by baclofen and adenosine in the hippocampus. *Neuron*. 9:919-927.
- Schmahmann JD, Pandya DN. 1997. Anatomic organization of the basilar pontine projections from prefrontal cortices in rhesus monkey. *The Journal of neuroscience : the official journal of the Society for Neuroscience*. 17:438-458.
- Schwindel CD, Ali K, McNaughton BL, Tatsuno M. 2014. Long-term recordings improve the detection of weak excitatory-excitatory connections in rat prefrontal cortex. *The Journal of neuroscience : the official journal of the Society for Neuroscience*. 34:5454-5467.
- Seltzer B, Pandya DN. 1989. Intrinsic connections and architectonics of the superior temporal sulcus in the rhesus monkey. *The Journal of comparative neurology*. 290:451-471.
- Seong HJ, Carter AG. 2012. D1 receptor modulation of action potential firing in a subpopulation of layer 5 pyramidal neurons in the prefrontal cortex. *The Journal of neuroscience : the official journal of the Society for Neuroscience*. 32:10516-10521.
- Silver RA, Lubke J, Sakmann B, Feldmeyer D. 2003. High-probability unquantal transmission at excitatory synapses in barrel cortex. *Science*. 302:1981-1984.
- Sohal VS, Zhang F, Yizhar O, Deisseroth K. 2009. Parvalbumin neurons and gamma rhythms enhance cortical circuit performance. *Nature*. 459:698-702.
- Staiger JF, Masannek C, Schleicher A, Zusratter W. 2004. Calbindin-containing interneurons are a target for VIP-immunoreactive synapses in rat primary somatosensory cortex. *The Journal of comparative neurology*. 468:179-189.
- Steger R, Blachorsky L, Yang Q, Brumberg JC. 2018. Synaptic properties of layer VI inverted pyramidal cells in the rodent somatosensory cortex. *Somatosens Mot Res*. 35:33-44.
- Steger RM, Ramos RL, Cao R, Yang Q, Chen CC, Dominici J, Brumberg JC. 2013. Physiology and morphology of inverted pyramidal neurons in the rodent neocortex. *Neuroscience*. 248:165-179.
- Strecker RE, Morairty S, Thakkar MM, Porkka-Heiskanen T, Basheer R, Dauphin LJ, Rainnie DG, Portas CM, Greene RW, McCarley RW. 2000. Adenosinergic modulation of basal forebrain and preoptic/anterior hypothalamic neuronal activity in the control of behavioral state. *Behav Brain Res*. 115:183-204.
- Stuss DT, Benson DF, Clermont R, Della Malva CL, Kaplan EF, Weir WS. 1986. Language functioning after bilateral prefrontal leukotomy. *Brain and language*. 28:66-70.
- Takashima A, Petersson KM, Rutter F, Tendolkar I, Jensen O, Zwartz MJ, McNaughton BL, Fernandez G. 2006. Declarative memory consolidation in humans: a prospective functional magnetic resonance imaging study. *Proceedings of the National Academy of Sciences of the United States of America*. 103:756-761.
- Takigawa T, Alzheimer C. 2002. Phasic and tonic attenuation of EPSPs by inward rectifier K⁺ channels in rat hippocampal pyramidal cells. *The Journal of physiology*. 539:67-75.
- Tawfik HE, Schnerrmann J, Oldenburg PJ, Mustafa SJ. 2005. Role of A1 adenosine receptors in regulation of vascular tone. *American journal of physiology Heart and circulatory physiology*. 288:H1411-1416.
- Thompson P, W Toga A. 2003. Cerebral Cortex Diseases and Cortical Localization.
- Thomson AM. 1997. Activity-dependent properties of synaptic transmission at two classes of connections made by rat neocortical pyramidal axons in vitro. *J Physiol*. 502 (Pt 1):131-147.

References

- Thomson AM. 2003. Presynaptic frequency- and pattern-dependent filtering. *J Comput Neurosci.* 15:159-202.
- Thomson AM. 2010. Neocortical layer 6, a review. *Front Neuroanat.* 4:13.
- Thomson AM, Deuchars J. 1997. Synaptic interactions in neocortical local circuits: dual intracellular recordings in vitro. *Cerebral cortex.* 7:510-522.
- Thomson AM, West DC, Wang Y, Bannister AP. 2002. Synaptic connections and small circuits involving excitatory and inhibitory neurons in layers 2-5 of adult rat and cat neocortex: triple intracellular recordings and biocytin labelling in vitro. *Cerebral cortex.* 12:936-953.
- Tomita H, Ohbayashi M, Nakahara K, Hasegawa I, Miyashita Y. 1999. Top-down signal from prefrontal cortex in executive control of memory retrieval. *Nature.* 401:699-703.
- Townsend-Nicholson A, Baker E, Schofield PR, Sutherland GR. 1995. Localization of the adenosine A1 receptor subtype gene (ADORA1) to chromosome 1q32.1. *Genomics.* 26:423-425.
- Tremblay R, Lee S, Rudy B. 2016. GABAergic Interneurons in the Neocortex: From Cellular Properties to Circuits. *Neuron.* 91:260-292.
- Uylings HB, Groenewegen HJ, Kolb B. 2003. Do rats have a prefrontal cortex? *Behav Brain Res.* 146:3-17.
- Valverde F. 1976. Aspects of cortical organization related to the geometry of neurons with intracortical axons. *J Neurocytol.* 5:509-529.
- van Aerde KI, Feldmeyer D. 2013. Morphological and Physiological Characterization of Pyramidal Neuron Subtypes in Rat Medial Prefrontal Cortex. *Cerebral cortex.*
- van Aerde KI, Qi G, Feldmeyer D. 2013. Cell Type-Specific Effects of Adenosine on Cortical Neurons. *Cerebral cortex.*
- van Calker D, Biber K. 2005. The role of glial adenosine receptors in neural resilience and the neurobiology of mood disorders. *Neurochem Res.* 30:1205-1217.
- Van Dort CJ, Baghdoyan HA, Lydic R. 2009. Adenosine A(1) and A(2A) receptors in mouse prefrontal cortex modulate acetylcholine release and behavioral arousal. *The Journal of neuroscience : the official journal of the Society for Neuroscience.* 29:871-881.
- Van Eden CG, Uylings HB. 1985. Cytoarchitectonic development of the prefrontal cortex in the rat. *The Journal of comparative neurology.* 241:253-267.
- Van Hoesen GW, Pandya DN, Butters N. 1972. Cortical afferents to the entorhinal cortex of the Rhesus monkey. *Science.* 175:1471-1473.
- Wang F, Zhu J, Zhu H, Zhang Q, Lin Z, Hu H. 2011. Bidirectional control of social hierarchy by synaptic efficacy in medial prefrontal cortex. *Science.* 334:693-697.
- Wang Y, Markram H, Goodman PH, Berger TK, Ma J, Goldman-Rakic PS. 2006. Heterogeneity in the pyramidal network of the medial prefrontal cortex. *Nature neuroscience.* 9:534-542.
- Wang Y, Toledo-Rodriguez M, Gupta A, Wu CZ, Silberberg G, Luo JY, Markram H. 2004. Anatomical, physiological and molecular properties of Martinotti cells in the somatosensory cortex of the juvenile rat. *J Physiol-London.* 561:65-90.
- Ward JH. 1963. Hierarchical Grouping to Optimize an Objective Function. *J Am Stat Assoc.* 58:236-&.

References

- West DC, Mercer A, Kirchhecker S, Morris OT, Thomson AM. 2006. Layer 6 cortico-thalamic pyramidal cells preferentially innervate interneurons and generate facilitating EPSPs. *Cerebral cortex*. 16:200-211.
- Wonders CP, Anderson SA. 2006. The origin and specification of cortical interneurons. *Nature reviews Neuroscience*. 7:687-696.
- Wood JN, Grafman J. 2003. Human prefrontal cortex: processing and representational perspectives. *Nature reviews Neuroscience*. 4:139-147.
- Wood JN, Romero SG, Makale M, Grafman J. 2003. Category-specific representations of social and nonsocial knowledge in the human prefrontal cortex. *Journal of cognitive neuroscience*. 15:236-248.
- Wu LG, Saggau P. 1994. Adenosine inhibits evoked synaptic transmission primarily by reducing presynaptic calcium influx in area CA1 of hippocampus. *Neuron*. 12:1139-1148.
- Wu LG, Saggau P. 1997. Presynaptic inhibition of elicited neurotransmitter release. *Trends Neurosci*. 20:204-212.
- Yang C, Franciosi S, Brown RE. 2013. Adenosine inhibits the excitatory synaptic inputs to Basal forebrain cholinergic, GABAergic, and parvalbumin neurons in mice. *Frontiers in neurology*. 4:77.
- Yang CR, Seamans JK, Gorelova N. 1996. Electrophysiological and morphological properties of layers V-VI principal pyramidal cells in rat prefrontal cortex in vitro. *The Journal of neuroscience : the official journal of the Society for Neuroscience*. 16:1904-1921.
- Zhang P, Bannon NM, Ilin V, Volgushev M, Chistiakova M. 2015. Adenosine effects on inhibitory synaptic transmission and excitation-inhibition balance in the rat neocortex. *The Journal of physiology*. 593:825-841.
- Zhang ZW, Deschenes M. 1997. Intracortical axonal projections of lamina VI cells of the primary somatosensory cortex in the rat: a single-cell labeling study. *The Journal of neuroscience : the official journal of the Society for Neuroscience*. 17:6365-6379.
- Zilles K, Amunts K. 2010. Centenary of Brodmann's map--conception and fate. *Nature reviews Neuroscience*. 11:139-145.
- Zucker RS, Regehr WG. 2002. Short-term synaptic plasticity. *Annu Rev Physiol*. 64:355-405.

Abbreviations

5HT: Serotonin

A₁AR: A₁ adenosine receptors

A_{2A}AR: A_{2A} adenosine receptors

A_{2B}AR: A_{2B} adenosine receptors

A₃AR: A₃ adenosine receptors

AC: adenylyl cyclase

ACC: anterior cingulate cortex

Ach: acetylcholine

ACSF: artificial cerebrospinal fluid

Ad: adapting

Ado: adenosine

AHP: after-hyperpolarisation potential

AMP: adenosine monophosphate

AP: action potential

ATP: adenosine triphosphate

CA: cluster analysis

cAMP: cyclic adenosine monophosphate

CNS: central nervous system

CPA: N⁶-cyclopentyladenosine

CPT: 8-Cyclopentyl-1,3-dimethylxanthine

CV: coefficient variation

DAG: diacylglycerol

EFT: event foot time

EPSP: excitatory postsynaptic potential

FS: fast spiking

GABA: gamma-aminobutyric acid

HCN channels: Hyperpolarisation-activated cyclic nucleotide-gated channels

IfL cortex: infralimbic cortex

IP₃: triphosphoinositol

IPSC: inhibitory postsynaptic current

IPSP: inhibitory postsynaptic potential
IS: irregular spiking
IEI: inter event interval
ISI: inter spike interval
LTS: low threshold spiking
mPFC: medial prefrontal cortex
nFS: non-fast spiking
OFC: orbital frontal cortex
PB: phosphate buffer
PC: principal component
PFA: paraformaldehyde
PIP₂: phosphatidylinositol 4,5-bisphosphate
PLC: phospholipase C
PN: pyramidal neuron
PPR: paired pulse ratio
PrL cortex: prelimbic cortex
PV: parvalbumin
REM: rapid eye movement
RS: regular spiking
SST: somatostatin
TTX: tetrodotoxin

Acknowledgement

Firstly I would like to express sincere appreciation to Prof. Dirk Feldmeyer for giving me patient guidances in the past five years. His insight and continuous advice provide the basis for this thesis. He is one of the best person I had met here and thanks to his apprehension and help that I could balance my family and work.

I wish to thank Prof. Andreas Bauer, who offered me an opportunity to pursuit my doctoral study in Germany. I also thank him for the supervision and advices he gave to me in the past years. I would like to thank Prof. Christoph Fahlke, who is my second supervisor, for reviewing this thesis.

I would like to thank Dr. Guanxiao Qi for coaching me all the experimental techniques and analysis. He was always available to help me with any problems and questions in my work as well as my personal life. Thanks to Dr. Shalini Emmenegger for introduced me the advanced skills of Neurolucida reconstructions.

I would like to thank Werner Hucko for all the experimental preparation and technical assistance. Thanks to Dr. Manual Marx for helpful suggestions and discussion. A special thank to them for all the unselfish helps they gave whenever I need with the administration and with my personal life.

A big thank to all the group members accompanying me during this wonderful time. They are Dr. Gabriele Radnikow, Dr. Robert Günter, Dr. Claudia Barz, Dr. Jiali Tang, Dr. Haijun Wang, Jawad Jawadi, Simone Schmitz, Ramya Rama and Irene Melati Aji.

I would like to thank China Scholarship Council and Forschungszentrum Jülich for financially support me during my doctoral study.

At last but not the least, I would like to thank my parents for giving me tremendous faith and trust. Thanks to my parents in law and my sister, who have also gave me unmatched supports. Most importantly, I wish to say ‘thank you’ to my wife, Danqing Yang, who is my best friend, my soul mate and the mother of my son. Thank you for always standing besides me and thank you for

believing me and believing us. You and Luca make the time of my doctoral study the best time in my life.

Curriculum Vitae

Personal details

Name: Chao Ding

Gender: Male

Date of birth: 01.25.1989

Place of Birth: Anhui, China

Marital status: Married

Nationality: Chinese

Email: ch.ding@fz-juelich.de

University Education

2013.10-Present: Ph.D. candidate in Neuroscience, Heinrich Heine Universität Düsseldorf; Institute of Neuroscience and Medicine (INM-2), Forschungszentrum Jülich, Germany

2010.9-2013.7: M.Sc. in Genomics/ Neuroscience, Key Laboratory of Brain Functional Genomics, Ministry of Education; Shanghai Institute of Brain Functional Genomics, East China Normal University, China

2006.9-2010.6: B.E. in Bioengineering, Engineering and Technology College, Hubei University Of Technology, China

2003.9-2006.6: High School Diploma, Wuwei middle school, Anhui, China

2000.9-2003.6: Middle School Diploma, Wuwei middle school, Anhui, China

Conferences

Oral presentation at the 1st iBrain annual meeting, 8th-9th May 2014, Düsseldorf, Germany

Poster presentation at the 7th annual retreat of the institute of neuroscience and medicine and the institute of complex systems, 2-3 July 2018, Jülich, Germany

Poster presentation at the 11th FENS forum of neuroscience, 7-11 July 2018, Berlin, Germany

Eidesstattliche Erklärung

Ich versichere hiermit an Eides statt, dass die vorliegende Dissertation von mir selbstständig und ohne unzulässige fremde Hilfe unter Beachtung der „Grundsätze zur Sicherung guter wissenschaftlicher Praxis an der Heinrich-Heine-Universität Düsseldorf“ erstellt worden ist. Diese Dissertation wurde keiner anderen Fakultät vorgelegt und es gab bisher keine erfolglosen Promotionsversuche.

Jülich, den 20. August 2018, Chao Ding